



저작자표시-비영리-변경금지 2.0 대한민국

이용자는 아래의 조건을 따르는 경우에 한하여 자유롭게

- 이 저작물을 복제, 배포, 전송, 전시, 공연 및 방송할 수 있습니다.

다음과 같은 조건을 따라야 합니다:



저작자표시. 귀하는 원저작자를 표시하여야 합니다.



비영리. 귀하는 이 저작물을 영리 목적으로 이용할 수 없습니다.



변경금지. 귀하는 이 저작물을 개작, 변형 또는 가공할 수 없습니다.

- 귀하는, 이 저작물의 재이용이나 배포의 경우, 이 저작물에 적용된 이용허락조건을 명확하게 나타내어야 합니다.
- 저작권자로부터 별도의 허가를 받으면 이러한 조건들은 적용되지 않습니다.

저작권법에 따른 이용자의 권리는 위의 내용에 의하여 영향을 받지 않습니다.

이것은 [이용허락규약\(Legal Code\)](#)을 이해하기 쉽게 요약한 것입니다.

[Disclaimer](#)

공학박사 학위 논문

센서 및 액추에이터 결함이 있는 전기 유압식 액추에이터에 대한 결함
진단 및 내결함성 추적 제어 개발

**DEVELOPMENT OF FAULT DIAGNOSIS AND FAULT-TOLERANT
TRACKING CONTROL FOR AN ELECTROHYDRAULIC ACTUATOR
WITH SENSOR AND ACTUATOR FAULT**

울산대학교 대학원

기계자동차 공학과

PHAN VAN DU

**DEVELOPMENT OF FAULT DIAGNOSIS AND FAULT-TOLERANT
TRACKING CONTROL FOR AN ELECTROHYDRAULIC ACTUATOR
WITH SENSOR AND ACTUATOR FAULT**

A thesis submitted in partial fulfillment of the requirement for the Degree of
Doctor of Philosophy to the School of Mechanical and Automotive
Engineering, University of Ulsan, Korea

Supervisor: **KYOUNG KWAN AHN**

By

PHAN VAN DU

June 2023

센서 및 액추에이터 결함이 있는 전기 유압식 액추에이터에 대한 결함
진단 및 내결함성 추적 제어 개발

**DEVELOPMENT OF FAULT DIAGNOSIS AND FAULT-TOLERANT
TRACKING CONTROL FOR AN ELECTROHYDRAULIC ACTUATOR
WITH SENSOR AND ACTUATOR FAULT**

지도교수 안경관

이논문을 공학박사 학위 논문으로 제출함

2023 년 06 월

울산대학교 대학원

기계자동차공학과

DEVELOPMENT OF FAULT DIAGNOSIS AND FAULT-TOLERANT TRACKING CONTROL FOR AN ELECTROHYDRAULIC ACTUATOR WITH SENSOR AND ACTUATOR FAULT

**This certifies that the dissertation of
PHAN VAN DU is approved by**

Committee Chairman: Prof. BYUNG RYONG LEE



Committee Member: Prof. CHEOL KEUN HA



Committee Member: Asst. Prof. GI SEO PARK



Committee Member: Prof. KYOUNG KWAN AHN



Committee Member: Prof. JI SUNG JANG



School of Mechanical and Automotive Engineering

University of Ulsan, Korea

June 2023

PHAN VAN DU 의
공학박사 학위 논문을 인준함

심사위원

이병룡



(인)

심사위원

하철근



(인)

심사위원

박기서



(인)

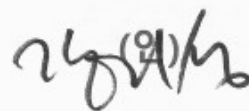
심사위원

안경관



심사위원

장지성



(인)

울산대학교 대학원

기계자동차공학과

2023 년 06

Acknowledgement

Time flies like an arrow, my doctoral research has come to the end. During the time in which this study was undertaken, I gained various experiences and had the best chance to work with excellent people. The thesis would not have been completed without encouragement, and kindly help from them to whom I dedicate my honest thanks.

Foremost, I would like to express my deep gratitude to my supervisor, Prof. Ahn Kyoung Kwan, for all of his help and support during my study in University of Ulsan. I will remember all of the opportunities, valuable advice, and careful guidance which he has provided me to take the first steps into becoming a scientist.

I would like to thank Prof. Byung Ryong Lee, Prof. Cheol Keun Ha, Prof. Gi-Seo Park, and Prof. Ji-Sung Jang, for kindly joining the advisory committee and providing me with many insightful suggestions and comments throughout my research.

I would also like to thank all of my friends and my colleagues in Korea, in Vinh University, Vietnam, and from abroad, especially my members of the Fluid Power and Machine Intelligence Lab. –and others – for their help and friendship.

Finally, I am grateful to my parents, my wife Nguyen Thi Thanh Huyen, my daughter, my parents-in-law, and all my sisters with the most wonderful members. Their love and encouragement have become the strongest power for me to stand up to difficulties during the time I studied abroad.

Ulsan, June 2023

Phan Van Du

Contents

Acknowledgments.....	i
Contents.....	ii
Abbreviations.....	v
List of Tables.....	vii
List of Figures.....	viii
Abstract.....	x
1 INTRODUCTION.....	1
1.1 Overview.....	1
1.2 Research objectives.....	4
1.3 Limitation of the dissertation.....	4
1.4 Dissertation outline.....	5
2 OVERVIEWS ON FAULT DIAGNOSIS AND FAULT-TOLERANT CONTROL.....	6
2.1 Introduction.....	6
2.2 Basic concepts.....	6
2.2.1 Basic definition.....	6
2.2.2 Fault classification.....	7
2.3 Fault diagnosis method.....	8
2.4 Fault tolerant control.....	9
3 MODELLING AND PROBLEM STATEMENTS OF THE EHA SYSTEM.....	10
3.1 Introduction.....	10
3.2 Nonlinear EHA model with fault and problem formulation.....	10
3.3 Matched, mismatched disturbance, and system faults.....	12
3.3.1 Matched and mismatched disturbance.....	12
3.3.2 System faults.....	13
3.4 Experiment apparatus.....	15
4 INTERNAL LEAKAGE FAULT-TOLERANT TRACKING CONTROL.....	18
4.1 Introduction.....	18
4.2 Problem formulation.....	19

4.3 Proposed control design for EHA.....	20
4.3.1 Coordinate transformation and system model transformation.....	21
4.3.2 Fault detection and identification using time delay estimation.....	23
4.3.3 Control law design.....	24
4.4 Simulation results.....	28
4.4.1 Simulation setup.....	28
4.4.2 Simulation result.....	29
4.5 Experimental verification.....	32
4.6 Chapter summary.....	36
5 ACTUATOR FAULT-TOLERANT TRACKING CONTROL WITH BIAS AND	
LOSS OF EFFECTIVENESS FAULT.....	37
5.1 Introduction.....	37
5.2 Problem description.....	38
5.3 FTC design and stability analysis.....	40
5.3.1 Nominal control design.....	41
5.3.2 Reconfigurable control design.....	43
5.4 Numerical simulation.....	47
5.4.1 Simulation setup.....	47
5.4.2 Simulation result.....	49
5.5 Comparative experimental results.....	51
5.5.1 Experiment setup.....	51
5.5.2 Experiment results.....	51
5.6 Chapter summary.....	54
6 ROBUST SENSOR FAULT-TOLERANT TRACKING CONTROL.....	56
6.1 Introduction.....	56
6.2 Problem statement.....	57
6.3 NUIO-based fault identification for EHA.....	59
6.4 Observer-based fault-tolerant tracking control.....	62
6.4.1 ESO design.....	62
6.4.2 FTC design with ESOs and NUIO.....	64

6.5 Simulation results.....	68
6.5.1 Simulation setup.....	68
6.5.2 Simulation result.....	70
6.6 Chapter summary.....	77
7 CONCLUSION AND FUTURE WORKS.....	79
7.1 Conclusion.....	79
7.2 Future works.....	80
PUBLICATIONS.....	82
REFERENCES.....	84

Abbreviations

Symbols	Descriptions
FTC	Fault-tolerant Control
FD	Fault diagnosis
FDe	Fault detection
FE	Fault estimation
FI	Fault isolation
FDI	Fault detection and identification
NUIO	Nonlinear unknown input observer
ESO	Extended state observer
NDO	Nonlinear disturbance observer
TDE	Time delay estimation
RBFNN	Radius basis function neural network
EHA	Electro-hydraulic actuator
NN	Neural network
FLS	Fuzzy logic system
DO	Disturbance observer
DSC	Dynamic surface control
CFC	Command filtered control
LOE	Loss of effectiveness
FDTDE	Fault detection using TDE
ILF	Internal leakage fault
AISMC	adaptive integral sliding mode control
FBL	Feedback linearization

BLF	Barrier Lyapunov function
LMI	Linear matrix inequality
DSESO	Dynamic surface control with ESOs
DSNUIO	Dynamic surface control with NUIOs
SOED	Second-order exact differentiation

List of Tables

Table 3.1	Setting parameters of the real EHA system.....	16
Table 3.2	Electro-hydraulic system parameters.....	17
Table 4.1	Performance indices of three controllers in simulation.....	31
Table 4.2	Performance indices of three controllers in experiment.....	36
Table 6.1	Summary of performance indices.....	74

List of Figures

Figure 1.1	Various applications of EHA.....	1
Figure 2.1	Fault classification with respect to location.....	7
Figure 2.2	The block diagram of FTC system.....	9
Figure 3.1	Schematic model of a double-rod EHA.....	10
Figure 3.2	Possible faults of a double-rod EHA.....	13
Figure 3.3	The experimental equipment of the EHA system.....	16
Figure 4.1	The schematic model of the EHA under ILF.....	19
Figure 4.2	Structure of the proposed control scheme.....	20
Figure 4.3	Lumped disturbance estimation in simulation: a) without fault, b) Abrupt fault.....	29
Figure 4.4	Performances of three controllers in simulation, scenario 1.....	30
Figure 4.5	Performances of three controllers in simulation, scenario 2.....	31
Figure 4.6	Lumped disturbance estimation in experiment: a) without fault, b) Abrupt fault.....	32
Figure 4.7	Performances of three controllers in experiment, scenario 1.....	33
Figure 4.8	Estimated velocity and acceleration of SEOD in experiment.....	34
Figure 4.9	Performances of three controllers in experiment, scenario 2.....	35
Figure 4.10	Adaptive gain in experiment.....	35
Figure 5.1	Schematic of the electro-hydraulic actuator with actuator faults.....	38
Figure 5.2	Sketch of the proposed control approach.....	40
Figure 5.3	Lumped disturbance and LOE fault estimation in the simulation.....	49
Figure 5.4	Performances of the proposed controller in the simulation.....	50

Figure 5.5	The overall tracking error of different control methods.....	50
Figure 5.6	Result of performance indexes in the simulation.....	51
Figure 5.7	Mismatched, matched disturbance and LOE fault estimation of the proposed method in the experiment.....	52
Figure 5.8	Performances of three control methods in experiment 1.....	53
Figure 5.9	Result of performance indexes in the experiment.....	53
Figure 5.10	Performances of three control methods in experiment 2.....	54
Figure 6.1	Schematic of the electro-hydraulic actuator with sensor faults.....	57
Figure 6.2	Schematic view of the proposed control scheme.....	59
Figure 6.3	FDEI of NUIOs in case of only fault in position sensor.....	70
Figure 6.4	FDEI of NUIOs in case of only fault in velocity sensor.....	71
Figure 6.5	FDEI of NUIOs in case of only fault in pressure sensor.....	71
Figure 6.6	FDEI of NUIOs in case of simultaneous fault.....	72
Figure 6.7	Performances of comparative controllers in case 1.....	73
Figure 6.8	Lumped disturbance estimation of ESOs in case 1.....	74
Figure 6.9	Tracking performance of different control methods in case 2.....	75
Figure 6.10	Lumped disturbance estimation of ESOs in case 2.....	76
Figure 6.11	Lumped disturbance estimation of ESOs in case 3.....	77
Figure 6.12	Tracking errors of two control methods in case 3.....	77

Abstract

In recent decades, electro-hydraulic actuator (EHA) is widely used in the model industry (i.e., aerospace systems, construction machines, robotic manipulators, and ships) due to their high-power weight ratio, low cost, efficient handling of heavy loads, and reliability. However, some negative factors affect the performance system such as nonlinear features, modeling uncertainties, and especially faults. In the EHA, the possible faults have normally happened relating to the mechanism, electronic amplifiers, servo valves, hydraulic cylinders, sensor components, or power supply with different features, which are divided into: sensor fault, component fault, and actuator fault. Therefore, this thesis develops a robust fault diagnosis and fault-tolerant tracking control scheme to not only overcome the influences of lumped disturbances/uncertainties and faults but also warrant stability, safety, and reliability.

In this thesis, various adaptive fault-tolerant controllers are proposed for a typical EHA in the presence of lumped disturbances, actuator fault (i.e., internal leakage fault and partial loss of effectiveness fault), and sensor fault. To construct the suggested controller, an observer-based (i.e., nonlinear unknown input observer, time delay estimation, extended state observer, nonlinear observer) is developed to effectively identify the sensor/actuator fault. Furthermore, various control strategies such as, conventional control, intelligent control, and modern control are applied to tackle the effect of the sensor/actuator fault. The integration of the above-mentioned techniques (i.e., observer-based, advanced control algorithm) is investigated to obtain acceptable tracking performance, robustness as well as fast convergence. The stability of the closed-loop system is proven by Lyapunov theory. Finally, the capability and effectiveness of the proposed approach are validated via the simulation and experiment results under different faulty scenarios.

CHAPTER 1

INTRODUCTION

1.1 Overview

Nowadays, with the development of modern industrials, the hydraulic actuator has been the most popular and widely used in many applications such as robotic manipulators, ships, aerospace systems, construction machinery, and so on. These applications are illustrated in Figure 1.1. Although this actuator has outstanding advantages of a high-power-to-weight ratio, high accuracy, cost, and fast response, the model uncertainty is a big challenge in ensuring operational efficiency. In detail, the hydraulic system always exists parametric uncertainties, external disturbance, and unmodeled nonlinearities as well as faults [1-4].

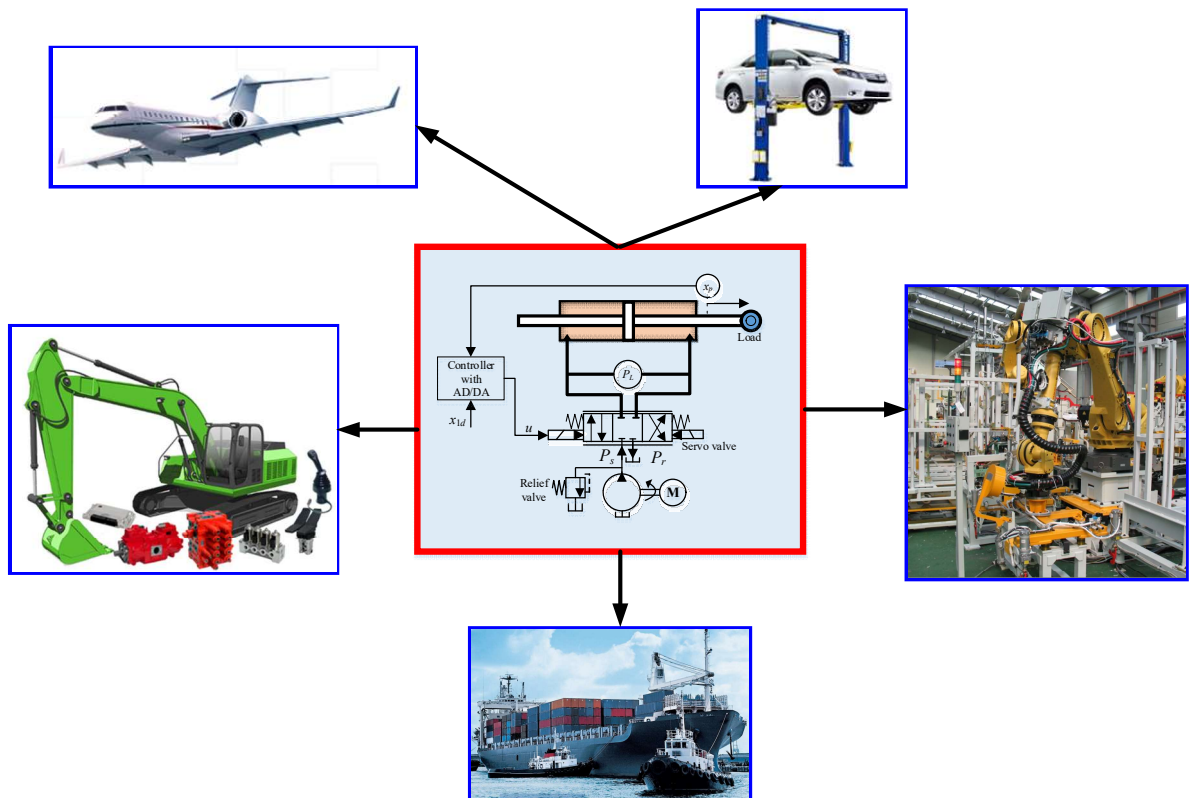


Figure 1.1 Various applications of EHA

In order to improve the system performance, the disturbance is not only needfully suppressed but also compensated by assisted techniques such as extended state observer [5], [6], neural network (NN) approximators [7-10] fuzzy logic system (FLS) [11], time-delay estimation (TDE) [12], [13], etc. In a certain way, the disturbances or uncertainties can be considered as faults, which seriously affect system performance and safety [14]. In an electro-hydraulic actuator (EHA), the possible faults have normally happened relating to the mechanism, electronic amplifiers, servo valves, hydraulic cylinders, sensor components, or power supply with different features [3]. For the closed-loop control in complex systems such as aircraft, construction machines, automobiles, serious accidents may occur due to system faults. Hence, the fault-tolerant controller (FTC) is developed to deal with the impact of faults on the system which can be classified into three main types [15]: component fault, sensor fault and actuator fault. In this thesis, the latter two faults will be studied.

In the engineering system, a measurement part plays an especially key role in the tracking control. For instance, the sensor fault could be happened in position sensors, pressure sensors, load cells in the hydraulic robot [16], in generators and rotor speed sensors of a wind turbine [17], in the sensor measuring jacket temperature of chemical plants [18], and on voltage sensors, current sensors and speed sensor of the electrical traction system [19], etc. Thus, any sensor fault occurs in the overall system that can affect significantly tracking performance [20], [21]. Inspired by fault estimation techniques, the alarm system failures and the suitable acts are decided as soon as possible to avoid heavy damage and dangerous situations. The idea of fault detection and identification (FDI) method becomes a powerful tool to reach the information of a sensor fault as well as an actuator fault [22-24]. In order to deploy the mentioned aim, several observer strategies have been investigated to estimate sensor faults such as adaptive observer [25-28], extended Kalman filter [29], [30], and Takagi-Sugeno fuzzy observer [17], [31]. Especially, an unknown input observer (UIO) is not only an accurate estimation but also a helpful method to distinguish disturbances and faults. It had thus become increasingly popular in the last decade in which observer gain is designed based on the linear matrix inequality (LMI) optimization algorithm [32-34]. In [35], the sensor faults including position and pressure with noise were presented for EHA, then an unknown input observer-integrated extended finite impulse response was investigated to determine the sensor

fault but the actuator fault has not been carried out. Meanwhile, a robust nonlinear unknown input observer (NUIO) [18] was also designed to detect only sensor fault without fault estimation. It has been applied to a continuous stirred tank reactor with respect to external disturbances. Furthermore, a higher-order sliding mode observer [36] was proposed to regulate the vehicle speed in the event of sensor faults/failures. Nevertheless, the effect of the disturbance has not been completely resolved yet. The common advantage of those methods is that they provide a valuable and uncomplicated design strategy to preserve an acceptable system performance in the presence of sensor faults and with/without disturbances. Besides sensor faults, another popular reason affecting control effectiveness is caused by actuator faults, especially the internal leakage fault.

From the actuator fault perspective, many recent studies determined actuator fault as loss-of-effectiveness faults or lumped unknown components [37-39]. In [40], [41] an internal leakage fault under the model uncertainties/time-varying load was accommodated via the adaptive parameter estimation. Then, the control performance was recovered by the FTC when the fault had been detected through the available sensor measurements. In another study, the actuator internal leakage and valve spool blockage were diagnosed by the NN without the presence of disturbances or sensor faults. Because the linearized model was used, it reduced the inherent nonlinearity of the system [42]. In [43], the position controller was tolerant with actuator internal leakage and robust with parametric uncertainties in the EHA in which the sensor fault was not considered. Different techniques like wavelet transform [44], Hilbert-Huang transform [45] applied to reduce the effects of the actuator fault. However, these techniques approach for FTC in general have not clearly analyzed the decoupling between actuator fault and disturbances/uncertainty.

As the above analysis literature, most of the previous studies only considered either the sensor fault or the actuator fault with/without disturbances for tracking control problem. However, it is noteworthy that in the practical hydraulic system, phenomena as mismatched disturbances, sensor faults, and actuator faults may happen simultaneously. Consequently, it is worth pointing out that most of all the above-mentioned challenges need to be handled. The goal of this thesis is to construct a robust fault diagnosis and fault-tolerant control for sensor or

actuator fault which helps to improve the safety and reliability as well as the control performance of the system.

1.2 Research objectives

In this thesis, the FD and FTC schemes are developed to ensure the safety and reliability of the hydraulic control system, especially in the presence of concerned faults (i.e., sensor and actuator faults) and lumped disturbances. This approach combines the FTC technique-assisted the fault information of FDI, called active FTC [46]. The proposed active FTC not only ensures the stability of the controlled system but also maintains acceptable control performances in the presence of faulty conditions. Based on the current demands for developing the FDI and FTC for EHA system, the main objectives of this thesis can be shown as follows:

- To investigate the effects of the relevant factors on the EHA system such as the lumped disturbances, multi-sensor faults, and actuator faults.
- To design the fault diagnosis for EHA, the observer-based FD is accommodated to successfully detect, isolate the sensor/actuator faults in real-time. Several observers such as ESO, NDO, TDE are conducted to not only estimate the lumped disturbances but also faults.
- To solve the effect of lumped disturbances, differential explosion, and system faults, the advanced control algorithms-based FTC scheme is performed. The appropriate methods for control applications of the EHA are proposed such as PID control, backstepping control, dynamics surface control, command filtered control, and feedback linearization integral sliding mode control.
- To analyze the system stability of the whole controlled system, the Lyapunov theory is applied.
- To confirm the effectiveness of the proposed controller, comparative simulation and experimental results are given on the EHA testbench.

1.3 Limitation of the dissertation

However, this dissertation still has some disadvantages.

First, the influences of the measurement noises and other types of sensor faults (i.e., outage and partial loss of effectiveness fault) to the system control performance are not considered. In addition, the valve dynamics is neglected. Finally, the relevant experimental data with multi-sensor and actuator fault diagnosis are not investigated.

1.4 Dissertation outline

The remainder of this dissertation is organized as the following: In Chapter 1 introduces motivations, research objectives, limitations, and outline of this dissertation. Chapter 2 presents an overview of fault diagnosis and fault-tolerant control. In Chapter 3, the system model of the EHA with the lumped disturbance/ uncertainty and sensor/actuator faults is described. Chapter 4 shows the FDI method for internal leakage fault and proposes a novel active FTC based on feedback linearization, adaptive integral sliding mode technique, and time delay estimation. Chapter 5 considers the actuator fault such as bias fault and a partial loss of effectiveness fault. Besides, this chapter suggests adaptive robust control-based command-filter control with the prescribed performance. Chapter 6 focuses on the sensor fault and proposed the novel nonlinear input observer based-dynamic surface controller with disturbance rejection. Lastly, the conclusions and future works are expressed in Chapter 7.

CHAPTER 2

OVERVIEW ON FAULT DIAGNOSIS AND FAULT-TOLERANT CONTROL

2.1 Introduction

In this chapter, background information of system faults, fault diagnosis, and fault-tolerant tracking control are reported. Section 2.2 presents the basic concepts of faults. It also gives the fault classification and FTC architecture. Section 2.3 discusses an overview of fault diagnosis. Finally, the comprehensive description of FTC is described in Section 2.4.

2.2 Basic concepts

With the development of modern control theory, the demand for reliability and safety of industrial systems subjected to potential process abnormalities and component faults has increased attention. Any faults appear in the overall system that can affect significantly tracking performance even resulting in serious accidents. Therefore, all types of potential failures should be studied and are early diagnosed (i.e., fault detection, identification, and FTC) which is crucial.

2.2.1 Basic definition

For the basic concepts of the faults, most of them are defined based on the work within the SAFE-PROCESS committee in the International Federation of Automatic Control (IFAC) [47].

- States and signals:

Fault: At least one variable, characteristic property, or parameter of the system has unacceptable deviation from the usual or standard condition value.

Failure: The system loses the ability to achieve its designed function permanently.

Disturbance: The uncontrolled and unknown input that acts on the system.

Residual: A fault indicator, based on a deviation between measurements and model-equation-based computations.

- Functions:

Fault detection: This module determines the occurrence of faults in a system and the time of detection.

Fault isolation: This module determines the kind, source, or location of a fault and the detection time. It follows fault detection.

Fault identification: This module determines the size or magnitude and time-variant behaviour of a fault. It follows fault isolation.

Fault diagnosis: This module determines the kind, size, location, and detection time of a fault. It comprises fault detection, isolation, and identification.

2.2.2 Fault classification

Faults are often classified into actuator fault, plant fault (or called component faults or parameter faults), and sensor fault by their location of occurrence [23]. The fault classification is shown in Figure 2.1.

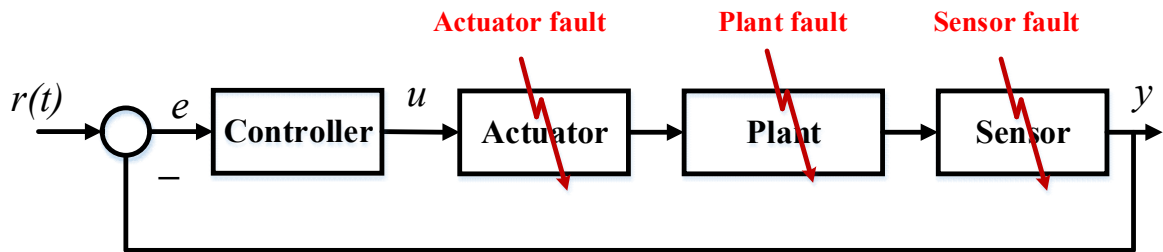


Figure 2.1 Fault classification with respect to location

- Actuator fault: Actuator is denoted as module that acts on the system by transferring the control signal into acting signal. When the actuator occurs a fault, the input control signal has a deviation as compared to the actuator output. This difference may negatively affect the controlled system and lead to a system failure. Basically, actuator faults have 3 modes: a bias fault (or floating fault), a loss of effectiveness fault, and damage (or outage). It can be formulated as follows:

$$u^f = \nu u + \zeta, \quad (2.1)$$

where u^f is the actuator output, u is the actuator input. ν and ζ denote the gain of LOE fault and the bias fault, respectively. When $0 < \nu < 1$, $\zeta = 0$, actuator fault is the LOE actuator fault. When $\nu = 1$, $\zeta \neq 0$, actuator fault is the bias actuator fault. When $\nu = 0$, actuator fault is outage.

- Plant fault: This is the fault that concerns the performance deterioration of process/components because of the inner parameter change.

- Sensor fault: Sensor is a device which is used to convert physical states into measurable signals after calibration process by a computer. When the sensor fault occurs, the feedback measured signal has a deviation as compared to the true value. This affects the system performance even instability system. Similar to actuator faults, sensor faults can be classified into three situations: bias sensor fault (i.e., offsets, poor calibration, scaling errors), partial loss of effectiveness sensor fault, and the outage case.

2.3 Fault diagnosis method

As is mentioned before, the fault diagnosis is a powerful component of designing an FTC for any system which includes fault detection (FD), fault estimation (FE), and fault isolation (FI) [49]. FD and FE point to the appearance of the fault, and the characteristic of the fault, while FI determines the location of the fault. Dependent on the obtained information about the fault, the damages caused by the fault can be eliminated. Fault diagnosis techniques can be broadly divided into two categories: Model-based FD method and Data (or Signal)-based FD method.

- Model-based FD method: In model-based methods, the models of the industrial processes or the practical systems need to be known. Based on the model, fault diagnosis algorithms are designed to monitor the consistency between the measured outputs of the practical systems and the model-predicted outputs. Several fault diagnosis algorithms using state observers have been explored by different researchers in the literature [50, 51]. In addition, various disturbance observers were induced to develop the FD module, such as adaptive disturbance observer, high-gain disturbance observer, time delay estimation, ESO, and so on.

- Data-based FD method: This method is built on the premise of achieving a large amount of historical data. Hence, data-based FD method includes statistical, neural networks, pattern recognition or fuzzy logic methods which do not require any system physical information.

2.4 Fault tolerant control

The main objective of a fault tolerant control scheme is to migrate/cancel the negative influences of faults and retain an acceptable level of control even after the appearance of the fault. FTC systems can be classified into two categories: passive FTC and active FTC systems. The structure of the FTC system is shown in Figure 2.2.

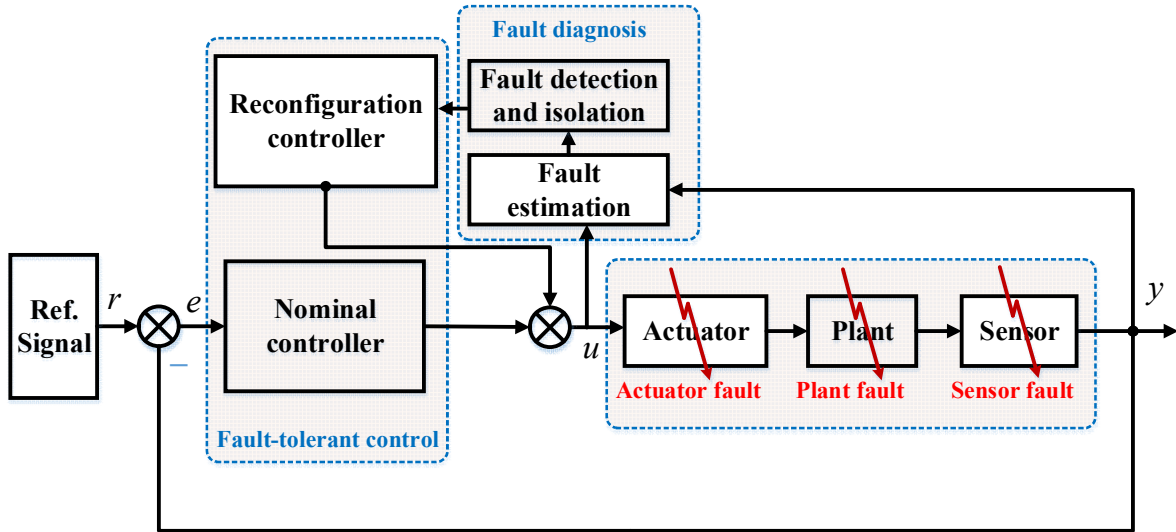


Figure 2.2 The block diagram of FTC system

- Passive FTC is designed to cope with a set of predefined faults. It uses a fix controller and close to robust control based on the control theory point of view. This approach does not require information of the fault. Nonetheless, the robustness properties of the passive FTC guarantee that a pre-defined level of performance is obtained in case of anticipated faults.

- Active FTC: This approach has a difference as compared passive FTC. Herein, the knowledge of online faults is adapted by fault diagnosis module. Hence, the active FTC includes both FD and reconfigurable controller as shown in Figure 2.2. Dependent on the obtained information about the fault of FD, the controller is properly re-designed. Therefore, the active FTC brings a better performance than passive FTC.

CHAPTER 3

MODELLING AND PROBLEM STATEMENTS OF THE EHA SYSTEM

3.1 Introduction

In this chapter, the problem descriptions and some required assumptions of the EHA system are derived in the presence of lumped disturbance and faults. Basically, EHA systems can be categorized into two main types: valve-controlled EHA and pump-controlled EHA. Herein, the valve-controlled is considered in this thesis. First, the component descriptions are introduced. Then, the mathematical model of EHA system is established in the presence of lumped disturbance and faults. Furthermore, some descriptions of system faults are presented such as internal leakage fault, loss of effectiveness actuator fault, and bias sensor faults. Finally, the experiment apparatus of the EHA is investigated.

3.2 Nonlinear EHA model with fault and problem formulation

The simplified schematic diagram of the EHA is described in Figure 3.1. The system consists of a hydraulic pump, a servo valve, a relief valve, a double-rod cylinder, an oil tank, and measurement components, i.e., a displacement transducer and two pressure sensors.

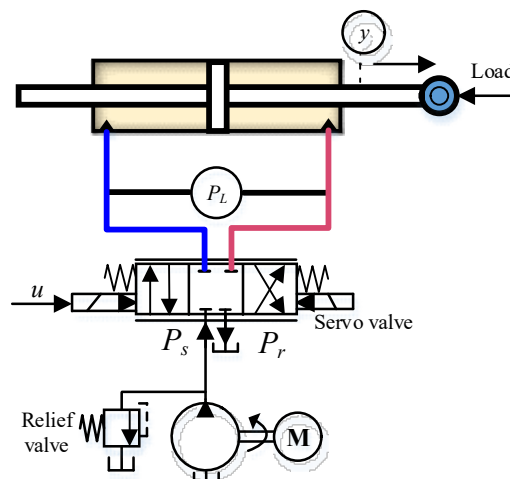


Figure 3.1 Schematic model of a double-rod EHA

A third-order EHA system is presented as follows:

By applying the continuity equation, the pressure dynamics through the cylinder is expressed by [7], [48]

$$\dot{P}_L = \frac{4\beta_e}{V_c}(-Ay - q_L + Q_L + Q_{Li}), \quad (3.1)$$

where A , V_c , and q_L are a ram area, a fixed control volume of the cylinder, and the internal leakage, respectively. β_e is the Bulk modulus. Q_{Li} is the time-varying deviation model including unmodeled pressure dynamics, modeling error, etc.

Assumed that the control supplied to the servo valve is directly proportional to the spool displacement. In addition, the valve dynamics is neglected. Hence, Q_L is load flow rate which is described with respect to control signal by

$$Q_L = k_t u \sqrt{P_s - \text{sign}(u) P_L}, \quad (3.2)$$

where P_s is the supply pressure, k_t is a proportional gain of the servo-valve, $P_L = P_1 - P_2$ denotes the difference of pressure, P_i is the pressure value of i^{th} chamber ($i = 1, 2$), u is the control signal supplied by the controller, and $\text{sign}(\bullet)$ is the standard signum function.

The internal leakage fault can be computed as

$$q_L = C_0 P_L, \quad (3.3)$$

where C_0 is the nominal coefficient of the internal leakage of the double cylinder.

Let us consider the mechanical dynamics given by Newton's second law as follows:

$$m\ddot{y} = P_L A - B\dot{y} + \Lambda(t, y, \dot{y}), \quad (3.4)$$

where y , m , and B represent the displacement, mass of the load, and viscous damping coefficient, respectively; $\Lambda(\bullet)$ is a lumped disturbance/uncertainty term including external load, nonlinear friction.

The parameter uncertainties Δ_1 and Δ_2 can be defined as follows:

$$\Delta_1 = -\Delta b_m \dot{y}, \Delta_2 = -\Delta p_b \dot{y} - \Delta p_c P_L, \quad (3.5)$$

where Δb_m , Δp_b , and Δp_c , in turn, represent the uncertainties of B/m , $p_b = 4\beta_e A/V_c$, $p_c = 4\beta_e C_0/V_c$.

Choosing $x = [x_1, x_2, x_3]^T \triangleq [y, \dot{y}, P_L]^T$ as the state variables. From (3.1)–(3.5), the EHA system can be described by the following third-order nonlinear state-space model:

$$\begin{aligned} &\text{Mechanical} \\ &\text{subsystem} \begin{cases} \dot{x}_1 = x_2, \\ \dot{x}_2 = f_2(x_2) + w_a x_3 + \varphi_1(x_1, x_2, t), \end{cases} \\ &\text{Hydraulic} \\ &\text{subsystem} \begin{cases} \dot{x}_3 = f_3(x_2, x_3) + w_b(x_3, u)u + \varphi_2(x_2, x_3, t), \end{cases} \end{aligned} \quad (3.6)$$

where

$$\begin{aligned} w_a &= \frac{A}{m}, f_2 = -\frac{B}{m}x_2, p_a = \frac{4\beta_e k_t}{V_c}, \\ w_b &= p_a \sqrt{P_s - x_3 \text{sign}(u)}, f_3 = -p_c x_3 - p_b x_2, \\ \varphi_1 &= \frac{\Lambda(\bullet)}{m} + \Delta_1, \varphi_2 = \frac{4\beta_e}{V_c} Q_{Li} + \Delta_2, \end{aligned}$$

denote the unmatched, matched disturbances, respectively.

3.3 Matched, mismatched disturbance, and system faults

In the EHA system, there are mismatched and matched disturbances as well as system faults from several sources that influence the tracking performance of the closed-loop system. The matched and mismatched disturbance can be distinguished via its appearance with respect to the control input u . If one above listed component is in a similar channel with u , it is considered as matched disturbance, and vice versa [1], [49], [50].

3.3.1 Matched and mismatched disturbance

In (3.6), the component of φ_2 is the matched disturbance that arises from leakages in the hydraulic dynamics, nonlinear uncertainties (i.e., parametric uncertainty and model uncertainty). Meanwhile, for mismatched disturbance, these components including viscous friction, Coulomb friction, unknown external load, and parametric uncertainty are lumped in φ_1 . In the real EHA system, the exact mathematical model of the mismatched disturbances is not easy to obtain. So, for the sake of convenience, without loss of generality, it is hypothetical and can be denoted according to the following expression [51], [52]:

$$\varphi_1 = \frac{\Lambda}{m} + \Delta_1 = -k_f x_2 - f_c \text{sign}(x_2) - F_{ext} + \Delta_1, \quad (3.7)$$

where k_f , f_c , and F_{ext} represent the ratio of viscous, Coulomb friction coefficient, and external load to mass, respectively.

3.3.2 System faults

The fault occurs in a practical system that can be categorized as three main groups: sensor fault, actuator fault, and component fault [22]. In this thesis, sensor fault and actuator fault are considered. It should be noted that sensor and actuator faults can be divided into three situations: bias fault, partial loss of effectiveness (LOE) fault, and the outage case [23]. In this thesis, the former two faults will be studied. The possible faults of EHA can be shown in Figure 3.2.

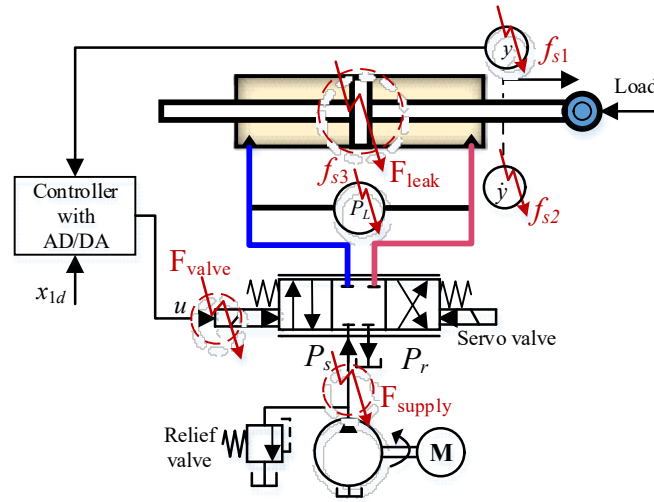


Figure 3.2 Possible faults of a double-rod EHA system

- Actuator fault (Internal leakage fault or bias fault): In the hydraulic system, the internal leakage fault is a relatively common malfunction that not only decreases the performance of the system but also causes serious damage. The internal leakage fault is captured as a bias fault in this thesis. This fault often comes from a piston seal or internal flow loss [53]. The reason for selecting the internal leakage fault is explained by its serious failures as well as the frequent occurrence in the practical EHA system. Since the internal leakage fault happens, it can be represented as [40], [37]:

$$q_L = C_0 P_L + C_t \sqrt{|P_L|} \text{sign}(P_L) \quad (3.8)$$

where C_t is the internal leakage fault coefficient. It is noteworthy that the leakage fault coefficient C_t has a value range analysis from the slight to the abrupt fault. In this article, to reflect the effect of fault, the slow-varying faulty coefficient is indicated as the following.

$$C_t = \begin{cases} 0 & \text{if } t < T_m \\ (1 - e^{-\alpha(t-T_m)})C_{t0} & \text{otherwise} \end{cases} \quad (3.9)$$

where T_m is the time of appearance of the fault, $\alpha > 0$ describes the evolution rate of the unknown fault. For the small value of α , the fault feature is increasing slowly, namely, an incipient fault. Otherwise, the leakage fault coefficient C_t approaches a step function in case of a large value of α and is called an abrupt fault. So, to overcome the effect of the above problem, it is necessary to design advantage control that can guarantee good tracking control as well as retain the stability system.

- Actuator fault (Loss of effectiveness fault): the faults in servo-valve and supply failure are considered as a partial loss of effectiveness fault. The LOE fault comes from incorrect supply pressure (F_{supply}) caused by a lack of pump pressure, or a relief failure which results in the limited performance of the system [58]. Besides, fault in the operational conditions of the servo valve (F_{valve}) can also be mentioned as the LOE fault [59]. Since the supply pressure drops from the nominal value or the servo valve may fail, it means that a fault has occurred. Then, a partial LOE type of actuator fault is considered as follows:

$$u_f = \nu u, \nu \in (0,1) \quad (3.10)$$

where u_f , ν , u represent the actuator faults input, the unknown effectiveness factor of the actuator, and the desired control input, respectively. For a normal operation, $\nu = 1$ while a complete failure (outage) happens with $\nu = 0$.

- Sensor fault: Three sensor faults of hydraulic driven actuator are considered: 1) position sensor fault (f_{s1}); 2) velocity sensor fault (f_{s2}); and 3) load pressure sensor fault (f_{s3}). In this thesis, only bias sensor fault (i.e., offsets, poor calibration, scaling errors) is carried out. When the sensor faults happen, the practical measured system state can be established as $y^F = y + f_{s1}$, $\dot{y}^F = \dot{y} + f_{s2}$, $P_L^F = P_L + f_{s3}$.

Assumption 1:

- a) The reference signal $y_d = x_{1d}(t)$, its velocity, and acceleration are bounded.
- b) The condition P_1 , P_2 , and $|P_L|$ sufficiently smaller than P_s is satisfied under a normal working condition in a real EHA system.
- c) There exist upper bounds for the matched (φ_1), unmatched disturbance (φ_2) and their derivatives $\dot{\varphi}_1, \dot{\varphi}_2$ such that they satisfy $|\varphi_i| \leq d_{im}, |\dot{\varphi}_i| \leq \Xi_i; i = 1, 2$, in which d_{im}, Ξ_i are positive constants.

Remark 3.1: The parameters w_a, w_b, p_a, p_b , and p_c are determined through the identification process which can be carried out on next sub-section. Meanwhile, k_t is computed from the servo valve's datasheet. Then, the physical parameters of the EHA system such as A, B, m, β_e, C_0 , and V_c can be achieved. The reader-interest can further find the details of several identification algorithms for the system parameters in [54-56].

Remark 3.2: Because of the impossible derivative of sign function, without loss of generality, the discontinuous term *sign* is replaced by a hyperbolic tangent function, namely, *tanh*. Besides, this hypothesis is to make the non-differentiable *sign* becoming continuously differentiable through *tanh* function and to support the control system design process [57], [51].

3.4 Experiment apparatus

The hardware of the hydraulic testbench is displayed in Figure 3.3. The EHA system comprises a double-rod cylinder (tube, rod diameter, and length of stroke, in turn, are 36, 12, and 35 mm), a servo valve (MOOG D633-317B), a hydraulic power unit (Kopack Engineering company), two pressure sensors (output 0~10 V, pressure range 0~300 bar), and displacement transducer (Rational WTB5-0500MM, displacement range 0~50 cm). Besides, an NI PCI-6014 card with an industrial computer was equipped. The setting parameters for the real EHA system are shown in Table 3.1.

To simulate the actuator fault in practice, a manual flow control valve was installed to connect two chambers of the symmetric cylinder. The internal leakage fault is generated by adjusting the manual valve, whilst a function block will be added after the control signal in Matlab/Simulink environment to cause the LOE fault.

Table 3.1 Setting parameters of the real EHA system

Components	Parameters	Specification
Double-rod cylinder	Tube diameter	36 [mm]
	Rod diameter	12 [mm]
	Length of stroke	25 [mm]
Servo valve	Model	MOOG – D633-317B
	Rated flow	10 [l/min]
Pressure sensor	Capacity	300 [bar]
	Rated output	30 [bar/V]
Displacement transducer	Model	Rational WTB5-0500MM
	Resolution	0.005mm
DAQ Card	Model	PCI-6014
	Resolution	AI/AO: 16 bit
Hydraulic Pump	Displacement	3.6 [cc/rev]
	Rated rotation speed	1730 [rpm]
	Relief pressure	160 [bar]

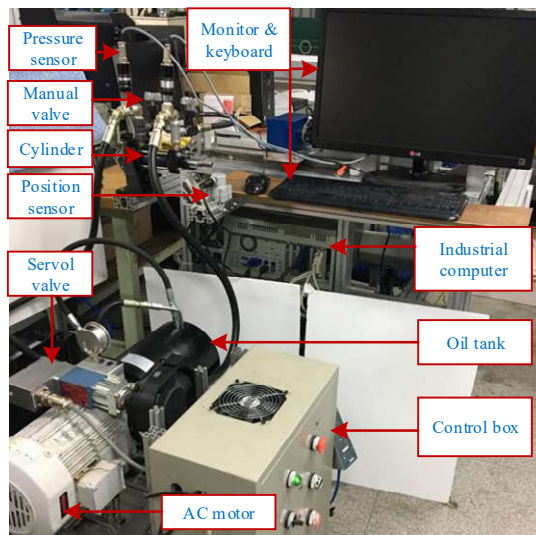


Figure 3.3 The experimental equipment of the EHA system.

Meanwhile, the setting parameters for the simulation EHA system are shown in Table 3.2 which is obtained via identification process. The following chapters will be developed based on the use of this EHA model approach in fault-tolerant control.

Table 3.2 Electro-hydraulic system parameters

Parameter	Symbol	Value	Unit
Oil bulk modulus	β_e	1.25×10^3	MPa
Proportional gain of valve	k_t	3.2×10^{-8}	$\text{m}^3/\text{s}/\text{V}/\text{Pa}^{-1/2}$
Viscous damping factor	B	450	Ns/m
Piston mass	m	4.5	kg
Effective area	A	4×10^{-4}	m^2
Supply pressure	P_s	16	MPa
Return pressure	P_r	0.1	MPa
Control volume	V_c	6×10^{-5}	m^3
Leakage coefficient	C_0	1.2×10^{-11}	m^5/Ns
Leakage fault coefficient	C_{f0}	1.4×10^{-10}	$\text{m}^4/(\text{N}^{1/2}\text{s})$
The rate of fault evolution	α	10	

CHAPTER 4

INTERNAL LEAKAGE FAULT-TOLERANT TRACKING CONTROL

4.1 Introduction

This chapter proposes a novel fault-tolerant controller for a double-rod EHA whilst the motion control system faces system disturbances/uncertainties and internal leakage fault. Firstly, taking advantage of the coordinate transformation, the nonlinear system is converted to a linear system to apply the control design tools in linear control theory. Besides, the matched, mismatched disturbances, and internal leakage fault are integrated into a new lumped uncertainty based on this transformation. Inspired by the great capability of time delay estimation technique, the suggested controller is developed to effectively detect and compensate for the internal leakage fault. To enhance the performance of the control system, an adaptive integral sliding mode control (AISMC) approach is deployed to effectively suppress the lump estimated error, and the effects of fault. The perfect combination of input-output feedback linearization (FBL), adaptive integral sliding mode, and time delay estimation is investigated to achieve high-precision tracking control and strong robustness in the presence of matched, mismatched disturbances, and faults, simultaneously. Moreover, the global stability of the suggested control algorithm is demonstrated by the Lyapunov theory. Finally, several tracking performance comparisons of the proposed approach with the existing controllers to demonstrate the efficiency are exhibited through simulation analyses and experiment results [58].

This chapter is organized as the following: In section 4.2, the system description of the EHA in the face of lumped disturbance and internal leakage fault is presented. Section 4.3 shows the fault detection (FD) method and develops a novel active FTC. Sections 4.4 and 4.5 discuss the simulation analyses and experiment results, respectively. Finally, the conclusions are summarized in Section 4.6.

4.2 Problem formulation

Choosing $x = [x_1, x_2, x_3]^T \triangleq [y, \dot{y}, P_L]^T$ as the state variables. As analysis in chapter 3, in case of the occurrence of the internal leakage fault, the total internal leakage is calculated by (3.8). The schematic model of the EHA under internal leakage fault (ILF) is shown in Figure 4.1. From (3.1)–(3.5) and (3.8), the EHA system can be established by the following third-order nonlinear state-space model:

$$\begin{cases} \dot{x}_1 = x_2, \\ \dot{x}_2 = f_2(x_2) + w_a x_3 + \varphi_1(x_1, x_2, t), \\ \dot{x}_3 = f_3(x_2, x_3) + w_b(x_3, u)u + \varphi_2(x_2, x_3, t), \end{cases} \quad (4.1)$$

where

$$w_a = \frac{A}{m}, f_2 = -\frac{B}{m}x_2, p_a = \frac{4\beta_e k_t}{V_c}, w_b = p_a \sqrt{P_s - x_3 \text{sign}(u)}, f_3 = -p_c x_3 - p_b x_2,$$

$\varphi_1 = \frac{\Lambda(\bullet)}{m}, \varphi_2 = \frac{4\beta_e}{V_c} (Q_{Li} - C_t \sqrt{|x_3|} \text{sign}(x_3))$, denote the unmatched, matched disturbances, respectively.

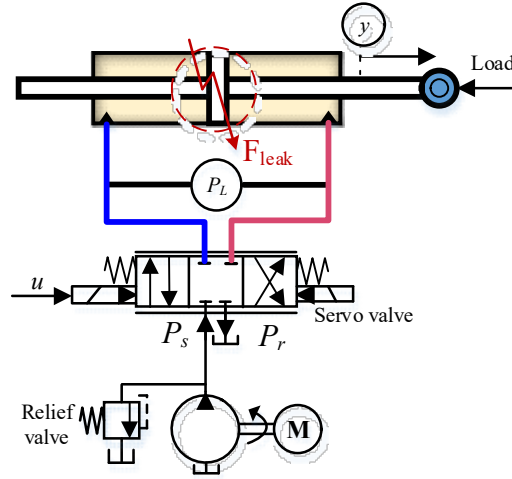


Figure 4.1 The schematic model of the EHA under ILF

Remark 4.1: The control objective is to design a controller u that drives the output y of the EHA to track the reference trajectory y_d , despite the external disturbance, model uncertainty, and actuator internal leakage fault. Motivated by the FDTDE and FBL, the novel FTC is developed such that the control objective for the nonlinear system (4.1) has been obtained.

4.3 Proposed control design for EHA

The overall structure of the proposed FTC is shown in Figure 4.2, which comprises three main steps. Firstly, the coordinate transformation using the Lie derivative is investigated in which the disturbance, uncertainty as well as fault are considered. Inspired by this transformation, the nonlinear characteristic of the system is eliminated. It is primary to apply the control design tools in linear control theory for the nonlinear object. Then, the TDE technique is developed to not only estimate matched and mismatched disturbance but also detect the fault. Finally, the tracking control law is achieved by the combination of a pole placement technique, adaptive integral sliding mode, and FDTDE. Although the simultaneously concerned faults, matched, and mismatched disturbance emerge in the EHA system, the proposed control scheme provides the system stability as well as a low steady-state error, and high precise control.

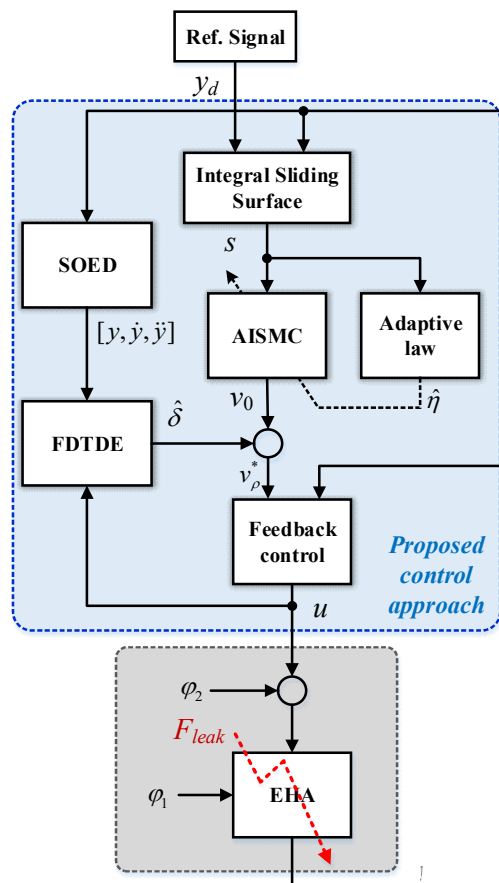


Figure 4.2 Structure of the proposed control scheme

4.3.1 Coordinate transformation and system model transformation

As above-mentioned, based on the differential geometry theory, a design procedure of coordinate transform is derived. For further convenience in designing the FBL, the nonlinear system (4.1) is rewritten as follows:

$$\begin{aligned}\dot{x} &= \phi(x) + \varphi(x)u + d(x, t), \\ y &= \xi(x),\end{aligned}\quad (4.2)$$

where $x \in R^m$, $u \in R^m$, $y \in R^m$ are state, control, and output vectors, respectively. $\phi = [x_2, f_2(x_2) + w_a x_3, f_3(x_2, x_3)]^T$, $\varphi = [0, 0, w_b(x_3, u)]^T$, and $\xi(x)$ are smooth functions. The lump disturbance is given by $d = [0, \varphi_1, \varphi_2]^T$. The Lie derivatives of the output ξ along the vector field $\phi(x)$ is denoted $L_\phi \xi(x)$. It can be calculated by using symbolic computation software or manual computation, and expressed by

$$L_\phi \xi(x) = \frac{\partial \xi(x)}{\partial x} \phi(x). \quad (4.3)$$

This notation can be used iteratively, that is

$$L_\phi^k \xi(x) = L_\phi L_\phi^{k-1} \xi(x) = \frac{\partial L_\phi^{k-1} \xi(x)}{\partial x} \phi(x), \quad (4.4)$$

where $k \geq 0$ is an integer with $L_\phi^0 \xi(x) = \xi(x)$

Definition 1: The system (4.2) has a relative degree ρ if the following conditions are satisfied [59]:

$$\begin{aligned}L_\phi L_\phi^k \xi(x) &= 0, \quad \text{for } k = 0, \dots, \rho - 2 \\ L_\phi L_\phi^{\rho-1} \xi(x) &\neq 0,\end{aligned}\quad (4.5)$$

With the definition of relative degree ρ , the system can be considered as full state feedback linearizable, if the system has a well-defined relative degree ρ which equals the system order. The change of coordinate is described by

$$\psi_i = \xi^{(i-1)}, i = \overline{1, \rho}. \quad (4.6)$$

Then, the exact input-output FBL is obtained, and the ρ^{th} derivation of output y can be expressed as [59]:

$$y^{(\rho)} = v_\rho = L_\phi^\rho \xi + L_\phi L_\phi^{\rho-1} \xi u. \quad (4.7)$$

By applying the FBL technique for the EHA system, the relative degree is firstly determined. Then, the original nonlinear system (4.2) taking into account the perturbation model can be changed into an integral chain pseudo linear system model with composite disturbance as follows:

$$\psi = \begin{bmatrix} \psi_1 \\ \psi_2 \\ \psi_3 \end{bmatrix} = \begin{bmatrix} y \\ \dot{y} \\ \ddot{y} \end{bmatrix} = \begin{bmatrix} \xi \\ L_\phi \xi + L_d \xi \\ L_\phi^2 \xi + L_d L_\phi \xi + \frac{d}{dt}(L_d \xi) \end{bmatrix}. \quad (4.8)$$

Then, the derivative of (4.8) is described by

$$\dot{\psi} = \begin{bmatrix} \dot{\psi}_1 \\ \dot{\psi}_2 \\ \dot{\psi}_3 \end{bmatrix} = \begin{bmatrix} \dot{y} \\ \ddot{y} \\ \ddot{y} \end{bmatrix} = \begin{bmatrix} \dot{y} \\ \ddot{y} \\ v_\rho + \delta \end{bmatrix}, \quad (4.9)$$

where $v_\rho = L_\phi^3 \xi + L_\phi L_\phi^2 \xi u$, $\delta = L_d L_\phi^2 \xi + \frac{d}{dt}(L_d L_\phi \xi) + \frac{d^2}{dt^2}(L_d \xi)$. Herein, v_ρ and δ denote a new input variable and a new lumped disturbance, respectively.

To simplify the notations, (4.9) can be rewritten by

$$\dot{\psi} = A\psi + Bv_\rho + \Omega, \quad (4.10)$$

where $A = \begin{bmatrix} 0 & 1 & 0 \\ 0 & 0 & 1 \\ 0 & 0 & 0 \end{bmatrix}$, $B = \begin{bmatrix} 0 \\ 0 \\ 1 \end{bmatrix}$, $\Omega = \begin{bmatrix} 0 \\ 0 \\ \delta \end{bmatrix}$.

Remark 4.2: The coordinate transformation converts the original system (4.1) to the equivalent linear system (4.10) in which the mismatched disturbance, matched disturbance (i.e., external load, parametric uncertainty), and fault are integrated into the new lumped disturbance. The benefit of this technique makes the initial complex system becoming simple and easy to implement control design procedures.

Remark 4.3: It is noted that the variable ψ is derived from the output signal y . Herein, the only available position sensor based on the displacement transducer information, $y = x_1$ can be measured. Nevertheless, in the control design procedure, other states such as the velocity and

acceleration need to be known. To obtain the information of the velocity and acceleration, a second-order exact differentiation (SOED) [60], [61] is employed as follows:

$$\begin{aligned}
\dot{\chi}_0 &= w_0 \\
w_0 &= -a_1 |\chi_0 - x_1|^{2/3} \text{sign}(\chi_0 - x_1) + \chi_1 \\
\dot{\chi}_1 &= w_1 \\
w_1 &= -a_2 |\chi_1 - w_0|^{2/3} \text{sign}(\chi_1 - w_0) + \chi_2 \\
\dot{\chi}_2 &= -a_3 \text{sign}(\chi_2 - w_1)
\end{aligned} \tag{4.11}$$

where a_1 , a_2 , and a_3 are chosen as suitable positive parameters.

Then, the estimation of velocity and acceleration can be reached as

$$\chi_1 = \dot{y}, \chi_2 = \ddot{y}. \tag{4.12}$$

4.3.2 Fault detection and identification using time delay estimation

After obtaining the new linear model, in order to effectively reduce the effect of disturbance/uncertainty as well as faults, the time delay estimation is proposed to estimate the new lumped disturbance. Then, robust FTC considering the FDTDE result can be investigated to compensate for the influence of the lumped disturbance and faults in the EHA system.

From (4.10), at time t , the new lumped disturbance is given by the following.

$$\Omega(t) = \dot{\psi}(t) - A\psi(t) - Bv_p(t) \tag{4.13}$$

Hence, the TDE technique is used to determine $\Omega(t)$ through $\Omega(t-t_d)$ that can be expressed as

$$\hat{\Omega} = \Omega(t-t_d) = \dot{\psi}(t-t_d) - A\psi(t-t_d) - Bv_p(t-t_d) \tag{4.14}$$

where t_d is the estimation time-delay. Mostly, t_d is the sampling time interval and $\hat{\Omega} = [0 \ 0 \ \hat{\delta}]^T$ is the estimated value of Ω .

The equation (4.14) indicates that the lumped disturbance can be formulated from the known dynamics of the linearized system and control input.

It is noted that the new lumped uncertainty includes lumped disturbance f_d (i.e., matched disturbance and mismatched disturbance) and fault φ_f . The estimated new lumped uncertainty can be re-expressed as

$$\hat{\Omega} = \hat{f}_d + \hat{\varphi}_f = f_d(t-t_d) + \varphi_f(t-t_d) \quad (4.15)$$

To realize the detection system fault process, a threshold μ is determined through conducting experiments under healthy and faulty conditions. In the case of the absence of the internal leakage fault, following (3.9), $\varphi_f = 0$ when $t < T_m$. Then, according to (4.15), one obtains

$$\hat{\Omega} = f_d(t) \leq \mu \quad (4.16)$$

Inspired by the FDTDE, relying on the predefined threshold value, the fault is detected immediately when $\hat{\Omega} > \mu$. In practice, to determine the threshold, the control system without fault is firstly tested to evaluate the limitations as well as the influence of the matched and mismatched terms f_d . Then, the threshold is selected bigger than the upper bound of f_d . It is concluded that the FDe system guarantees sensitive to the leakage fault, however, it also suppresses the impact of lumped uncertainty of the system.

4.3.3 Control law design

In this sub-section, the combining of the FBL, TDE, and AISMC is investigated to not only enhance the tracking control accuracy but also achieve system stability in the presence of disturbances/uncertainties and actuator faults. Input-output feedback linearization is developed to alleviate the nonlinearity of the system. Then, the ISMC is applied to reduce steady-state error and pursue the finite-time stability for the EHA. The robustness of the controller is enhanced to against the appearance of fault and the TDE error with the assist of the adaptation gain parameter. Moreover, the new lumped disturbance is approximated by the FDTDE technique. It is efficiently compensated through the proposed control algorithm and helpfully improves the tracking performance. The stability of the whole system is verified using the Lyapunov method.

The tracking errors of the linearized system are defined as

$$e_{\psi_i} = \psi_{id} - \psi_i, \quad i = \overline{1,3} \quad (4.17)$$

where $\psi_d = [\psi_{1d} \quad \psi_{2d} \quad \psi_{3d}]^T = [y_d \quad \dot{y}_d \quad \ddot{y}_d]^T$ is the desired trajectory.

The error dynamics are formulated as follows:

$$\begin{aligned}
\dot{e}_{\psi_1} &= e_{\psi_2} \\
\dot{e}_{\psi_2} &= e_{\psi_3} \\
\dot{e}_{\psi_3} &= \dot{\psi}_{3d} - (v_\rho + \delta)
\end{aligned} \tag{4.18}$$

The sliding mode control law is established to secure that the tracking error in (4.18) converges to zero. The sliding manifold is designed as

$$s = k_0 \int_0^t e_{\psi_1} d\tau + k_1 e_{\psi_1} + k_2 e_{\psi_2} + e_{\psi_3} \tag{4.19}$$

where k_0 , k_1 , and k_2 are positive constant; the integral component is supplemented to degrade the steady-state error, and these control gains are selected, in such a way, that the ideal conditions $s = 0$, and $\dot{s} = 0$ are satisfied.

To receive a good dynamic process, the gain parameters can be figured out by following the pole placement method.

$$p_s = (p + \varpi)^3 = p^3 + 3\varpi p^2 + 3\varpi^2 p + \varpi^3 \tag{4.20}$$

where p is Laplace operator, ϖ is a positive constant.

Hence, the poles are p_1 , p_2 , p_3 that lie in the left-half plane. So, (4.20) is a Hurwitz polynomial. The gain parameters are computed as follows:

$$k_0 = \varpi^3, k_1 = 3\varpi^2, k_2 = 3\varpi \tag{4.21}$$

The derivative of s can be represented as

$$\begin{aligned}
\dot{s} &= k_0 e_{\psi_1} + k_1 \dot{e}_{\psi_1} + k_2 \dot{e}_{\psi_2} + k_3 \dot{e}_{\psi_3} \\
&= k_0 e_{\psi_1} + k_1 e_{\psi_2} + k_2 e_{\psi_3} + \dot{\psi}_{3d} - (v_\rho + \delta)
\end{aligned} \tag{4.22}$$

To stabilize the system (4.10), with the estimated lumped uncertainty and fault in (4.15), the auxiliary control law is designed as follows:

$$v_\rho^* = \underbrace{v_{com} + v_{rob} + v_z}_{v_0} + v_{ide} \tag{4.23}$$

where v_{com} is a dynamics compensation term, v_{rob} is a robust term that is used to alleviate the estimation error, v_z helps the sliding surface from an arbitrary place back to the vicinity of zero, and v_{ide} is a lumped compensation term that is obtained by using TDE. These designs are given as follows:

$$\begin{aligned} v_{com} &= \dot{\psi}_{3d} + k_0 e_{\psi_1} + k_1 e_{\psi_2} + k_2 e_{\psi_3}; \\ v_{ide} &= -\hat{\delta}; v_z = k_s s; v_{rob} = \eta \text{sign}(s). \end{aligned} \quad (4.24)$$

where k_s, η are positive constants, and $\dot{\psi}_{3d} = \ddot{y}_d$.

Denotes $\tilde{\delta} = \delta - \hat{\delta}$ that is the estimation error of the lumped disturbance term.

Assumption 4.1: The boundedness of the time-delay estimation error $\tilde{\delta}$ is defined by D . This hypothesis has been verified in [12], [62] with a sufficiently small time delay t_d .

The robust gain η is investigated to cope with the occurrence of fault and the TDE error. To promote the robustness feature of the controller, the adaptive gain algorithm is developed. Hence, the robust component can be modified by

$$v_{rob} = \hat{\eta} \text{sign}(s) \quad (4.25)$$

where $\hat{\eta}$ is the adapt value of the gain η .

The effective gain adaption is given by

$$\dot{\hat{\eta}} = \Gamma^{-1} |s| \quad (4.26)$$

where Γ is a positive adaption parameter.

The feedback control law is constructed as follows:

$$u = \frac{1}{L_\varphi L_\phi^2 \xi} (v_\rho^* - L_\phi^3 \xi) \quad (4.27)$$

Theorem 4.1: Considering the system (4.1) satisfying Assumption 1, with the TDE in (4.14), if the control input signal is proposed as (4.27) together with the auxiliary control law (4.23), the adaptive law (4.26) that does not only guarantee the stability of the whole system but also retain acceptable tracking control in the event of faulty conditions, matched and mismatched disturbance.

Proof:

Let consider the candidate Lyapunov function

$$V = \frac{1}{2} s^2 + \frac{1}{2} \Gamma (\hat{\eta} - D)^2 \quad (4.28)$$

Taking the time derivative of V with noting (4.24), (4.26), one obtains

$$\begin{aligned}
\dot{V} &= s\dot{s} + \Gamma(\hat{\eta} - D)\dot{\hat{\eta}} \\
&= s(k_0 e_{\psi_1} + k_1 e_{\psi_2} + k_2 e_{\psi_3} + \dot{\psi}_{3d} - (v + \delta)) + \Gamma(\hat{\eta} - D)\dot{\hat{\eta}} \\
&= s(-k_s s - \hat{\eta} \text{sign}(s) - \tilde{\delta}) + \Gamma(\hat{\eta} - D)\dot{\hat{\eta}} \\
&= -k_s s^2 - (\hat{\eta} - D)(|s| - \Gamma \dot{\hat{\eta}}) - |s|(\tilde{\delta} \text{sign}(s) + D) \\
&\leq -k_s s^2
\end{aligned} \tag{4.29}$$

Then, the derivative of Lyapunov function \dot{V} is negative semidefinite which shows that s will converge to zero in a certain time, and $e_{\psi_i} \rightarrow 0$ as $t \rightarrow \infty$. Thus, it can be concluded that the stabilization of the closed-loop system can be achieved according to Lyapunov criteria [63]. Theorem 4.1 is proved.

Remark 4.4: To eliminate the chattering phenomenon, the saturation function $\text{sat}(\bullet)$ is utilized to replace the $\text{sign}(\bullet)$ function in (4.25) as [12]

$$\text{sat}\left(\frac{s}{\varepsilon}\right) = \begin{cases} \text{sign}(s) & \text{if } |s| \geq \varepsilon \\ \frac{s}{\varepsilon} & \text{otherwise} \end{cases} \tag{4.30}$$

where ε is a small and positive coefficient.

Remark 4.5: To avoid the continuous increase of the adaptive gain in (4.26), some tips, e.g., dead-zone technique is developed to ensure the feasibility in practice as follows [46]:

$$\dot{\hat{\eta}} = \begin{cases} \Gamma^{-1}|s| & \text{if } |s| > \varepsilon_d \\ 0 & \text{otherwise} \end{cases} \tag{4.31}$$

where ε_d is a small positive scalar.

Remark 4.6: From the developed control law, the guidelines to select the parameters are given as follows:

- 1) For fault detection, the threshold μ is carefully selected which is the boundness of the matched and mismatched terms f_d .
- 2) For control module, a pole placement technique is used to select the desired pole ϖ . Next, the gain parameters k_0, k_1, k_2 of the sliding manifold are determined via (4.21). Then, the gain k_s is tuned to approach the switching manifolds faster. Lastly, the parameter adaptation rate Γ is increased gradually to guarantee the convergence of the adaptive parameter. In addition, the

effects on the system behavior will be evaluated by trial and error through simulation analysis and experimental tests.

4.4 Simulation results

4.4.1 Simulation setup

In this part, the effectiveness of the proposed controller is demonstrated through numerical simulation and experiments using MATLAB Simulink software. The sampling time is set as $0.005s$ and the simulation time is chosen as $T = 30s$. The setting parameters for the simulation EHA system are shown in Table 3.2. For the purpose of comparison, the desired input signal is selected as $q_d = 20\sin(0.2\pi t - \pi/2)$ (mm).

To evaluate the improved performance of the suggested FTC, i.e., adaptive integral sliding mode feedback linearization controller using FDTDE, a PID controller, and a backstepping controller with TDE (BCTDE), in turn, have been derived for the EHA as a comparison. The following control gain of the controllers are tuned via the trial error method or based on the trade-off between the convergence speed and oscillatory and shown as: BCTDE $k_{b1} = 15$, $k_{b2} = 100$, $k_{b3} = 20$; proposed controller $\varpi = 40$, $k_s = 5.5$, $\Gamma = 80$. The selection of threshold value is set as $\mu = 150$ in simulation. In the different control scheme, PID controller is tuned by Ziegler-Nichols method with $K_p = 120$, $K_i = 20$, $K_d = 0.001$.

For the sake measurement of the quality of each control algorithm, the root mean square (RMS) error (index 1) or control effort (index 2) is computed as follows:

$$RMS = \sqrt{\frac{1}{N} \sum_{i=1}^n z_i^2} \quad (4.32)$$

where i and n are the current and total of sample number, respectively; z_i is the interested index for the current sample. The index 1 (mm) shows the tracking accuracy whilst the index 2 (V) evaluates the control effort.

In order to show the superior properties of the proposed control in case of the appearance of fault, two working scenarios are considered as

- 1) Both matched and mismatched disturbances, and without fault.
- 2) Simultaneous abrupt internal leakage fault, matched, and mismatched disturbances.

4.4.2 Simulation result

The effectiveness of the FDTDE is first validated for detection and identification of the internal leakage fault in the simulation. As the above-mentioned analysis, the matched, mismatched, and fault is integrated into the new lumped uncertainty through the coordinate transformation. Then, the FDTDE is applied to exactly estimate it. The estimation results in the absence of fault are displayed in Figure 4.3a. From Figure 4.3a, we can see that the FDTDE brings a high accuracy estimation. And the selection threshold preserves the boundness of the new lumped uncertainty under healthy conditions. A fault is subsequently generated with internal leakage coefficient $C_{l0} = 2.5 \times 10^{-8} \text{ m}^4 / (\text{N}^{1/2} \text{ s})$. When the fault happens at the time $t = 6\text{s}$, the estimated lumped uncertainty overshoots the predetermined threshold. The response of the residual in the occurrence of the fault is depicted in Figure 4.3b. From this figure, in the presence of the fault, it is clear that the fault has been successfully detected and accurately estimated thanks to the FDTDE.

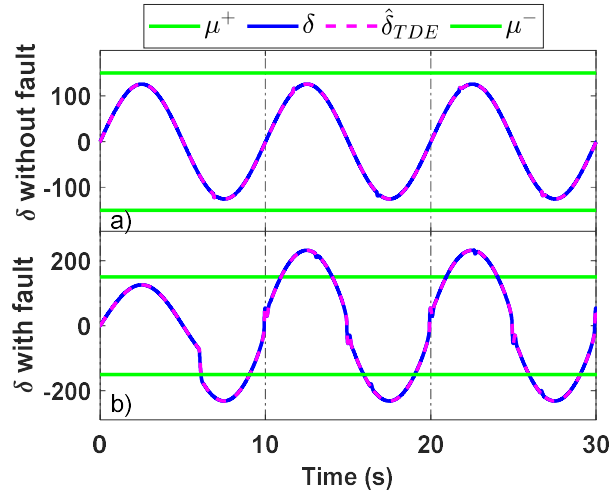


Figure 4.3 Lumped disturbance estimation in simulation: a) without fault, b) Abrupt fault

1) Scenario 1

In this working scenario, the system operates in healthy condition, the fault does not occur. Meanwhile, there exists the matched and mismatched disturbance, the FDTDE is used to approximate the uncertainty component. We investigate the performance comparison of the proposed FTC with the PID and BCTDE. Comparisons of three controllers including the tracking position, the error state, and the control input are shown in Figure 4.4. As can be seen

in Figure 4.4, due to the assistance of the TDE, the lumped uncertainty is compensated. Except for PID, the relevant methods have no significant differences, the response is still ensured with small errors. It is observed that the performance of the PID controller was worse in the presence of the lumped uncertainty due to the lack of uncertainty compensation. The BCTDE has a larger tracking error than the proposed controller because of non-possession a robustness term to tackle the certain estimation error of the TDE. Furthermore, from the performance indices in Table 4.1, the PID, BCTDE, and proposed controllers lead to the RMS errors of 0.6031, 0.041, and 0.0229 *mm*, respectively. Whilst the three controllers consume the RMS control efforts of 1.4671, 1.4464, and 1.3527 *V*, respectively. Evidently, the suggested controller complementing the adaptive gain and integral term yields the best performance with minimum tracking error and the requirement of the lowest control effort.

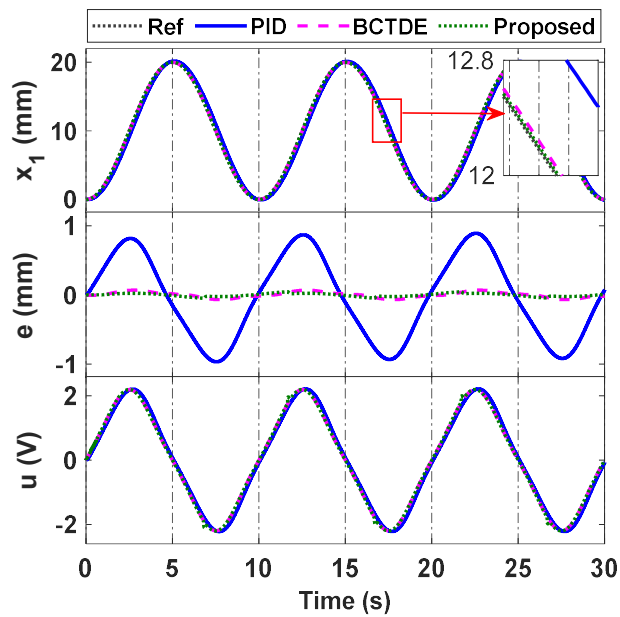


Figure 4.4 Performances of three controllers in simulation, scenario 1

2) Scenario 2

In order to verify the robustness of the proposed controller, the abrupt internal leakage fault is augmented as a partial loss of effectiveness. It is noteworthy that the fault changes from slight to abrupt depending on the evolution rate and the internal leakage coefficient [40], however, the abrupt fault is only presented in this article. So, the internal leakage coefficient is chosen as $C_{l0} = 2.5 \times 10^{-8} m^4 / (N^{1/2} s)$ to indicate the influence of the internal leakage fault and

the time of the occurrence fault is 6s. The transient responses of the output position, the error state, and the control input, in turn, are illustrated in Figure 4.5. It can be seen that the control effort of relevant controllers is significantly changed to against both disturbance and the fault at the time 6s. On the other hand, the comprise of adaptive gain and TDE upgrades the effectiveness of the suggested methodology which is visibly evident from the error state plot. Hence, we can see that the proposed FTC provided better performance than the BCTDE and PID despite the addition of internal leakage fault. The RMS error and the effort of signal control of three controllers in the simulation are shown in Table 4.1 that again confirmed the effectiveness of the proposed FTC.

Table 4.1 Performance indices of three controllers in simulation.

	Controller	PID	BCTDE	Proposed
Scenario 1	Index 1	0.6031	0.0410	0.0229
	Index 2	1.4671	1.4464	1.3527
Scenario 2	Index 1	0.8301	0.3812	0.1824
	Index 2	2.0179	1.9940	1.9776

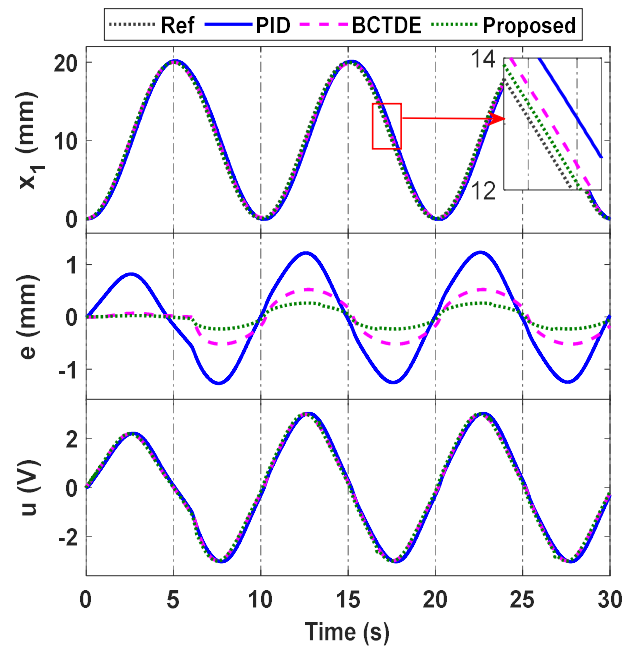


Figure 4.5. Performances of three controllers in simulation, scenario 2

4.5 Experimental verification

The experiment setup is depicted in Chapter 3, Figure 3.3. The artificial internal leakage fault is generated through a manual flow control valve that connects two chambers of the hydraulic cylinder. The threat level of the fault depends on the range adjustment of the flow control valve. Considering the mechanical limitation of the length of the cylinder stroke, the reference trajectory is chosen as $q_d = 20\sin(0.6\pi t - \pi/2)$ (mm). In the experiment, all the parameters of the EHA system, as well as the control gains, are set similar to the corresponding values in simulation.

The sequent implementation experimental is the same as in simulation. The experiment results are shown in Figures. 4.6 – 4.10. First of all, the effectiveness of the FDTDE is confirmed and the threshold value is again determined for suitable in practice, $\mu = 2 \times 10^3$ in Figure 4.6a. When the flow control valve is adjusted to create the internal leakage fault at the time $t = 12s$, the lumped estimation including matched, mismatched disturbance, and fault, is larger than the threshold. The fault is successfully detected in Figure 4.6b. Next, two experiment scenarios are exploited corresponding to with and without the appearance of fault.

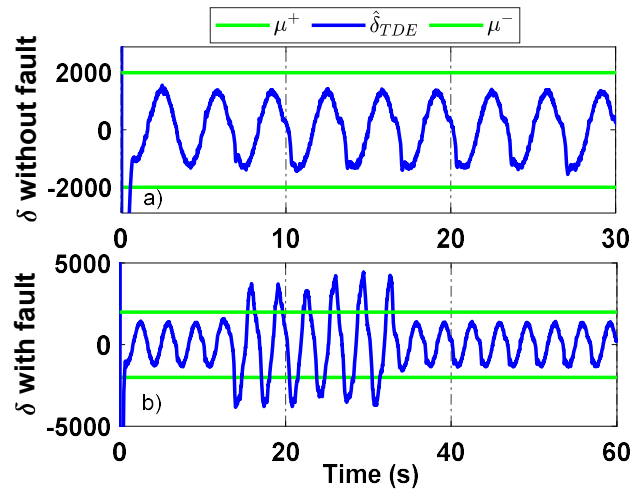


Figure 4.6. Lumped disturbance estimation in experiment: a) without fault, b) Abrupt fault.

1) Scenario 1

This working scenario considers the situation that there are matched and mismatched disturbance from the EHA system whilst a fault doesn't appear. The corresponding experimental results of scenario 1 are depicted in Figure 4.7. It is obvious that the traditional

PID controller presents large errors in the presence of lumped uncertainties. Although the lumped uncertainties are compensated by the TDE, the BCTDE is still poorer than the suggested controller because of not belonging any measure to treat the undesired estimation error as well as the deviation in the parameter identification method for the EHA system. In contrast, the proposed controller provides a significant improvement of the performance due to the robustness properties of the adaptive law as well as the ISMC technique to alleviate the estimation error. The performance indices of the comparative controllers are calculated from $t = 10$ s and described in Table 4.2. It can be seen that the tracking accuracy of the proposed controller has been improved by 57% and 54% over PID and BCTDE methods, respectively. The result of data analysis proves the superior properties of the proposed control compared to the remaining controllers. Figure 4.8 illustrates the velocity and acceleration estimation via the constructed SEOD. As shown, the information via the SOED can be given by differential and filtering, which facilitates the control design procedure of the proposed controller.

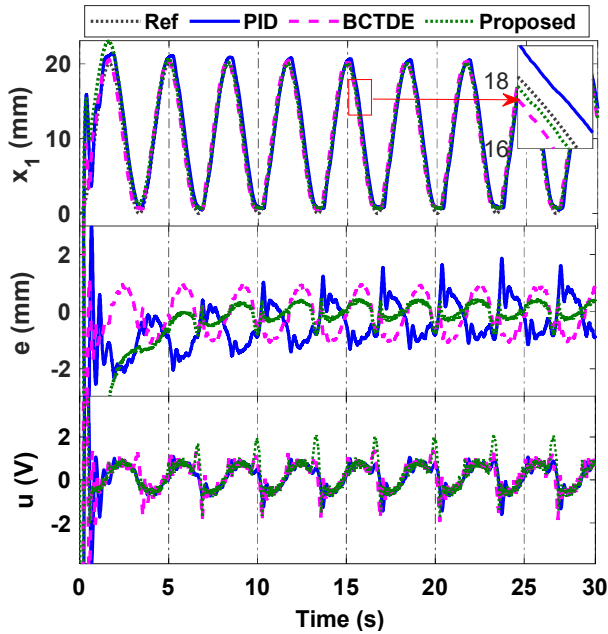


Figure 4.7 Performances of three controllers in experiment, scenario 1

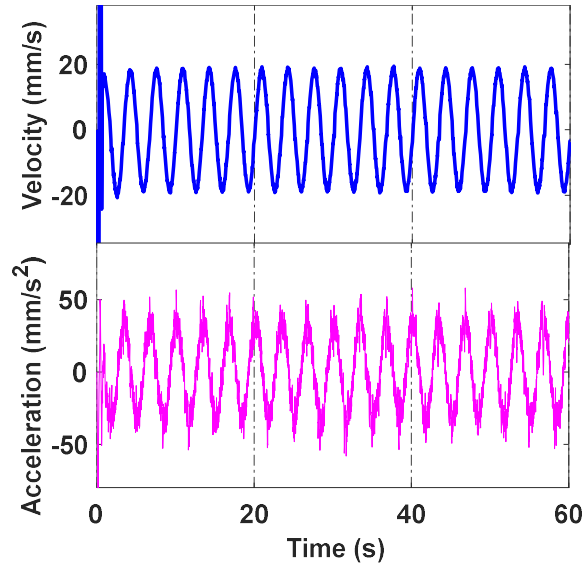


Figure 4.8 Estimated velocity and acceleration of SEOD in experiment.

2) Scenario 2

In the experiment of scenario 2, the robustness of the suggested method is validated under the matched, mismatched and internal leakage fault. The abrupt fault is generated by the manual flow control valve. Because of the serious damage and safety problem in the appearance of the fault, the fault experiment is implemented from 12s to 33s. The experiment results are shown in Figure 4.9. As seen in this figure, the control performance of the PID and BCTDE became much worse in the heavy fault condition. The control effort and the error state significantly increase at the time $t = 12s$. These results are explained by the insufficient compensation of relevant controllers against the abrupt fault. Meanwhile, due to the robust FTC scheme, a great improvement was achieved by taking advantage of the integration of TDE into the integral sliding mode, FBL technique, and adaptable property. The efficiency of comparative controllers is evaluated through RMS error in Table 4.2. The RMS tracking errors of PID, BCTDE, suggested controller, in turn, are obtained as 1.791, 0.977 and 0.3597 mm. In addition, RMS control efforts are calculated as 1.7329, 1.6639, and 1.6020 V, respectively. It reveals that the outstanding efficiency of the proposed control algorithm once again is confirmed in case of the occurrence of faults.

Furthermore, the responses of the adaptive gains for two working scenarios are illustrated in Figure 4.10. It can be observed from Figure 4.10 that this parameter is adapted to

suppress the effects on the appearance of fault and TDE error. Since the fault occurs at time $t = 12s$, the adaption gain, ie, $\hat{\eta}$ will be significantly regulated to approximate the value η , and then, to further enhance the tracking performance.

Therefore, the simulation and experiment results indicate that the suggested fault-tolerant controller can be applied for EHA and exhibits the best performance despite the matched, mismatched disturbances, and internal leakage fault.

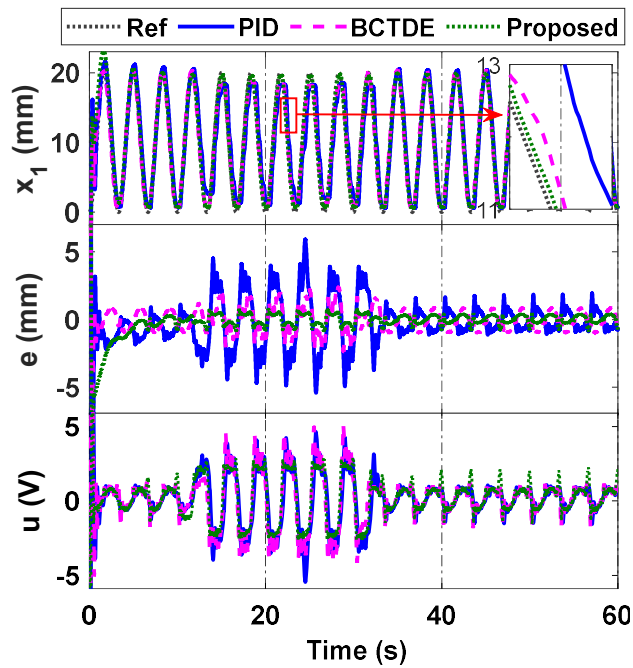


Figure 4.9 Performances of three controllers in experiment, scenario 2

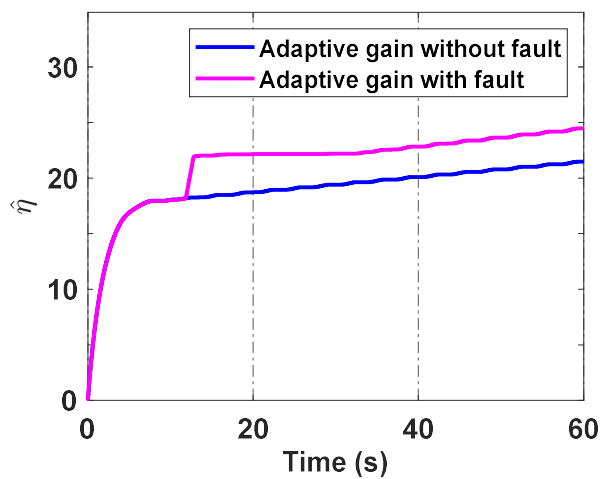


Figure 4.10. Adaptive gain in experiment

Table 4.2 Performance indices of three controllers in experiment.

	Controller	PID	BC-TDE	Proposed
Scenario 1	Index 1	0.7118	0.6794	0.3062
	Index 2	0.7238	0.7004	0.6955
Scenario 2	Index 1	1.7910	0.9770	0.3597
	Index 2	1.7329	1.6639	1.6020

4.6 Chapter summary

On the premise of the synthesis of adaptive integral sliding mode, feedback linearization technique, and time delay estimation, the proposed FTC scheme has been investigated in this chapter. Firstly, the descriptor of the EHA system in presence of matched, mismatched disturbance, and internal leakage fault is established. Then, we linearize the nonlinear EHA system by using the coordinate transformation. Next, the new lumped disturbance including disturbance/uncertainty, and the concerned fault is estimated by the assist of the TDE. Moreover, the TDE-based fault detection is developed. Lastly, the incorporation of adaptive integral sliding mode-based feedback linearization technology and TDE is proposed to guarantee high precision tracking control and maintain the stability system in spite of disturbances as well as faults. The Lyapunov approach is used to verify the stability of the closed-loop system. The simulation analyses and experiment results have demonstrated the efficiency of the suggested methodology.

CHAPTER 5

ACTUATOR FAULT-TOLERANT TRACKING CONTROL WITH BIAS AND LOSS OF EFFECTIVENESS FAULT

5.1. Introduction

Due to their outstanding features, electro-hydraulic actuators (EHAs) have been widely deployed in modern industries, i.e., aerospace and construction fields. Specifically, the position/force tracking control problem for these applications has mainly been focused on developing [1, 64, 65]. However, there exist different factors against the control performance as well as the system stability, i.e., disturbances, uncertainties, nonlinearities, and some malfunctions [66], [67]. On the other hand, the practical EHA system regularly copes with output constraints in the type of physical limitations, performance specifications, and safety bounds in the position tracking control tasks [68]. Therefore, it is of significant challenge to obtain good tracking qualifications for the EHA system in the presence of these above disadvantages.

In this chapter, the design and experimental evaluation of a fault-tolerant controller are introduced for a double-rod EHA subjected to actuator faults and disturbances. The internal leakage fault is captured as a bias fault, whilst the faults in servo-valve and supply failure are considered as a partial loss of effectiveness (LOE) fault. The design obstacles caused by the disturbances and bias fault are suppressed by nonlinear disturbance observers (NDO) while an asymmetric barrier Lyapunov function is used to ensure the non-violated boundary of the output position. To tackle the LOE fault, the development of an enhanced adaptive compensation technique for actuator fault-tolerant control (FTC) is then constructed. Moreover, to mitigate the “explosion of complexity” in the traditional backstepping design, the command-filtered control is utilized to elaborate the FTC scheme. It is shown by theoretical analysis that system stability is ensured under faulty conditions. Finally, simulation/experiment results and comparison studies are performed to further verify the effectiveness of the proposed approach.

This chapter is arranged as follows: In section 5.2, the mathematical model of the EHA is given which includes the problem statements and some lemmas. The proposed FTC consists of the nominal controller and reconfigurable controller that is presented in section 5.3. Sections 5.4 and 5.5 show the numerical simulation and experiment studies, respectively. Finally, the conclusions and future works are discussed in Section 5.6.

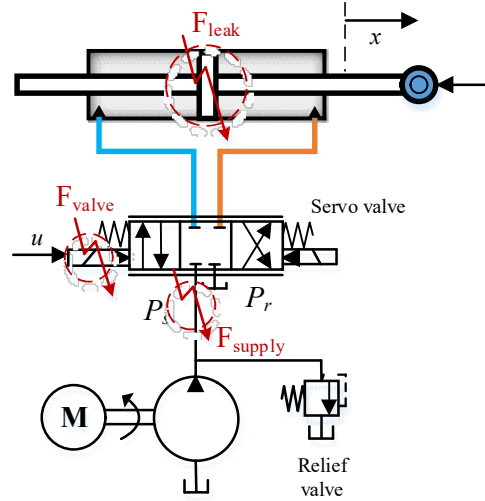


Figure 5.1 Schematic of the electro-hydraulic actuator with actuator faults

5.2 Problem description

The schematic diagram of the EHA with actuator faults is shown in Figure 5.1. Three main faults of the hydraulic-driven actuator are studied: 1) drop in supply pressure of a hydraulic power supply (F_{supply}); 2) fault in a servo-valve (F_{valve}); and 3) internal leakage fault (F_{leak}), which can be classified into two types of actuator fault: bias fault and LOE fault.

From (3.8) and (3.10), actuator fault includes the partial LOE or the bias fault which can be formulated as follows:

$$u_f = \nu u + \zeta, \nu \in (0,1) \quad (5.1)$$

where $\zeta = -\frac{4\beta_e C_t}{g_3 V_c} \sqrt{|P_L|} \text{sign}(P_L)$, g_3 will be denoted latter.

Choosing $x = [x_1, x_2, x_3]^T \triangleq [y, \dot{y}, w_a P_L]^T$ as the state variables. From (3.1)–(3.5) and (5.1), the EHA system can be established by the following third-order nonlinear state-space model:

$$\begin{cases} \dot{x}_1 = x_2, \\ \dot{x}_2 = f_2 + x_3 + \varphi_1, \\ \dot{x}_3 = \varphi_3(x_2, x_3) + g_3(x_3, u)vu + \varphi_2(x_3, t), \end{cases} \quad (5.2)$$

where

$$w_a = \frac{A}{m}, f_2 = -\frac{B}{m}x_2, p_a = \frac{4\beta_e k_t}{V_c}, \varphi_3 = -\frac{4\beta_e C_0}{V_c}x_3 - \frac{4\beta_e A^2}{mV_c}x_2, g_3 = \frac{4A\beta_e k_t}{mV_c} \sqrt{P_s - \frac{m}{A}x_3 \text{sign}(u)},$$

$$\varphi_1 = \frac{\Lambda(\bullet)}{m}, \varphi_2 = \frac{4A\beta_e}{mV_c} Q_{Li} + g_3 \zeta, \text{ denote the unmatched, matched disturbances, respectively.}$$

Lemma 5.1 [69]: There exists any positive constant $\varepsilon_g \in R$, for $\forall x_a \in R$ satisfying $|x_a| < \varepsilon_g$; the following inequality holds

$$\log \frac{\varepsilon_g^2}{\varepsilon_g^2 - x_a^2} \leq \frac{x_a^2}{\varepsilon_g^2 - x_a^2}. \quad (5.3)$$

Lemma 5.2 [70]: For any scalar positive function $\sigma(t): [0, \infty] \rightarrow R^+$, the following inequality holds

$$\left| z \right| - \frac{z^2}{\sqrt{z^2 + \sigma(t)}} < \sqrt{\sigma(t)}, \quad \forall z \in R. \quad (5.4)$$

Lemma 5.3 [71]: For a time-varying positive function $L_f(t) \geq 0, \forall t \in [0, \infty]$ and $L_f(0)$ bounded. If the following inequality holds

$$\dot{L}_f \leq -aL_f + b, \quad (5.5)$$

where a and b are two positive constants, then it can be concluded that $L_f(t)$ will lie in a bounded region ($L_f(t) \leq b/a$ when $t \rightarrow \infty$).

Remark 5.1: For practical EHA systems, they appear constrained motions caused by narrow space, precision machining, performance specifications, or rescue tasks. We suppose that the output position x_1 of the EHA is required to satisfy

$$y_l(t) < x_1(t) < y_u(t), \quad \forall t \geq 0, \quad (5.6)$$

where y_l and y_u define lower and upper bounds of the desirable safe working range.

Remark 5.2: The control objective is to synthesize a control signal u such that the output position x_1 tracks the desired trajectory x_{1d} to a bounded compact set, in the face of the lumped

disturbances and actuator faults. Inspired by the CFC, NDO, and reconstruction of the last virtual control law, the proposed FTC is developed to obtain the system stability and acceptable performance specifications for the plant (5.2)

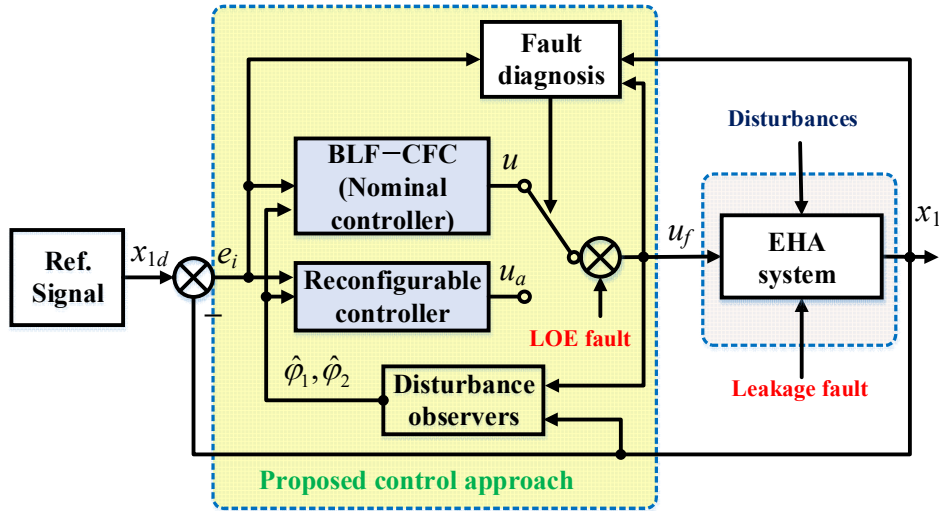


Figure 5.2 Sketch of the proposed control approach

5.3 FTC design and stability analysis

The structure of the proposed controller is illustrated in Figure 5.2, which consists of three main parts: DO, fault diagnosis (FD) scheme, and main FTC controller. By considering the lumped disturbances and the bias fault as lumped uncertainties, two DOs are designed to handle their impacts. Then, the FD including fault detection and identification is investigated to diagnose the LOE fault. There are two components in the main FTC controller. A nominal controller is first constructed to solve the impacts of negative factors on a system, such as lumped disturbances, uncertainties, and bias fault. Meanwhile, the reconfigurable controller is developed to cope with the influences of LOE fault that can be active based on the fault information from FD. The FTC is proposed by combining the NDO, FD, and nominal/reconfigurable controller such that the output position does not violate the expected bounds and all signal states are bounded.

5.3.1 Nominal control design

The nonlinear system (5.2) without LOE fault ($\nu = 1$) is first considered. Consequently, the control design procedure for the nominal controller is presented in this subsection.

The error states are defined as follows:

$$\begin{aligned} e_1 &= x_1 - x_{1d}, \\ e_i &= x_i - \alpha_{i-1}^c \text{ for } i = 2, 3, \end{aligned} \quad (5.7)$$

where α_i^c is the filtered signal of the virtual controller α_i . By using a first-order filter, the command filtered is formulated as

$$o_i \dot{\alpha}_i^c + \alpha_i^c = \alpha_i; i = 1, 2, \quad (5.8)$$

where $o_i > 0; \alpha_i^c(0) = \alpha_i(0)$

Then, the compensated tracking error signals are given by $z_i = e_i - v_i$ where the compensation signals v_i are defined as

$$\dot{v}_i = -k_i v_i + v_{i+1} + \alpha_i^c - \alpha_i; i = 1, 2, \quad (5.9)$$

with $v_i(0) = 0$, k_i is a positive scalar. For $i = 3$, define $\dot{v}_3 = -k_3 v_3$.

Step 1: The derivative of z_1 can be expressed as

$$\dot{z}_1 = \dot{e}_1 - \dot{v}_1 = \alpha_1 + z_2 + k_1 v_1 - \dot{x}_{1d}, \quad (5.10)$$

A change of error coordinates is given by

$$\begin{aligned} \omega_x &= \frac{z_1}{k_x}, \omega_y = \frac{z_1}{k_y}, \omega = q\omega_x + (1-q)\omega_y, \\ q &= \begin{cases} 1 & \text{if } z_1 \geq 0 \\ 0 & \text{if } z_1 < 0 \end{cases} \end{aligned} \quad (5.11)$$

where k_x and k_y are positive terms.

The virtual control law α_1 of step 1 is designed as

$$\alpha_1 = -k_1 e_1 - k_u z_1 + \dot{x}_{1d}, \quad (5.12)$$

where $k_1 > 0, k_u = \sqrt{\left(\frac{\dot{k}_x}{k_x}\right)^2 + \left(\frac{\dot{k}_y}{k_y}\right)^2} + \gamma_1, \gamma_1 > 0$.

Consider the time-varying asymmetric BLF V_1 as

$$V_1 = \frac{q}{2} \log \frac{k_y^2}{k_y^2 - z_1^2} + \frac{1-q}{2} \log \frac{k_x^2}{k_x^2 - z_1^2} = \frac{1}{2} \log \frac{1}{1-\omega^2}. \quad (5.13)$$

The derivative of V_1 can be given by

$$\dot{V}_1 = \frac{q\omega_y}{k_y(1-\omega_y^2)} \left(\dot{z}_1 - z_1 \frac{\dot{k}_y}{k_y} \right) + \frac{(1-q)\omega_x}{k_x(1-\omega_x^2)} \left(\dot{z}_1 - z_1 \frac{\dot{k}_x}{k_x} \right) = -k_1 \frac{\omega^2}{1-\omega^2} + z_1 z_2 \phi_1, \quad (5.14)$$

where $\phi_1 = \frac{q}{k_y^2 - z_1^2} + \frac{1-q}{k_x^2 - z_1^2}$.

Step 2: Differentiating z_2 with respect to time yields that

$$\begin{aligned} \dot{z}_2 &= \dot{e}_2 - \dot{v}_2 = f_2 + \xi_3 + \varphi_1 - \dot{\alpha}_1^c - (-k_2 v_2 + v_3 + \alpha_2^c - \alpha_2) \\ &= f_2 + \varphi_1 - \dot{\alpha}_1^c + \alpha_2 + z_3 + k_2 v_2. \end{aligned} \quad (5.15)$$

The virtual control law α_2 is designed as

$$\alpha_2 = -k_2 e_2 - \varphi_2 - \hat{\varphi}_1 + \dot{\alpha}_1^c - \phi_1 z_1, \quad (5.16)$$

where $\hat{\varphi}_1$ is the estimation of φ_1 .

The DO for mismatched disturbance φ_1 is constructed as

$$\begin{aligned} \dot{\hat{\varphi}}_1 &= \chi_1 + L_1 x_2, \\ \dot{\chi}_1 &= -L_1 \chi_1 + z_2 - L_1 (f_2 + x_3 + L_1 x_2), \end{aligned} \quad (5.17)$$

where χ_1, L_1 are internal states, observer gain of the first DO.

Define the disturbance error $\tilde{\varphi}_1 = \varphi_1 - \hat{\varphi}_1$. Taking the derivative of $\tilde{\varphi}_1$ as

$$\begin{aligned} \dot{\tilde{\varphi}}_1 &= \dot{\varphi}_1 - \dot{\hat{\varphi}}_1 = \varphi_1 - \dot{\chi}_1 - L_1 \dot{x}_2 \\ &= \dot{\varphi}_1 + L_1 \chi_1 - z_2 + L_1 (f_2 + x_3 + L_1 x_2) - L_1 (f_2 + x_3 + \varphi_1) \\ &= \dot{\varphi}_1 - L_1 \tilde{\varphi}_1 - z_2. \end{aligned} \quad (5.18)$$

Lyapunov function candidate V_2 is adopted as

$$V_2 = V_1 + \frac{1}{2} z_2^2 + \frac{1}{2} \tilde{\varphi}_1^2. \quad (5.19)$$

Taking the derivative of V_2 yields:

$$\begin{aligned}
\dot{V}_2 &= -k_1 \frac{\omega^2}{1-\omega^2} + z_1 z_2 \dot{\phi}_1 + z_2 \left(-k_2 z_2 + \tilde{\Delta}_1 - \phi_1 z_1 + z_3 \right) + \tilde{\varphi}_1 \left(\dot{\phi}_1 - L_1 \tilde{\varphi}_1 - z_2 \right) \\
&= -k_1 \frac{\omega^2}{1-\omega^2} - k_2 z_2^2 - L_1 \tilde{\varphi}_1^2 + z_2 z_3 + \tilde{\varphi}_1 \dot{\phi}_1.
\end{aligned} \tag{5.20}$$

Step 3: Differentiating z_3 with respect to time yields that

$$\dot{z}_3 = \dot{e}_3 - \dot{v}_3 = \varphi_3 + g_3 u + \varphi_2 - \dot{\alpha}_2^c + k_3 v_3. \tag{5.21}$$

The DO is constructed to estimate both matched disturbance and the bias fault φ_2 as

$$\begin{aligned}
\hat{\varphi}_2 &= \chi_2 + L_2 x_3, \\
\dot{\chi}_2 &= -L_2 \chi_2 + z_3 - L_2 (\varphi_3 + g_3 u + L_2 x_3),
\end{aligned} \tag{5.22}$$

where $\hat{\varphi}_2$ is the estimation of φ_2 ; χ_2, L_2 are internal states, observer gain of the second DO.

Define the disturbance error $\tilde{\varphi}_2 = \varphi_2 - \hat{\varphi}_2$. Taking the derivative of $\tilde{\varphi}_2$, one obtains

$$\begin{aligned}
\dot{\tilde{\varphi}}_2 &= \dot{\varphi}_2 - \dot{\hat{\varphi}}_2 = \dot{\varphi}_2 - \dot{\chi}_2 - L_2 \dot{x}_3 \\
&= \dot{\varphi}_2 - L_2 \tilde{\varphi}_2 - z_3.
\end{aligned} \tag{5.23}$$

The final control law u of the nominal controller is elaborated as

$$u = \frac{1}{g_3} \left(-k_3 e_3 - \varphi_3 - \hat{\varphi}_2 + \dot{\alpha}_2^c - z_2 \right). \tag{5.24}$$

Remark 5.3: The control law (5.24) is given to exhibit good tracking qualification and disturbance rejection despite the presence of lumped disturbances and the bias fault. However, it cannot ensure the system performance under the appearance of the LOE fault. Therefore, it is indispensable to construct the control law that can attenuate the impact of the severity of the LOE fault.

5.3.2 Reconfigurable control design

For the mentioned reason, the final control law u is reconstructed to overcome the effect of the LOE fault. In this regard, the LOE fault coefficient can be identified, and the achieved information is then used to compare with the detector threshold. Based on the compared result, the normal operation or faulty operation can be determined. If the LOE fault occurs, the reconfigurable controller is implemented instead of the nominal controller (5.24) to eliminate the influences of actuator failures. The system stability and acceptable performance of the

whole closed-loop system can be preserved. The control design procedure in step 3, section 5.3.1 is rewritten as follows:

From (5.21), by adding and subtracting the intermediate factor α_3 , we have

$$\dot{z}_3 = \varphi_3 + g_3 u + \varphi_2 - \dot{\alpha}_2^c + k_3 v_3 + \alpha_3 - \alpha_3 \quad (5.25)$$

The intermediate controller α_3 is elaborated as

$$\alpha_3 = k_3 e_3 + \varphi_3 + \hat{\varphi}_2 - \dot{\alpha}_2^c + z_2 \quad (5.26)$$

Substituting (5.26) into (5.25), one obtains:

$$\dot{z}_3 = g_3 v u_a + \tilde{\varphi}_2 - k_3 z_3 - z_2 + \alpha_3 \quad (5.27)$$

where u_a is the reconfigurable controller.

The Lyapunov function candidate V is defined as

$$V = V_2 + \frac{1}{2} z_3^2 + \frac{1}{2} \tilde{\varphi}_2^2 + \frac{g_3 V}{2\Gamma} \tilde{\Phi}^2. \quad (5.28)$$

where $\Gamma > 0$, $\tilde{\Phi} = \Phi - \hat{\Phi}$, $\hat{\Phi}$ is the estimation of $\Phi = \frac{1}{g_3 V}$.

Differentiating (5.28) with respect to time, it follows that:

$$\begin{aligned} \dot{V} &= k_1 \frac{\omega^2}{1-\omega^2} - k_2 z_2^2 - L_1 \tilde{\varphi}_1^2 + z_2 z_3 + \tilde{\varphi}_1 \dot{\varphi}_1 + z_3 (g_3 v u_a + \tilde{\varphi}_2 - k_3 z_3 - z_2 + \alpha_3) \\ &\quad + \tilde{\varphi}_2 (\dot{\varphi}_2 - L_2 \tilde{\varphi}_2 - z_3) - \frac{g_3 V}{\Gamma} \tilde{\Phi} \dot{\Phi} \\ \dot{V} &\leq -k_1 \log \frac{1}{1-\omega^2} - k_2 z_2^2 - L_1 \tilde{\varphi}_1^2 - k_3 z_3^2 - L_2 \tilde{\varphi}_2^2 + \tilde{\varphi}_1 \dot{\varphi}_1 + \tilde{\varphi}_2 \dot{\varphi}_2 \\ &\quad + z_3 g_3 v u_a + z_3 \alpha_3 - \frac{g_3 V}{\Gamma} \tilde{\Phi} \dot{\Phi}. \end{aligned} \quad (5.29)$$

Using Young's inequality, one obtains

$$\begin{aligned} \tilde{\varphi}_1 \dot{\varphi}_1 &\leq \frac{1}{2} \tilde{\varphi}_1^2 + \frac{1}{2} \Xi_1^2, \\ \tilde{\varphi}_2 \dot{\varphi}_2 &\leq \frac{1}{2} \tilde{\varphi}_2^2 + \frac{1}{2} \Xi_2^2, \end{aligned} \quad (5.30)$$

The derivative of V is further derived as

$$\dot{V} \leq \Psi + z_3 g_3 v u_a + z_3 \alpha_3 - \frac{g_3 V}{\Gamma} \tilde{\Phi} \dot{\Phi}, \quad (5.31)$$

where $\Psi = -k_1 \log \frac{1}{1-\omega^2} - k_2 z_2^2 - k_3 z_3^2 - \sum_{i=1}^2 \left(L_i - \frac{1}{2} \right) \tilde{\varphi}_i^2 + \frac{1}{2} \sum_{i=1}^2 \Xi_i^2$.

The final control law of the reconfigurable controller can be constructed as follows:

$$u_a = -\frac{z_3 \hat{\Phi}^2 \alpha_3^2}{\sqrt{z_3^2 \hat{\Phi}^2 \alpha_3^2 + \sigma_1^2}}, \quad (5.32)$$

where σ_1 is a positive scalar.

The adaptive law of parameter $\hat{\Phi}$ is determined as

$$\dot{\hat{\Phi}} = \Gamma z_3 \alpha_3 - b_0 \hat{\Phi}, \quad (5.33)$$

where b_0 is a positive constant.

Applying u_a and $\dot{\hat{\Phi}}$ to (5.31), yields

$$\dot{V} \leq \Psi - g_3 \nu \frac{z_3^2 \hat{\Phi}^2 \alpha_3^2}{\sqrt{z_3^2 \hat{\Phi}^2 \alpha_3^2 + \sigma_1^2}} + z_3 \alpha_3 - \frac{g_3 \nu}{\Gamma} \tilde{\Phi} (\Gamma z_3 \alpha_3 - b_0 \hat{\Phi}). \quad (5.34)$$

Making use of Lemma 2, and noting that g_3, ν are positive parameters, we have

$$\begin{aligned} -g_3 \nu \frac{z_3^2 \hat{\Phi}^2 \alpha_3^2}{\sqrt{z_3^2 \hat{\Phi}^2 \alpha_3^2 + \sigma_1^2}} &\leq g_3 \nu \sigma_1 - g_3 \nu z_3 \hat{\Phi} \alpha_3, \\ -\frac{g_3 \nu}{\Gamma} \tilde{\Phi} (\Gamma z_3 \alpha_3 - b_0 \hat{\Phi}) &= -g_3 \nu z_3 \tilde{\Phi} \alpha_3 + \frac{g_3 \nu b_0}{\Gamma} \tilde{\Phi} \hat{\Phi}, \end{aligned} \quad (5.35)$$

and considering the definition of Φ , the following equality is derived:

$$\begin{aligned} z_3 \alpha_3 - g_3 \nu z_3 \hat{\Phi} \alpha_3 - g_3 \nu z_3 \tilde{\Phi} \alpha_3 &= z_3 \alpha_3 (1 - g_3 \nu (\hat{\Phi} + \tilde{\Phi})) \\ &= z_3 \alpha_3 (1 - g_3 \nu \Phi) = 0. \end{aligned} \quad (5.36)$$

From (5.35), (5.36), and (5.34) can then be simplified to

$$\dot{V} \leq \Psi + g_3 \nu \sigma_1 + \frac{g_3 \nu b_0}{\Gamma} \tilde{\Phi} \hat{\Phi}. \quad (5.37)$$

By applying Young's inequality, one obtains

$$\frac{b_0}{\Gamma} \tilde{\Phi} \hat{\Phi} \leq \frac{b_0}{2\Gamma} (\Phi^2 - \tilde{\Phi}^2). \quad (5.38)$$

The derivative of V becomes as

$$\begin{aligned} \dot{V} \leq & -k_1 \log \frac{1}{1-\omega^2} - k_2 z_2^2 - k_3 z_3^2 - \sum_{i=1}^2 \left(L_i - \frac{1}{2} \right) \tilde{\varphi}_i^2 \\ & - \frac{b_0}{2\Gamma} \tilde{\Phi}^2 + \frac{1}{2} \sum_{i=1}^2 \Xi_i^2 + \frac{b_0}{2\Gamma} \Phi^2 + g_3 \nu \sigma_1. \end{aligned} \quad (5.39)$$

Then, we obtain

$$\dot{V} \leq -a_1 V + b_1, \quad (5.40)$$

where

$$a_1 = \min \left(2\lambda_{\min}(k_1), 2\lambda_{\min}(k_2), 2\lambda_{\min}(k_3), \lambda_{\min}(2L_1 - 1), \lambda_{\min}(2L_2 - 1), \lambda_{\min} \left(\frac{b_0}{\Gamma} \right) \right),$$

$$b_1 = \frac{1}{2} \sum_{i=1}^2 \Xi_i^2 + \frac{b_0}{2\Gamma} \Phi^2 + g_3 \nu \sigma_1.$$

Theorem 5.1: With the EHA system (5.2), if the two NDOs are designed as (5.17), (5.22); the virtual/intermediate control law is presented in (5.12), (5.16), (5.26) and the enhanced adaptive law for the LOE fault is presented in (5.33), the actuator FTC controller is indicated by (5.32). Then, all closed-loop signals, i.e., tracking errors, disturbance errors, and $\tilde{\Phi}$ are uniformly ultimately bounded, and the position constraint is unviolated in the simultaneous presence of lumped disturbances, bias and LOE fault.

Proof:

Further analysis of (5.40) can get

$$V \leq \left(V(0) - \frac{b_1}{a_1} \right) e^{-a_1 t} + \frac{b_1}{a_1} \leq \mathcal{G}, \quad (5.41)$$

where $\mathcal{G} = V(0) + b_1/a_1$.

The error variables z_1 , z_2 , and z_3 are bounded by the compact sets Y_{e1} , Y_{e2} , and Y_{e3} respectively, defined as follows:

$$\begin{aligned}
Y_{e1} &= \left\{ z_1 \in R \mid -\sqrt{k_b^2 (1-e^{-g})} \leq z_1 \leq \sqrt{k_a^2 (1-e^{-g})} \right\}, \\
Y_{e2} &= \left\{ z_2 \in R \mid z_2 \leq \sqrt{\frac{g}{\lambda_{\min}(k_2)}} \right\}, \\
Y_{e3} &= \left\{ z_3 \in R \mid z_3 \leq \sqrt{\frac{g}{\lambda_{\min}(2k_3-1)}} \right\},
\end{aligned} \tag{5.42}$$

Based on the above analysis, we can be concluded that the result of Theorem 5.1 can be achieved. The proof is completed.

Remark 5.4: From (5.33), the exact fault information \hat{v} can be provided. Then, the fault decision scheme is carried out by comparing the estimation of v with a predefined threshold T_h which is decided through performing experiments. It can be described by

$$\hat{v} = \frac{1}{\hat{\Phi}_{g_3}} \begin{cases} \geq T_h \rightarrow \text{faulty operation,} \\ < T_h \rightarrow \text{normal operation.} \end{cases} \tag{5.43}$$

In the case of faulty operation, the reconfigurable controller is conducted to retain key properties of the overall system, such as stability and disturbance/fault rejection.

Remark 5.5: It is noted that by designing the larger the $k_1, k_2, k_3, L_1, L_2, b_0$ and smaller the Γ , the smaller the tracking errors, disturbance errors, and adaptor error will be. However, since the selection of these parameters is over a certain value, the qualification of the EHA system will be impacted (i.e., overshoot, chattering phenomenon). Thus, it is essential to choose suitable control parameters according to the controlled system.

5.4 Numerical simulation

5.4.1 Simulation setup

To demonstrate the improved performance of the proposed FTC, simulation studies are first conducted in the EHA system by using Matlab/Simulink (R2021a version). The desired trajectory, i.e., the sinusoidal signals, is described as

$$x_{1d} = 10 + 10\sin(\pi t - \pi/2) \text{ (mm)}. \tag{5.44}$$

The setting parameters for the simulation EHA system are shown in Table 3.2.

Three control strategies are given and compared to prove the superior tracking performance of the suggested FTC method in the numerical simulation and experiments.

C1: Strategy 1 is BLF-BC with two DOs. The control law is designed as follows:

$$\begin{aligned}
e_1 &= x_1 - x_{1d}, \alpha_1 = -(k_b^2 - e_1^2)k_1 e_1, e_2 = x_2 - \dot{x}_{1d} - \alpha_1, \\
\alpha_2 &= -f_2 - \hat{\varphi}_1 + \dot{\alpha}_1 - k_2 e_2 - \frac{e_1}{k_b^2 - e_1^2}, e_3 = x_3 - \ddot{x}_{1d} - \alpha_2, \\
u &= \frac{1}{g_3} (-\varphi_3 - \hat{\varphi}_2 + \ddot{x}_{1d} + \dot{\alpha}_2 - k_3 e_3 - e_2).
\end{aligned} \tag{5.45}$$

C2: Strategy 2 is the BLF-CFC with adaptive actuator controller which is given by (5.32), without two DOs and the updating law is described by (5.33).

Proposed controller: Strategy 3 is BLF-CFC with two DOs and an adaptive actuator controller.

The control parameters and filter parameters of the proposed controller are carefully adjusted and tuned via the trial error method and shown as: $k_1 = 50$; $k_2 = 150$; $k_3 = 25$; $o_1 = o_2 = 0.05$; $\gamma_1 = 0.1$. The parameters for adaption part are set as $\Gamma = 0.5$, $b_0 = 1.3$, $\sigma_1 = 0.2e^{(-0.03t)}$. As noted in Remark 1, the EHA is applied for different applications resulting in different constrain motions. In this paper, one type of the time-varying barriers for output displacement is set as $y_u = 25 + 2\cos(\pi t - \pi)$ (mm), $y_l = -5 + 2\cos(\pi t - \pi)$ (mm); $k_x = \xi_{1d} - y_l$, $k_y = y_u - \xi_{1d}$. The parameters for the NDO are set as $L_1 = 50$; $L_2 = 65$. The predefined threshold value is chosen as $T_h = 0.05$. The LOE fault coefficient is set as $v = 0.4$.

In a fair comparison, the control parameters of the **C1** and **C2** controller are set as the same as the proposed controller, i.e., the same value of k_1 ; k_2 ; k_3 ; L_1 ; L_2 .

To evaluate the qualification of the proposed control method in the appearance of actuator faults, the different operational fault conditions are implemented during 20 cycles. The system starts the simulation in ideal condition from 0 to 10 s. The system operates in healthy condition with lumped disturbances from 10 to 20 s. From 20 to 30 s, the bias fault occurs, and the partial LOE fault happens in the remaining time.

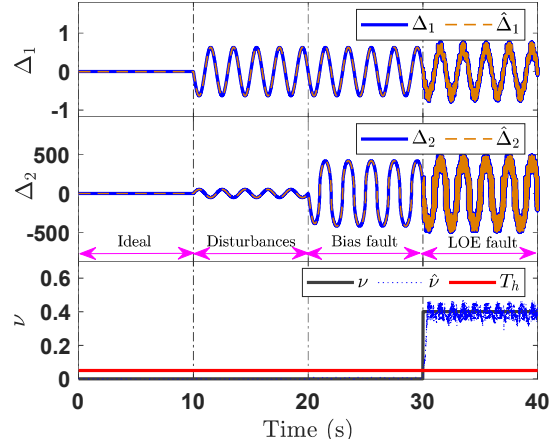


Figure 5.3 Lumped disturbance and LOE fault estimation in the simulation.

5.4.2 Simulation result

In the simulations, the mismatched disturbance, and the matched disturbance with bias fault are approximated by two disturbance observers where the estimation results are depicted in Figure 5.3. From Figure 5.3, it shows that the observed values track their physical values from ideal conditions to faulty conditions. Once the mismatched, matched disturbances, and LOE coefficient appear, they are successfully estimated. For the matched disturbance containing the bias fault, the estimated value increases when the internal leak fault appears at the time $t = 20s$. Furthermore, despite the occurrence of both the bias fault and the LOE fault after $t = 30s$, the estimation value of the lumped uncertainties, including the matched disturbance and the bias fault has still been effectively preserved. Meanwhile, the LOE fault information is provided in the third subgraph of Figure 5.3 thanks to the assistance of the enhanced adaptive law. This value $\hat{\nu}$ will be used for fault diagnosis that makes an exact decision. Consequently, the reconfigurable controller can be active. We can see that the LOE fault is immediately detected when the estimation of the LOE coefficient is bigger than the threshold value. Hence, the flexible switch between the nominal controller and reconfigurable controller has been performed that ensures the system stability and some key feature performances despite disturbances/faults.

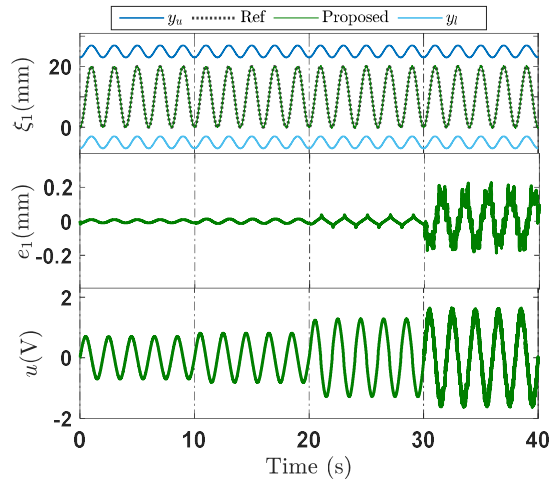


Figure 5.4 Performances of the proposed controller in the simulation.

Figure 5.4 illustrates, in turn, the position tracking performance, the tracking error, and the control inputs. With reference to Figure 5.4, the proposed FTC controller accommodates not only the lumped disturbance but also the generated actuator faults. However, the tracking error and control action has changed since the ideal condition, disturbances, bias, and LOE fault are sequentially applied. The input signal is significantly increased against the bias fault and LOE fault during the operation, as expected. After 30 s, the LOE fault is detected and identified by the received information from FD, then the reconfigurable controller instead of the nominal controller is enhanced to reduce the effects of the LOE fault. It is obvious that the control effort of the reconfigurable controller is enriched to effectively compensate for the actuator LOE failure. Moreover, the position tracking performance remains within the specified tolerance and without violating the predefined boundary, as shown in Figure 5.4.

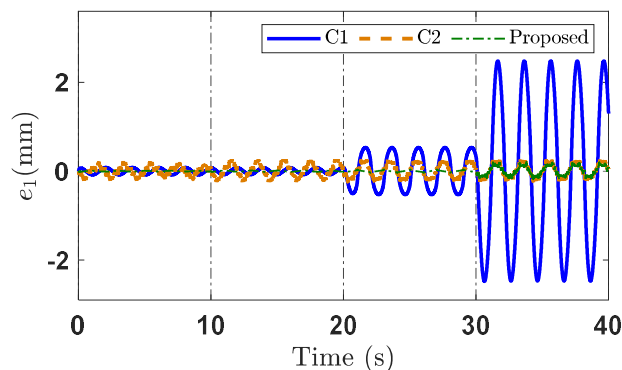


Figure 5.5. The overall tracking error of different control methods

For the sake of comparison with other approaches, the tracking errors are also plotted in Figure 5.5. As one can see, the position error of the relevant controllers increases as a result of starting the ideal condition, introducing the disturbance, bias fault, and LOE fault, respectively. However, there is a significant difference between the three controllers. The proposed controller brings the best performance among the three controllers. Meanwhile, the C1 and C2 cannot exhibit good performance as expected due to the lack of some compensation components. Furthermore, some of the true root mean square (RMS) values ($\sqrt{(1/T) \int_0^T e_i^2(t) dt}$, where T is the time period) and maximum errors ($\max(e_i)$) of the corresponding controller in Figure 5.6 confirm again the outstanding of the suggested method.

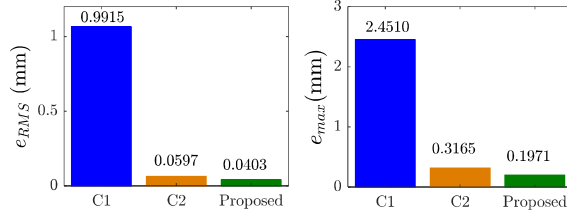


Figure 5.6 Result of performance indexes in the simulation

5.5 Comparative experimental results

5.5.1 Experiment setup

The hardware of the hydraulic testbench is displayed in Figure 3.3. The tracking reference signal (5.44) is also applied to evaluate the tracking performance of the different control methods. In the experiment, the EHA system parameters are set similar to the corresponding values in simulation while some control gain parameters are returned as $k_1 = 45$; $k_2 = 120$; $k_3 = 30$ and the parameters for adaption part are set as $\Gamma = 0.9$, $b_0 = 0.45$. The NDO gains are selected $L_1 = 40$; $L_2 = 75$.

5.5.2 Experiment results

Two experiments were executed to appraise the effectiveness of the suggested FTC scheme. The various operational fault conditions are performed during 30 cycles. Experiment 1 considered only the LOE fault while both the internal leakage fault and LOE fault were tested in Experiment 2. The experiment results are described as follows.

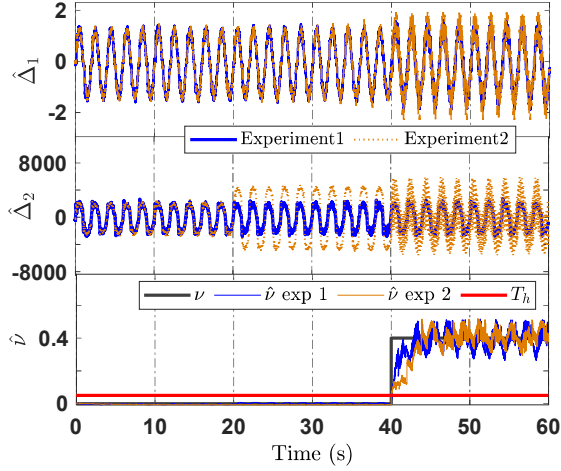


Figure 5.7 Mismatched, matched disturbance and LOE fault estimation of the proposed method in the experiment.

Firstly, the precise estimation results of the two experiments for the matched, mismatched disturbances and LOE fault coefficient of the proposed approach are plotted in Figure 5.7. It can be seen in the first and second subgraphs of Figure 5.7, the mismatched, and matched disturbances rise after the appearance of the bias fault or LOE fault; and the matched DO can approximate the lumped uncertainties including disturbances and the bias faults in a timely manner. As seen in the third subgraph of Figure 5.7, the LOE coefficient is also successfully estimated and compared with the threshold value. Then the reconfigurable controller is used to replace the nominal controller that maintains the acceptable tracking performance.

Experiment 1: In this experiment, the electro-hydraulic system operates in healthy condition with inherent lumped disturbances from 0 to 40 s. Then the LOE fault experiment is implemented which occurs from 40 to 60 s. Figure 5.8 shows the experiment results with sinewave response. As seen in this figure, the output position of three control methods satisfies the output constraint condition in both healthy and faulty modes. However, the tracking error of the proposed controller is the smallest in comparison with the **C1** and **C2** because the proposed method possesses both the actuator FTC controller and two DOs to compensate for the lumped disturbances as well as LOE fault. It is noteworthy that the error state of the proposed controller after 40 s and the **C2** controller has some structural vibrations because of the enhanced effort of the actuator controller to suppress the influences of LOE fault. On the

other hand, the control input of **C1** decreases due to the impact of the LOE fault that causes the big error after 40 s. Meanwhile, the control action of **C1** and the proposed controller increase against the LOE fault. The efficacy of comparative controllers is evaluated through two performance indexes and summarized in Figure 5.9a. It is noteworthy that the RMS error and maximum error of the proposed controller, in turn, 0.2634 and 0.8854 mm are the smallest during the tracking desired signal. This reconfirms the outstanding efficiency of the proposed control algorithm.

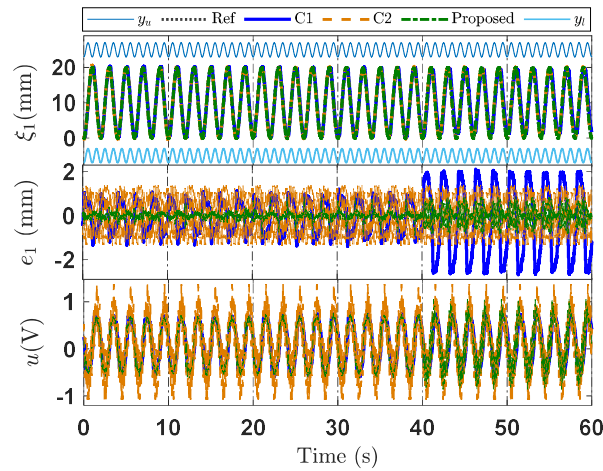


Figure 5.8 Performances of three control methods in experiment 1

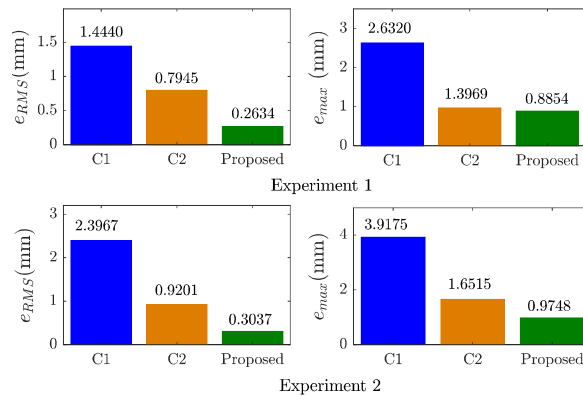


Figure 5.9 Result of performance indexes in the experiment.

Experiment 2: In scenario 2, the internal leakage fault experiment is performed from 20 to 40 s, whilst the LOE fault appears from 40 to 60 s. The internal leakage fault arises when the manual flow control valve is opened. Figure 5.10 describes the experiment results which indicated that the position error of the **C1**, **C2**, and the proposed method all rise under the

occurrence of the leakage fault and LOE fault. Nonetheless, in comparison with **C1**, the tracking error of the proposed method is better due to a compensation system of CFC. Meanwhile, compared with the **C2** control method, the proposed controller can observe and effectively compensate for the matched, mismatched disturbances, and bias fault through two NDOs as shown in Figure 5.7. Consequently, the FTC proposed approach obtained better performance and stronger robustness when the bias fault and LOE fault simultaneously occur. Figure 5.9b presents the results of two performance indexes of three controllers. It indicates that the tracking performance of the proposed controller is improved by 87%, and 66% in comparison with the other two controllers, respectively. This clearly validates the effectiveness of the proposed method.

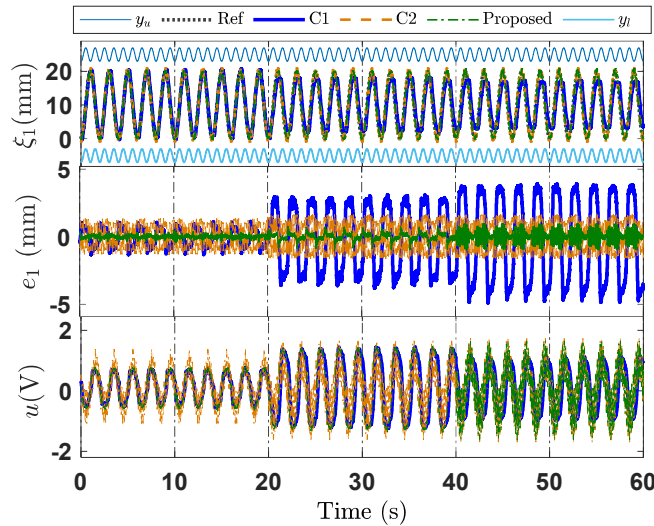


Figure 5.10 Performances of three control methods in experiment 2

According to the aforementioned comparative simulation and experiment studies, it is revealed that the proposed FTC can be warranted the stability condition and output non-violating the prebound in all situations. Furthermore, it provides superior tracking performance in the face of the matched, mismatched disturbances, bias, and LOE fault among the four controllers.

5.6 Chapter summary

Even though there are meaningful explorations in the tracking control for the EHA system, the experimental research of FTC to tackle the challenging problem such as lumped

disturbances, bias faults, and LOE fault is scarce. Come up with this shortcoming, the proposed FTC scheme was constructed by combining NDO, CFC, and an adaptive compensation technique to improve tracking qualification and guarantee safety issues subjected to the presence of lumped uncertainties, bias fault and partial LOE fault. In detail, the NDO was deployed to cope with the lumped uncertainties including matched, mismatched disturbances, and bias fault. The BLF was introduced to ensure the position constraint for the EHA system was not violated. Meanwhile, the LOE fault was successfully detected and identified, which was then fed back to the reconfigurable controller. The CFC approach was applied to solve the problem of “explosion of complexity” in the backstepping design process, and a compensation system was developed to decrease the tracking error. Both numerical simulation and experiment results were implemented to demonstrate superior tracking performance and system stability even in faulty conditions.

CHAPTER 6

ROBUST SENSOR FAULT-TOLERANT TRACKING CONTROL

6.1 Introduction

The electro-hydraulic servo system (EHA) usually faces multiple sensor faults and disturbances, which is difficult to achieve good tracking control, reliability, and stability control [72]. In this chapter, an advanced fault-tolerant controller is proposed for an EHA to deal with the above challenge. The three fault observers, called nonlinear unknown input observers (NUIOs), are developed to effectively estimate the position, velocity, pressure sensor faults and the system states. The fault detection, estimation, and isolation (FDEI) are then presented as effective for multiple sensors failure at a time. The first NUIO for position sensor fault is utilized for the tracking control, whilst the other NUIOs are used for alarm proposal. The adverse effects caused by the matched and unmatched disturbances are eliminated by two extended state observers (ESOs). In addition, to avoid the “explosion of complexity” when computing the derivatives of virtual control laws, the dynamic surface control (DSC) is applied to design the fault-tolerant control (FTC) scheme. The Lyapunov principle ensures system stability under lumped disturbance and faulty conditions. Finally, simulation studies and evaluation results are performed to demonstrate the validity of the proposed FTC algorithm.

The architecture of this chapter is arranged as follows. Section 6.2 derives the problem statements, including system description of the EHA, and some required assumptions. In Section 6.3, the proposed NUIO on the basis of LMI approach is presented. Section 6.4 presents the ESOs and the DSC-based FTC design. Simulation studies on the proposed algorithm are shown in Section 6.5. Finally, the conclusions are discussed, and future works are put forward in Section 6.6.

6.2 Problem statement

The block diagram of the symmetric EHA in the presence of multiple sensor faults is illustrated in Figure 6.1. From Figure 6.1, three sensor faults of hydraulic driven actuator are considered: 1) position sensor fault (f_{s1}); 2) velocity sensor fault (f_{s2}); and 3) load pressure sensor fault (f_{s3}).

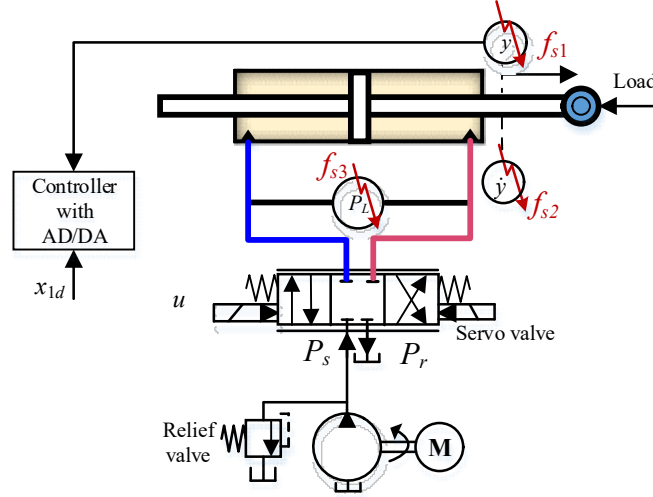


Figure 6.1 Schematic of the electro-hydraulic actuator with sensor faults

Defines $\mathbf{x} = [x_1, x_2, x_3]^T \triangleq [y, \dot{y}, P_L]^T$. From (3.4)–(3.5) the system modeled with system uncertainties, Δ_1 and Δ_2 , can be expressed by:

$$\begin{cases} \dot{x}_1 = x_2, \\ \dot{x}_2 = f_2(x_2) + w_a x_3 + \varphi_1(x_1, x_2, t), \\ \dot{x}_3 = f_3(x_2, x_3) + w_b(x_3, u)u + \varphi_2(x_2, x_3, t), \end{cases} \quad (6.1)$$

where

$$w_a = \frac{A}{m}, f_2 = -\frac{B}{m}x_2, p_a = \frac{4\beta_e k_t}{V_c},$$

$$w_b = p_a \sqrt{P_s - x_3 \text{sign}(u)}, f_3 = -p_c x_3 - p_b x_2,$$

$$\varphi_1 = \frac{\Lambda(\bullet)}{m} + \Delta_1, \varphi_2 = \frac{4\beta_e}{V_c} Q_{Li} + \Delta_2, \text{ denote the unmatched, matched disturbances, respectively.}$$

In the case of sensor faults, the practical measured system state can be established as $y^F = x_p + f_{s1}, \dot{x}_p^F = \dot{x}_p + f_{s2}, P_L^F = P_L + f_{s3}$. Hence, the sensor fault dynamics is formulated by

$$\begin{cases} \dot{\mathbf{f}}_s = \mathbf{d}_s \mathbf{f}_s + \boldsymbol{\theta}_s, \\ \mathbf{y} = \mathbf{C} \mathbf{x} + \mathbf{D}_s \mathbf{f}_s, \end{cases} \quad (6.2)$$

where $\mathbf{f}_s = [f_{s1} \ f_{s2} \ f_{s3}]^T$ denotes the concerned sensor fault, i.e., position sensor fault and load pressure sensor fault, $\mathbf{d}_s = [d_{s1} \ 0 \ 0; 0 \ d_{s2} \ 0; 0 \ 0 \ d_{s3}]$, d_{si} is a scalar that describes the evolution of the i^{th} sensor fault, $\boldsymbol{\theta}_s = [\theta_{s1} \ \theta_{s2} \ \theta_{s3}]^T$ is an unknown input signal, $\mathbf{C} = \mathbf{I}_3$ is output matrix, $\mathbf{I}_3 \in \mathcal{R}^{3 \times 3}$ is a unit matrix $\in \mathcal{R}^{3 \times 3}$ is, $\mathbf{D}_s = [\mathbf{d}_1 \ \mathbf{d}_2 \ \mathbf{d}_3]$, $\mathbf{d}_1 = [1 \ 0 \ 0]^T$, $\mathbf{d}_2 = [0 \ 1 \ 0]^T$, $\mathbf{d}_3 = [0 \ 0 \ 1]^T$, denotes a standard vector. Based on (6.1) and (6.2), the augmented system including sensor fault can be rewritten as follows [73]:

$$\begin{cases} \dot{\boldsymbol{\xi}}_i = \mathbf{g}_i(\boldsymbol{\xi}_i, u) + \mathbf{E}_i \boldsymbol{\chi}_i, \\ \mathbf{y}_i = \mathbf{S}_i \boldsymbol{\xi}_i, \end{cases} \quad (6.3)$$

where $\boldsymbol{\xi}_i = [\mathbf{x}, f_{si}]^T$ is an augmented state vector, \mathbf{E}_i represents the known fault distribution matrix, $\mathbf{S}_i = [\mathbf{C} \ \mathbf{d}_i]^T$, $\mathbf{g}_i = [x_2, w_a x_3 + f_2, w_b u + f_3, d_{si} f_{si}]^T$, $\boldsymbol{\chi}_i = [\varphi_1, \varphi_2, \theta_{si}]^T$.

Assumption 6.1: The sensor faults can simultaneously appear at the position, velocity, or load pressure sensor at the same time.

Assumption 6.2: For the nonlinear function $\mathbf{g}(\boldsymbol{\xi})$, $\hat{\boldsymbol{\xi}}$ is the estimated state vector, there exist a Lipschitz constant σ such that

$$\left| \mathbf{g}(\boldsymbol{\xi}) - \mathbf{g}(\hat{\boldsymbol{\xi}}) \right| \leq \sigma \left| \boldsymbol{\xi} - \hat{\boldsymbol{\xi}} \right|. \quad (6.4)$$

Remark 6.1: The first objective is to design three NUIO observers for estimating the position, velocity, load pressure sensor fault, and then the FDEI is given. The second objective of this study is to organize an appropriate u that drives the output x_1 of the EHA (6.1) to track the desired trajectory x_{1d} in spite of the lumped disturbances and sensor faults.

Remark 6.2: It should be noted that sensor faults can be divided into three situations: bias fault (i.e., offsets, poor calibration, scaling errors), partial loss of effectiveness sensor fault, and the outage case [17]. In this paper, a bias sensor fault case model formulated by (6.2) is used. The latter two faults will be studied in our future works.

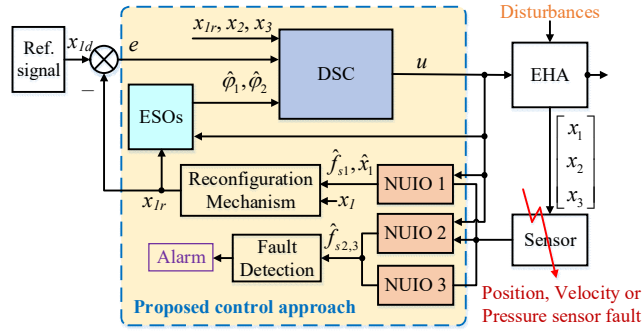


Figure 6.2 Schematic view of the proposed control scheme

6.3 NUIO-based fault identification for EHA

The architecture of proposed control approach is described in Figure 6.2, which comprises of three main parts: three NUIOs (sensor faults and states estimation), two ESOs, and DSC control approach. In this section, the procedure of three NUIOs design is described whilst the remaining parts are presented in the next section. It is noted that the sensor faults may be simultaneously at a time in this study. By considering the matched, unmatched disturbances, unknown input signal as the unknown input terms, three NUIOs are designed to approximate the internal system states and position, velocity, or load pressure sensor fault, respectively. Then, the sensor faults are detected when the estimated value is bigger than a predefined threshold. In addition, the location of the faults is determined through the three NUIOs. When the sensor faults were identified and detected, only the position sensor fault information is used to feed to the integrated controller. Other sensor faults, i.e., velocity, load pressure sensor fault, are detected for the alarm proposal.

The procedure design observer process is built based on the separate sensor fault warrants the independent operation of the designed fault observer. Without loss of generality, a typical observer is constructed to provide a unified approach, other observers will be similarly designed. For the sake of simplicity, ξ , \mathbf{g} , φ , \mathbf{E} , \mathbf{y} , \mathbf{S} denote ξ_i , \mathbf{g}_i , φ_i , \mathbf{E}_i , \mathbf{y}_i , \mathbf{S}_i , respectively.

Considering the NUIO for a fault estimation process:

$$\begin{aligned} \dot{\psi} &= \mathbf{H}\hat{\mathbf{g}} + \mathbf{K}(\mathbf{y} - \mathbf{S}\hat{\xi}), \\ \hat{\xi} &= \psi + \mathbf{R}\mathbf{y}, \end{aligned} \quad (6.5)$$

where $\hat{\mathbf{g}} = \mathbf{g}(\hat{\xi}, u)$, $\mathbf{R} \in \mathcal{R}^{4 \times 3}$, $\mathbf{H} = \mathbf{I} - \mathbf{RS}$, $\mathbf{I} \in \mathcal{R}^{4 \times 4}$ is a unit matrix, $\mathbf{K} \in \mathcal{R}^{4 \times 3}$ are the gain matrices to be designed.

Defining estimation error $\tilde{\xi} = \xi - \hat{\xi}$, and using (6.3), one has

$$\tilde{\xi} = \xi - \psi - \mathbf{RS}\xi = (\mathbf{I} - \mathbf{RS})\xi - \psi. \quad (6.6)$$

From (6.3), (5.7), (5.8), the derivative of $\tilde{\xi}$ is given by

$$\dot{\tilde{\xi}} = (\mathbf{I} - \mathbf{RS})(\mathbf{g} - \hat{\mathbf{g}}) + (\mathbf{I} - \mathbf{RS})\mathbf{E}\varphi - \mathbf{KS}\tilde{\xi}. \quad (6.7)$$

If one can make the following relationship holds:

$$(\mathbf{I} - \mathbf{RS})\mathbf{E} = \mathbf{0}. \quad (6.8)$$

Hence, the unknown input vector φ has been decoupled. The state estimation error dynamics (6.7) simplify to

$$\dot{\tilde{\xi}} = \mathbf{H}(\mathbf{g} - \hat{\mathbf{g}}) - \mathbf{KS}\tilde{\xi}. \quad (6.9)$$

The solution of (6.8) relies on the rank of matrix \mathbf{SE} . If the condition $\text{rank}(\mathbf{SE}) = \text{rank}(\mathbf{E})$ is satisfied, \mathbf{R} exists. Therefore, the robust NUIO (6.5) for the EHA (6.3) can be designed, and a special solution of (6.8) is derived by

$$\mathbf{R} = \mathbf{R}_1 + \mathbf{Y}\mathbf{R}_2, \quad (6.10)$$

where

$$\begin{aligned} \mathbf{R}_1 &= \mathbf{E} \left[(\mathbf{SE})^T (\mathbf{SE}) \right]^{-1} (\mathbf{SE})^T, \\ \mathbf{R}_2 &= \mathbf{I}_3 - \mathbf{SE} \left[(\mathbf{SE})^T (\mathbf{SE}) \right]^{-1} (\mathbf{SE})^T, \end{aligned} \quad (6.11)$$

and \mathbf{Y} is a gain matrix to be designed.

Theorem 6.1: If there exist a positive definite symmetric matrix $\mathbf{P} \in \mathcal{R}^{4 \times 4}$, and two matrices \mathbf{Y} , \mathbf{K} that satisfy the following inequality

$$-(\mathbf{PKS} + (\mathbf{KS})^T \mathbf{P} - \sigma \mathbf{PHH}^T \mathbf{P} - \sigma \mathbf{I}) < 0, \quad (6.12)$$

then (6.5) is the NUIO for sensor fault estimation of (6.3), and $\tilde{\xi} \rightarrow 0$ in a certain time.

Proof: Consider the Lyapunov function candidate V_{uio}

$$V_{uio} = \tilde{\xi}^T \mathbf{P} \tilde{\xi}. \quad (6.13)$$

Using (6.4), (6.9), the derivative of V_{uio} can be given by

$$\begin{aligned}
\dot{V}_{uio} &= -\tilde{\xi}^T (\mathbf{PKS} + (\mathbf{KS})^T \mathbf{P}) \tilde{\xi} + 2\tilde{\xi}^T \mathbf{PH} (\mathbf{g} - \hat{\mathbf{g}}) \\
&\leq -\tilde{\xi}^T (\mathbf{PKS} + (\mathbf{KS})^T \mathbf{P}) \tilde{\xi} + 2\sigma \|\tilde{\xi} \mathbf{PH}\| \|\tilde{\xi}\| \\
&\leq -\tilde{\xi}^T (\mathbf{PKS} + (\mathbf{KS})^T \mathbf{P}) \tilde{\xi} + \sigma \left(\|\tilde{\xi} \mathbf{PH}\|^2 + \|\tilde{\xi}\|^2 \right) \\
&= -\tilde{\xi}^T \left(\mathbf{PKS} + (\mathbf{KS})^T \mathbf{P} - \sigma \mathbf{PHH}^T \mathbf{P} - \sigma \mathbf{I} \right) \tilde{\xi} \\
&= -\tilde{\xi}^T \mathbf{\Pi} \tilde{\xi}.
\end{aligned} \tag{6.14}$$

Since $\mathbf{\Pi} > 0$ in terms of (6.12), one has $V_{uio} < 0$, which shows $\tilde{\xi}$ tends to zero asymptotically, i.e., $\tilde{\xi}_i \leq \zeta_{im}$ with ζ_{im} is a small positive constant. The Theorem 1 is proven.

Procedure 1: On the premise of Theorem 6.1, the design procedure of the NUIO for sensor fault estimation can be summarized as follow:

- 1) Determine $\mathbf{R}_1, \mathbf{R}_2$ according to formulas (6.11)
- 2) Solve the LMI (6.12) to achieve the matrices $\mathbf{P}, \mathbf{Y}, \mathbf{K}$.
- 3) Compute the other observer gain matrices \mathbf{R}, \mathbf{H} .

Remark 6.3: The NUIO in (6.5) is built for a sensor fault that depends on the structure of the vector \mathbf{D}_i . In this work, the three NUIOs are independently constructed to identify and detect the sensor fault. Among these observers, NUIO 1 is used for the position sensor fault that will feed the state estimation to the control law. Meanwhile, the NUIO 2 and NUIO 3 are utilized for the detection, and alarming proposes the velocity and load pressure sensor fault.

Remark 6.4: The control error is generated by subtracting displacement output with desired signal, and it is reconstructed under the position sensor fault. Because the aim is to perform a position tracking control task, the control errors of other sensor faults are not considered within the scope of this paper. In detail, the estimation value is compared with a threshold, once the i^{th} sensor becomes faulty, the control error will be calculated as $e_{1r} = x_{1r} - x_{1d}$. x_{1r} denotes the output value of the reconfiguration mechanism which is given by

$$x_{1r} = \begin{cases} y_1 & \text{if } |f_{s1}| \leq \mu_1, \\ \hat{y}_1 & \text{if } |f_{s1}| > \mu_1, \end{cases} \tag{6.15}$$

where μ_1 is a predefined threshold, x_{d1} is the desired signal. And the alarm of velocity and load pressure sensor is set when $|f_{si}| > \mu_i, i = 2, 3$ with μ_i are threshold values.

6.4 Observer-based fault-tolerant tracking control

As abovementioned, to handle the influence of the multiple sensor faults and matched, unmatched disturbance for the tracking problem, the FTC controller based on DSC method, NUIOs, and ESOs is constructed. Since the position, velocity, and load pressure sensor fault occurs, the estimation values of the component sensor of NUIO 1–3 are implemented instead of the measurement value to eliminate the influences of the sensor failure. Meanwhile, the design obstacle of lumped disturbance is mitigated by ESOs which provide real-time lumped disturbance compensation for the controller. The proposed FTC can preserve the system stability and acceptable performance of the whole closed-loop system under the effect of the multiple sensor faults and disturbances. The procedure control design procedure is presented as the following.

6.4.1 ESO design

The disturbance compensation module is designed to improve the performance tracking control for EHA. In this work, the ESOs are utilized to estimate both matched and unmatched disturbances in which the disturbance is extended as a new state. Then, the nonlinear system (6.3) with only position sensor fault can be reorganized as follows:

$$\begin{cases} \dot{x}_2 = f_2(x_2) + w_a x_3 + \varphi_1, \\ \dot{\varphi}_1 = q_1, \\ \dot{x}_3 = f_3(x_2, x_3) + w_b(x_3, u)u + \varphi_2, \\ \dot{\varphi}_2 = q_2. \end{cases} \quad (6.16)$$

Therefore, two ESOs can be elaborated as follows:

$$\begin{cases} \dot{\hat{x}}_2 = f_2(x_2) + w_a x_3 + \hat{\varphi}_1 + r_1 \varepsilon_1 (x_2 - \hat{x}_2), \\ \dot{\hat{\varphi}}_1 = r_2 \varepsilon_1^2 (x_2 - \hat{x}_2), \\ \dot{\hat{x}}_3 = f_3(x_2, x_3) + w_b(x_3, u)u + \hat{\varphi}_2 + r_3 \varepsilon_2 (x_3 - \hat{x}_3), \\ \dot{\hat{\varphi}}_2 = r_4 \varepsilon_2^2 (x_3 - \hat{x}_3), \end{cases} \quad (6.17)$$

where $\hat{\varphi}_1, \hat{\varphi}_2$ denote the estimate of φ_1, φ_2 ; r_1, r_2, r_3, r_4 , are positive constants; $\varepsilon_1, \varepsilon_2$ are the observer gain parameters which can be considered as the bandwidths of the ESOs.

The observer error dynamics are calculated by subtracting (6.16) to (6.17) and shown as

$$\begin{cases} \dot{\tilde{x}}_2 = -r_1 \varepsilon_1 \tilde{x}_2 + \tilde{\varphi}_1, \\ \dot{\tilde{\varphi}}_1 = -r_2 \varepsilon_1^2 \tilde{x}_2 + q_1, \end{cases} \leftrightarrow \begin{cases} \dot{\tilde{x}}_2 = -r_1 \varepsilon_1 \tilde{x}_2 + \tilde{\varphi}_1, \\ \frac{\dot{\tilde{\varphi}}_1}{\varepsilon_1} = -r_2 \varepsilon_1 \tilde{x}_2 + \frac{q_1}{\varepsilon_1}, \end{cases} \quad (6.18)$$

$$\begin{cases} \dot{\tilde{x}}_3 = -r_3 \varepsilon_2 \tilde{x}_3 + \tilde{\varphi}_2, \\ \dot{\tilde{\varphi}}_2 = -r_4 \varepsilon_2^2 \tilde{x}_3 + q_2, \end{cases} \leftrightarrow \begin{cases} \dot{\tilde{x}}_3 = -r_3 \varepsilon_2 \tilde{x}_3 + \tilde{\varphi}_2, \\ \frac{\dot{\tilde{\varphi}}_2}{\varepsilon_2} = -r_4 \varepsilon_2 \tilde{x}_3 + \frac{q_2}{\varepsilon_2}. \end{cases}$$

Define the disturbance error $\varpi_1 = \begin{bmatrix} \tilde{x}_2 & \tilde{\varphi}_1 / \varepsilon_1 \end{bmatrix}^T$, $\varpi_2 = \begin{bmatrix} \tilde{x}_3 & \tilde{\varphi}_2 / \varepsilon_2 \end{bmatrix}^T$. Take the derivative of ϖ_1, ϖ_2 as

$$\dot{\varpi}_i = \varepsilon_i \mathbf{A}_i \varpi_i + \mathbf{C}_i \frac{q_i}{\varepsilon_i}, i = 1, 2 \quad (6.19)$$

where $\mathbf{A}_1 = \begin{bmatrix} -r_1 & 1 \\ -r_2 & 0 \end{bmatrix}$, $\mathbf{A}_2 = \begin{bmatrix} -r_3 & 1 \\ -r_4 & 0 \end{bmatrix}$, $\mathbf{C}_1 = \begin{bmatrix} 0 \\ 1 \end{bmatrix}$, $\mathbf{C}_2 = \mathbf{C}_1$.

If \mathbf{A}_i ($i = 1, 2$) is the Hurwitz matrix, a positive definite matrix \mathbf{P}_i exists so that the following equality holds selected

$$\mathbf{A}_i^T \mathbf{P}_i + \mathbf{P}_i \mathbf{A}_i = -\mathbf{Q}_i, \quad (6.20)$$

where \mathbf{Q}_i is the symmetric positive definite matrix.

Theorem 6.2: For the EHA (6.1), with a set of big enough design parameters $\varepsilon_1, \varepsilon_2$ are selected, the ESO is constructed in (6.17) which can ensure the bounded estimation performance.

Proof:

Lyapunov function candidate V_{esoi} is selected as

$$V_{esoi} = \varpi_i^T \mathbf{P}_i \varpi_i. \quad (6.21)$$

Using (6.20), Assumption 1c, the derivative of V_{esoi} is calculated as

$$\begin{aligned} \dot{V}_{esoi} &= \dot{\varpi}_i^T \mathbf{P}_i \varpi_i + \varpi_i^T \mathbf{P}_i \dot{\varpi}_i \\ &= \varepsilon_i \varpi_i^T \left(\mathbf{A}_i^T \mathbf{P}_i + \mathbf{P}_i \mathbf{A}_i \right) \varpi_i + 2 \varpi_i^T \mathbf{P}_i \mathbf{C}_i \frac{q_i}{\varepsilon_i}. \end{aligned} \quad (6.22)$$

Applying Young's inequality, one obtains

$$2\varpi_i^T \mathbf{P}_i \mathbf{C}_i \frac{q_1}{\varepsilon_i} \leq \varpi_i^T \varpi_i + \frac{\Xi_i^2}{\varepsilon_i^2} (\mathbf{P}_i \mathbf{C}_i)^T \mathbf{P}_i \mathbf{C}_i. \quad (6.23)$$

The derivative of V_{esoi} is rewritten as

$$\dot{V}_{esoi} \leq -\varpi_i^T (\varepsilon_i \mathbf{Q}_i - \mathbf{I}) \varpi_i + \frac{\Xi_i^2}{\varepsilon_i^2} (\mathbf{P}_i \mathbf{C}_i)^T \mathbf{P}_i \mathbf{C}_i. \quad (6.24)$$

Then (6.24) becomes

$$\dot{V}_{esoi} \leq -a_i V_{esoi} + \frac{1}{\varepsilon_i^2} b_i, \quad (6.25)$$

where

$$\begin{aligned} a_i &= 2\lambda_{\min}(\varepsilon_i \mathbf{Q}_i - \mathbf{I}), \\ b_i &= \Xi_i^2 (\mathbf{P}_i \mathbf{C}_i)^T \mathbf{P}_i \mathbf{C}_i. \end{aligned} \quad (6.26)$$

From (17) and noting Lemma 1, the ESO errors for matched and unmatched disturbances are bounded by the compact sets as

$$\|\varpi_i\| \leq \sqrt{\frac{b_i}{\varepsilon_i^2 a_i}}, \quad (6.27)$$

Theorem 6.2 is verified.

6.4.2 FTC design with ESOs and NUIO

Since the position sensor fault is successfully detected and identified by NUIO 1, the reconfiguration mechanism is performed by switching between estimation and measurement value. Meanwhile, the matched, unmatched disturbance are estimated by two ESOs. Both the obtained results of NUIO 1 and ESOs will feed to the DSC-based FTC controller that is presented as follows:

Step 1: Define tracking errors, we have

$$\begin{aligned} e_1 &= x_1 - x_{1d}, \\ \varsigma_1 &= x_1 - x_{1r}, \\ e_i &= x_i - \alpha_{i-1}, \quad i = 2, 3 \end{aligned} \quad (6.28)$$

where x_{1d} is the reference signal, α_{i-1} represents the virtual controller, which need to be designed.

To eliminate the influences of ‘‘explosion of complexity’’ caused by the backstepping iteration and achieve the objective, we will deploy the DSC technique to perform the design task. Considering a first-order filter κ_1 , the command filter is elaborated as

$$\tau_1 \dot{\kappa}_1 + \kappa_1 = x_{1d}, \kappa_1(0) = x_{1d}(0), \quad (6.29)$$

where τ_1 is positive coefficient.

Defining the error compensation $z_1 = \kappa_1 - x_{1d}$ for the filter, its derivative is computed as:

$$\dot{z}_1 = \dot{\kappa}_1 - \dot{x}_{1d} = -\tau_1^{-1} z_1 - \dot{x}_{1d}, \quad (6.30)$$

The virtual control law α_1 is constructed with noting Remark 6.2 and (6.28), one yields

$$\alpha_1 = \dot{\kappa}_1 - \lambda_1 e_{1r} = \dot{\kappa}_1 - \lambda_1 e_1 + \lambda_1 \varsigma_1, \quad (6.31)$$

where λ_1 is a control gain and a positive constant.

Lyapunov function candidate V_1 is chosen as

$$V_1 = \frac{1}{2} e_1^2 + \frac{1}{2} z_1^2. \quad (6.32)$$

Differentiating (6.32) with respect to time, it follows that:

$$\begin{aligned} \dot{V}_1 &= e_1 (\dot{z}_1 - \lambda_1 e_1 + \lambda_1 \varsigma_1 + e_2) + z_1 (-\tau_1^{-1} z_1 - \dot{x}_{1d}) \\ &= -\lambda_1 e_1^2 + \lambda_1 \varsigma_1 e_1 + e_1 e_2 + e_1 (-\tau_1^{-1} z_1 - \dot{x}_{1d}) + z_1 (-\tau_1^{-1} z_1 - \dot{x}_{1d}), \end{aligned} \quad (6.33)$$

Using Young’s inequality, one yields

$$\begin{aligned} -e_1 \tau_1^{-1} z_1 &\leq \frac{1}{2\tau_1^2} e_1^2 + \frac{1}{2} z_1^2, -e_1 \dot{x}_{1d} \leq \frac{1}{2} e_1^2 + \frac{1}{2} \|\dot{x}_{1d}\|^2, \\ \varsigma_1 e_1 &\leq \frac{1}{2} \varsigma_{1m}^2 + \frac{1}{2} e_1^2, -z_1 \dot{x}_{1d} \leq \frac{1}{2} z_1^2 + \frac{1}{2} \|\dot{x}_{1d}\|^2, \end{aligned} \quad (6.34)$$

where ς_{1m} is a positive constant.

The derivative of V_1 reduces as

$$\dot{V}_1 \leq -\left(\frac{\lambda_1}{2} - \frac{\tau_1^{-2} + 1}{2}\right) e_1^2 + e_1 e_2 - (\tau_1^{-1} - 1) z_1^2 + \frac{1}{2} \rho_1^2 + \frac{\lambda_1}{2} \varsigma_{1m}^2. \quad (6.35)$$

Step 2: Then, a similar approach to step 1 is applied to derive the virtual controller α_2 . The command filter can be constructed as follows:

$$\tau_2 \dot{\kappa}_2 + \kappa_2 = \alpha_1, \kappa_2(0) = \alpha_1(0), \tau_2 > 0, \quad (6.36)$$

where τ_2 is a positive scalar.

Denotes $z_2 = \kappa_2 - \alpha_1$ for command filter, the filter error dynamics is given by:

$$\begin{aligned}\dot{z}_2 &= \dot{\kappa}_2 - \dot{\alpha}_1 = -\tau_2^{-1}z_2 + \left(\frac{\partial \alpha_1}{\partial e_1} \dot{e}_1 + \frac{\partial \alpha_1}{\partial \kappa_1} \dot{\kappa}_1 \right) \\ &= -\tau_2^{-1}z_2 + \gamma_1,\end{aligned}\quad (6.37)$$

where $\gamma_1(e_1, \kappa_1)$ represents a continuous function, and $\|\gamma_1(e_1, \kappa_1)\| \leq \gamma_{1m}$.

The virtual control law α_2 is constructed as

$$\alpha_2 = \frac{1}{w_a} (\dot{\kappa}_2 - \lambda_2 e_2 - e_1 - f_2 - \hat{\varphi}_1), \quad \lambda_2 > 0, \quad (6.38)$$

where λ_2 is a control gain and a positive constant.

Considering the Lyapunov function as follows:

$$V_2 = \frac{1}{2} e_2^2 + \frac{1}{2} z_2^2. \quad (6.39)$$

and differentiating V_2 with respect to time, we have:

$$\begin{aligned}\dot{V}_2 &= e_2 \left(-\tau_2^{-1}z_2 + \gamma_1 - \lambda_2 e_2 + e_3 + \tilde{\varphi}_1 - e_1 \right) \\ &\quad + z_2 \left(-\tau_2^{-1}z_2 + \gamma_1 \right).\end{aligned}\quad (6.40)$$

Applying Young's inequality, one gets:

$$\begin{aligned}-e_2 \tau_2^{-1} z_2 &\leq \frac{1}{2} \tau_2^{-2} e_2^2 + \frac{1}{2} z_2^2, \\ e_2 \gamma_1 &\leq \frac{1}{2} e_2^2 + \frac{1}{2} \gamma_{1m}^2, \\ e_2 \tilde{\varphi}_1 &\leq \frac{1}{2} e_2^2 + \frac{1}{2} \Xi_1^2.\end{aligned}\quad (6.41)$$

From (5.35), (5.36), (5.34) can then be simplified to

$$\begin{aligned}\dot{V}_2 &\leq -\left(\lambda_2 - \frac{\tau_2^{-2} + 2}{2} \right) e_2^2 + e_2 e_3 - \left(\tau_2^{-1} - \frac{1}{2} \right) z_2^2 \\ &\quad - e_1 e_2 + \frac{1}{2} \gamma_{1m}^2 + \frac{1}{2} \Xi_1^2.\end{aligned}\quad (6.42)$$

Step 3: This step gives the final control input. The virtual controller α_2 pass through a first-order filter κ_3 as

$$\tau_3 \dot{\kappa}_3 + \kappa_3 = \alpha_2, \kappa_3(0) = \alpha_2(0), \tau_3 > 0. \quad (6.43)$$

Define $z_3 = \kappa_3 - \alpha_2$, one has

$$\begin{aligned} \dot{z}_3 &= \dot{\kappa}_3 - \dot{\alpha}_2 = -\tau_3^{-1} z_3 + \left(\frac{\partial \alpha_2}{\partial e_2} \dot{e}_2 + \frac{\partial \alpha_2}{\partial \kappa_2} \dot{\kappa}_2 \right) \\ &= -\tau_3^{-1} z_3 + \gamma_2. \end{aligned} \quad (6.44)$$

where $\gamma_2(e_2, \kappa_2)$ represents a continuous function and satisfies $\|\gamma_2(e_2, \kappa_2)\| \leq \gamma_{2m}$.

The input signal u can be designed by

$$u = \frac{1}{w_b} (\dot{\kappa}_3 - \lambda_3 e_3 - f_3 - e_2 - \hat{\varphi}_2), \lambda_3 > 0. \quad (6.45)$$

The Lyapunov function be selected as follows:

$$V_3 = \frac{1}{2} e_3^2 + \frac{1}{2} z_3^2. \quad (6.46)$$

The time derivative of V_3 is achieved as follows:

$$\begin{aligned} \dot{V}_3 &= e_3 (-\tau_3^{-1} z_3 + \gamma_2 - \lambda_3 e_3 + \tilde{\varphi}_2 - e_2) + z_3 (-\tau_3^{-1} z_3 + \gamma_2) \\ &\leq -\left(\lambda_2 - \frac{\tau_3^{-2} + 2}{2} \right) e_3^2 - e_2 e_3 - \left(\tau_3^{-1} - \frac{1}{2} \right) z_3^2 + \frac{1}{2} \gamma_{2m}^2 + \frac{1}{2} \Xi_2^2. \end{aligned} \quad (6.47)$$

Theorem 6.3: For the EHA dynamics reported by (6.3), with the designed NUIO in (6.5), if the ESOs are developed as (6.17), the control law carried out by (6.45). It can be revealed that all system states e_i, z_i are uniformly ultimate boundedness in the presence of lumped disturbances, and faulty conditions.

Proof:

The positive-definite Lyapunov function candidate expressed as

$$V = V_1 + V_2 + V_3. \quad (6.48)$$

Taking the derivative of V , we obtain

$$\begin{aligned} \dot{V} &\leq -\left(\frac{\lambda_1}{2} - \frac{\tau_1^{-2} + 1}{2} \right) e_1^2 - \sum_{i=2,3} \left(\lambda_i - \frac{\tau_i^{-2} + 2}{2} \right) e_i^2 - (\tau_1^{-1} - 1) z_1^2 \\ &\quad - \sum_{i=2,3} \left(\tau_i^{-1} - \frac{1}{2} \right) z_i^2 + \frac{1}{2} \rho_1^2 + \frac{\lambda_1}{2} \varsigma_{1m}^2 + \sum_{j=1,2} \left(\frac{1}{2} \gamma_{jm}^2 + \frac{1}{2} \Xi_j^2 \right) \\ &\leq -a_l V + b_l, \end{aligned} \quad (6.49)$$

where

$$a_t = \min \left(\begin{array}{l} \lambda_{\min}(\lambda_1 - \tau_1^{-2} - 1), \lambda_{\min}(2\lambda_i - \tau_i^{-2} - 2), \\ \lambda_{\min}(2\tau_1^{-1} - 2), \lambda_{\min}((2\tau_i^{-1} - 1)) \end{array} \right),$$

$$b_t = \frac{1}{2}\rho_1^2 + \frac{\lambda_1}{2}\zeta_{1m}^2 + \sum_{j=1}^2 \left(\frac{1}{2}\gamma_{jm}^2 + \frac{1}{2}\Xi_j^2 \right).$$

Further analysis of (5.40) can get

$$V \leq \left(V(0) - \frac{b_t}{a_t} \right) e^{-at} + \frac{b_t}{a_t} \leq \Lambda, \quad (6.50)$$

where $\Lambda = V(0) + b_t/a_t$.

From (6.50), we have $\lim_{t \rightarrow \infty} V = b_t/a_t$ and according to the Lemma 1, it can imply that the variables e_i , z_i are uniformly bounded. In addition, the error variables e_1 , e_2 , and e_3 are bounded by the compact sets U_{e1} , U_{e2} , U_{e3} respectively, defined as follows:

$$U_{e1} = \left\{ e_1 \in R \mid e_1 \leq \sqrt{\frac{b_t}{\lambda_{\min}(\lambda_1 - (\tau_1^{-2} + 1))}} \right\},$$

$$U_{e2} = \left\{ e_2 \in R \mid e_2 \leq \sqrt{\frac{b_t}{\lambda_{\min}(\lambda_2 - 0.5(\tau_2^{-2} + 2))}} \right\}, \quad (6.51)$$

$$U_{e3} = \left\{ e_3 \in R \mid e_3 \leq \sqrt{\frac{b_t}{\lambda_{\min}(\lambda_3 - 0.5(\tau_3^{-2} + 2))}} \right\}.$$

Therefore, Theorem 6.3 is proven.

6.5 Simulation results

6.5.1 Simulation setup

Simulations were performed by MATLAB/Simulink to evaluate the position tracking performance of the proposed controller under the impact of sensor fault and lumped uncertainties. The displacement demand is sinusoidal signal, i.e., $x_{1d} = 10(1 - \cos(\pi t))(1 - \exp(-t))$ (mm) and multistep reference tracking. Table 3.2 provides the actuator physical parameters.

The controller parameters of the suggested controller, i.e., DSC technique-based FTC controller with two ESOs and NUIO, described in Section 6.3, are listed as: $\lambda_1 = 50$; $\lambda_2 = 150$; $\lambda_3 = 25$; $\tau_1 = \tau_2 = \tau_3 = 0.05$. The ESO parameters are tuned as $r_1 = r_3 = 2$; $r_2 = r_4 = 1$; $\varepsilon_1 = 100$; $\varepsilon_2 = 150$. The predefined threshold value of position, velocity, and load pressure sensor are carefully set as $\mu_1 = \pm 4$ (mm), $\mu_2 = \pm 30$ (mm/s), $\mu_3 = \pm 1.5$ (bar), respectively. The NUIO parameters are determined by following the Procedure 1, shown as:

$$\begin{aligned} \text{NUIO1: } \mathbf{H} &= \begin{bmatrix} 1 & 0 & 0 & 0 \\ 0 & 1 & 0 & 0 \\ 0 & 0 & 1 & 0 \\ -1 & 0 & 0 & 0 \end{bmatrix}, \mathbf{K} = \begin{bmatrix} 0 & -0.005 & 0 \\ 0 & 300 & 0 \\ 0 & 0 & 260 \\ 1.99 & -0.005 & 0 \end{bmatrix}, \mathbf{R} = \begin{bmatrix} 0 & 0 & 0 \\ 0 & -1 & 0 \\ 0 & 0 & -1 \\ 1 & 0 & 0 \end{bmatrix}, \\ \text{NUIO2: } \mathbf{H} &= \begin{bmatrix} 1 & 0 & 0 & 0 \\ 0 & 1 & 0 & 0 \\ 0 & 0 & 1 & 0 \\ 0 & -1 & 0 & 0 \end{bmatrix}, \mathbf{K} = \begin{bmatrix} 300 & 0 & 0 \\ 0 & 0 & -0.005 \\ 0 & 0 & 260 \\ 777 & 1.99 & -0.005 \end{bmatrix}, \mathbf{R} = \begin{bmatrix} 0 & 0 & 0 \\ 0 & 0 & 0 \\ 0 & 0 & -1 \\ 0 & 1 & 0 \end{bmatrix}, \\ \text{NUIO3: } \mathbf{H} &= \begin{bmatrix} 1 & 0 & 0 & 0 \\ 0 & 1 & 0 & 0 \\ 0 & 0 & 1 & 0 \\ 0 & 0 & -1 & 0 \end{bmatrix}, \mathbf{K} = \begin{bmatrix} 300 & -0.005 & 0 \\ 0 & 300 & 0 \\ 0 & 0.015 & 0 \\ 777 & 0.015 & 1.99 \end{bmatrix}, \mathbf{R} = \begin{bmatrix} 0 & 0 & 0 \\ 0 & -1 & 0 \\ 0 & 0 & 0 \\ 0 & 0 & 1 \end{bmatrix}. \end{aligned}$$

To make a comparison, the other two controllers are also applied for the EHA: Strategy 1 is the control algorithm which is same as the proposed controller but without NUIO (DSESO) while Strategy 2 is the same as proposed controller but without two ESOs (DSNUIO). For fairness, all design parameters of these controllers are set the same as the corresponding parameters of the suggested controller.

In order to study the validity of the proposed control in the presence of sensor faults and lumped disturbances, the following two parts were performed:

1) Sensor faults separately and simultaneously occur one at a time such as position, velocity, and load pressure sensor fault. The purpose of this part is to verify the effectiveness of the three NUIOs for fault detection and fault estimation.

2) Sensor faults simultaneously happen in above-mentioned sensor fault. Besides, the matched and unmatched disturbances are also appeared. The purpose of this part is to

demonstrate the effectiveness of the proposed controller for position tracking control problem under multiple sensor fault conditions.

6.5.2 Simulation result

a) NUIO performance validation

In this simulation, the fault detection of the three different fault types was conducted: 1) Fault in position sensor with $d_{s1} = -1$; $\theta_{s1} = 20 + 5\sin\pi t$; 2) Fault in velocity sensor with $d_{s2} = -1$; $\theta_{s2} = -70 + 10\text{sawtooth}(\pi t)$; 3) Fault in load pressure sensor with $d_{s3} = -1$; $\theta_{s3} = 5$.

For the case separately occurrence fault, at the time $t = 5\text{s}$, the sensor fault happens. The estimation performance of three NUIOs is given in Figures 6.3–6.5. As seen in Figures 6.3–6.5, it is clear that three NUIOs estimated the fault accurately. Moreover, the estimation value of every sensor fault is within the thresholds in the normal state while it exceeds the thresholds in the fault state. For fault detection, the value “1” and “0” reveals whether a fault can be detected or not. When the sensor fault is identified, and its estimation value exceeds the predefined thresholds, the NUIO successfully detects a fault. This indicated that the faults happened in position, velocity, or load pressure sensor and the respective fault flag was set as 1. Hence, the alarm will be activated to notify the operator or engineer, and the fault then needs to be fixed. Besides, three above sensor fault types can be effectively isolated via three NUIOs.

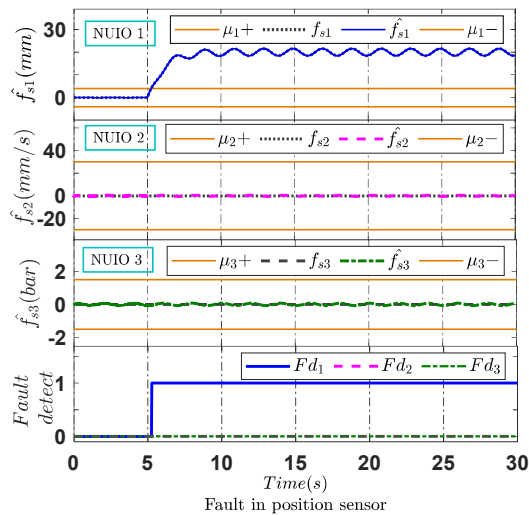


Figure 6.3 FDEI of NUIOs in case of only fault in position sensor.

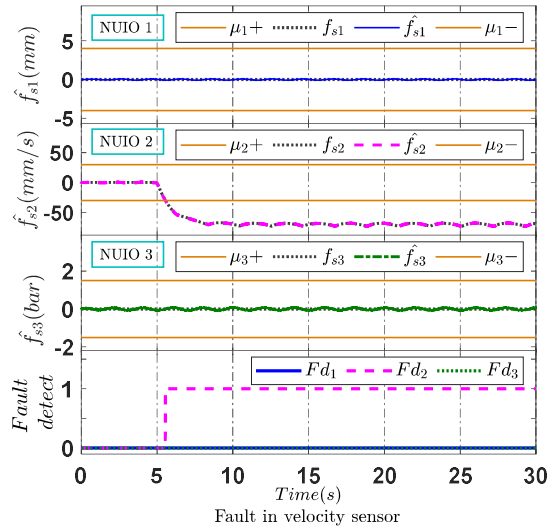


Figure 6.4 FDEI of NUIOs in case of only fault in velocity sensor.

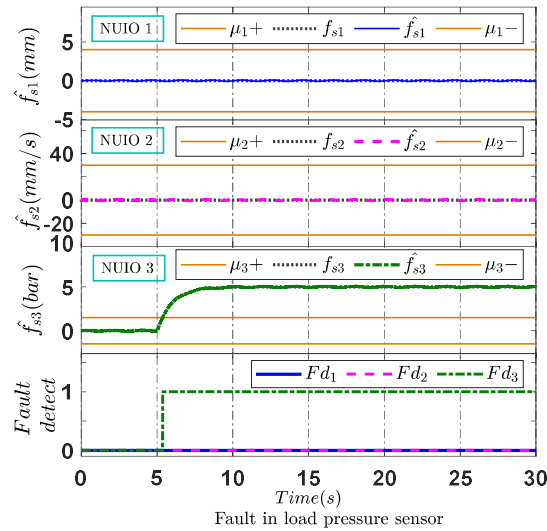


Figure 6.5 FDEI of NUIOs in case of only fault in pressure sensor.

For the case simultaneously occurrence fault, at the time $t = 5s$, three sensor faults happen. The estimation performance of three NUIOs is given in Figure 6.6. It can be seen that every designed fault observer can effectively approximate the relevant sensor fault. Furthermore, the location of the faults is determined through the three NUIOs. The simulation results confirm the reliability and the effectiveness of the fault diagnosis algorithm in both case studies including separately and simultaneously fault appearance.

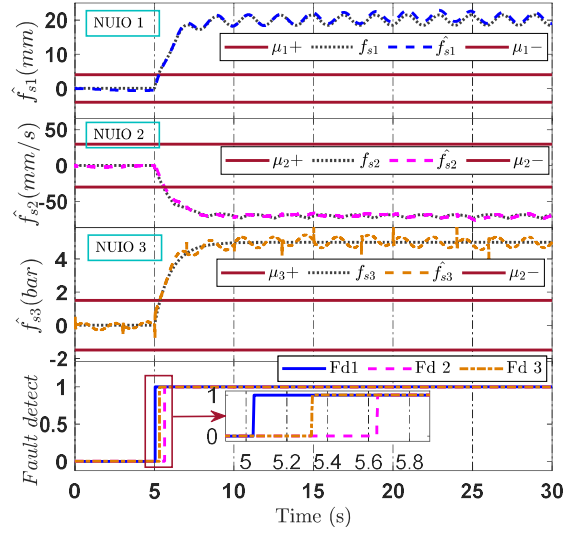


Figure 6.6 FDEI of NUIOs in case of simultaneous fault.

Remark 6.5: In this study, although the all-sensor faults occur at the same time $t = 5s$, the sensor faults (i.e., position, velocity, and pressure sensor faults) are detected at different times, in turn, 5.26s, 5.55s, 5.37s. This fact ensures that the condition $rank(\mathbf{SE}) = rank(\mathbf{E})$ for (13) is satisfied. Therefore, the proposed FTC scheme with three NUIOs can effectively work under sensor faulty conditions.

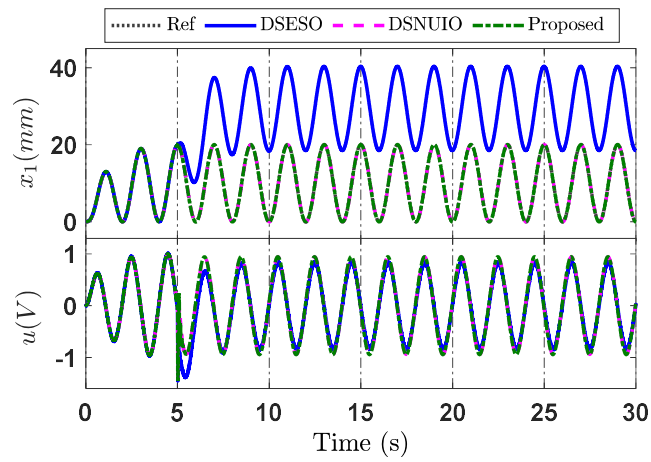
b) Tracking performance validation

In this part, to demonstrate the performance of the proposed controller in position tracking control problem, two demand signals are applied under the displacement sensor fault and lumped uncertainties. The position sensor fault and other sensor faults appear at the time $t = 5s$. Hereby, a reconfigurable mechanism is introduced for position tracking control issue. By using the achieved sensor fault information, the faulty sensor is switched to the estimated output from the NUIO 1 since a position sensor fault is detected.

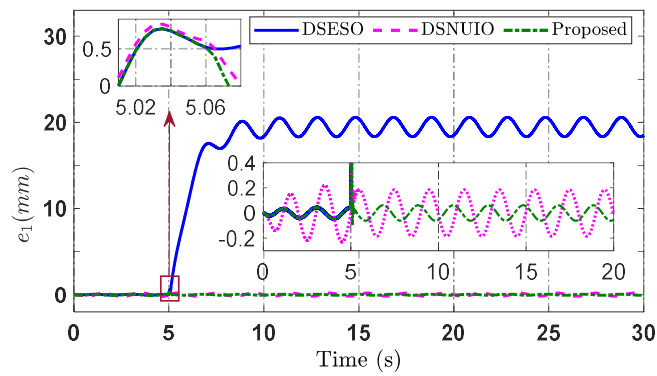
Case 1: Sinusoidal reference tracking

Firstly, the obtained results of three controllers are depicted in Figure 6.7 that indicates the position tracking performance, the tracking error, and the control inputs, respectively. With reference to Figure 6.7a, the DSESO performs the worst tracking performance under the position sensor fault due to the lack of compensation of NUIO. Especially, the tracking error of DSESO is great since the sensor fault occurs at time $t = 5s$. On the contrary, the relevant controllers, i.e., the proposed controller, DSNUIO can tackle the effect of the displacement

sensor fault because of the support of the NUIO. However, the proposed controller provides better tracking performance than the DSNUIO controller by benefiting from ESOs to approximate matched and unmatched disturbances in real time. The zoom in of tracking error in Figure 6.7b implies that the suggested controller has the smallest error as compared to other controllers. Besides, the control effort u of the contrastive three controllers can be exhibited in the second subgraph of Figure 6.7a, which is significantly adjusted after the detection of a fault.



a)



b)

Figure 6.7 Performances of comparative controllers in case 1

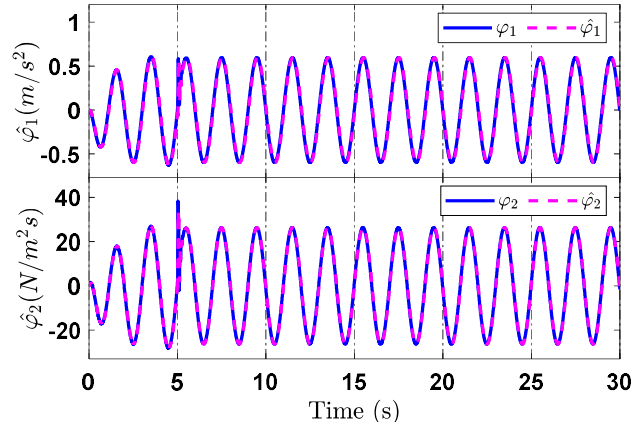


Figure 6.8 Lumped disturbance estimation of ESOs in case 1

In addition, the estimation performance of the two ESOs are displayed in Figure 6.8. From Figure 6.8, we can see that the lumped disturbances are successfully estimated. Hence, it will be compensated feedforwardly through the procedure control design. It is noteworthy that their estimation performance can be further enhanced when the design parameters ε_1 , ε_2 are increased. Nonetheless, this causes a trade-off between the estimation performance and the system stability.

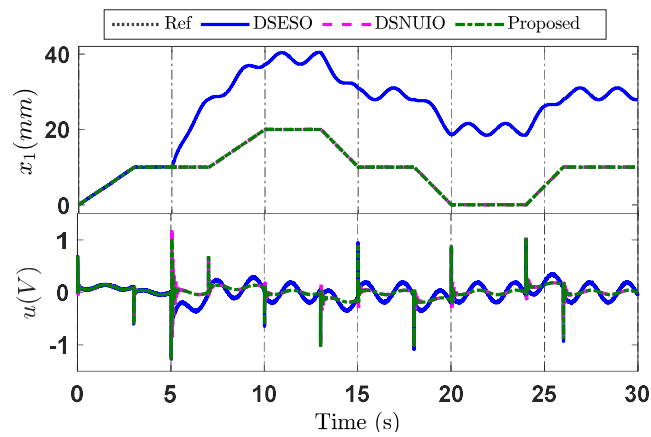
Table 6.1 Summary of performance indices

	Controller	Proposed	DSNUIO	DSESO
Case 1	RMS (mm)	0.046	0.1337	17.1859
	$\max(e_i)$ (mm)	0.5087	0.5336	20.5805
Case 2	RMS (mm)	0.0179	0.0466	17.2089
	$\max(e_i)$ (mm)	0.4843	0.4916	21.5574

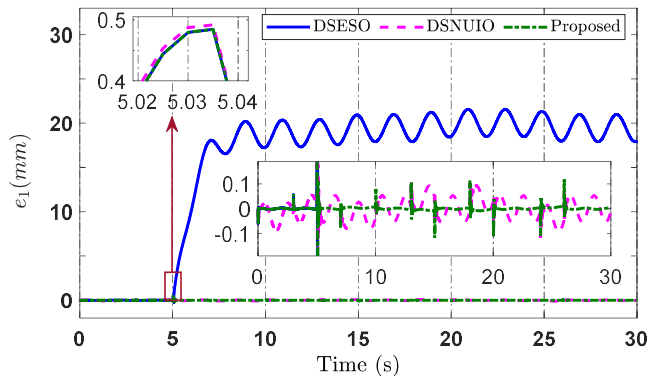
Case 2: Multistep reference tracking

To further verify the robustness of the proposed methodology, the multistep trajectory is given. The position tracking performance of three controllers are displayed in the first subgraph of Figure 6.9a which reveals that x_1 can track x_{1d} under healthy condition ($t < 5s$). However, since multiple sensor faults happen, the output response of the DSESO without NUIO cannot tracking the reference signal x_{1d} . Meanwhile, owing the effectiveness of the fault detection and estimation from NUIO, the DSNUIO and proposed can ensure the tracking

error as small as possible. Furthermore, as seen from the zoom in of the tracking error in Figure 6.9b, the proposed controller exhibits better tracking performance than that of DSNUIO, this demonstrates the advantage of the synthesized ESOs. The control input of all controllers shown on the final subgraph of Figure 6.9a, which are strongly regulated to adopt the sensor fault at $t = 5$ s. It can be observed that the control efforts are impacted when the fault is detected.



a)



b)

Figure 6.9 Tracking performance of different control methods in case 2

The estimation performance of two ESOs in this case is presented in Figure 6.10. From Figure 6.10, it indicates that the estimated matched and unmatched disturbance can track its physical value as closely as possible, which further verifies good estimate performance of the designed ESO observers.

Furthermore, to quantitatively evaluate the robustness of the three controllers, the two performance indexes are computed, i.e., the RMS value ($\sqrt{(1/T)\int_0^T e_i^2(t)dt}$, where T is the time period) and maximum error ($\max(e_i)$). Using the tracking error data from Figure 6.7 and Figure 6.9, the result of performance indexes of the relevant controller is summarized in Table 2. It is worth mentioning that for each case, the suggested controller has the smallest RMS error as well as maximum error in comparison with other controllers. This reconfirms the high control precision and strong robustness of the proposed algorithm under the multiple sensor faults and lumped disturbances.

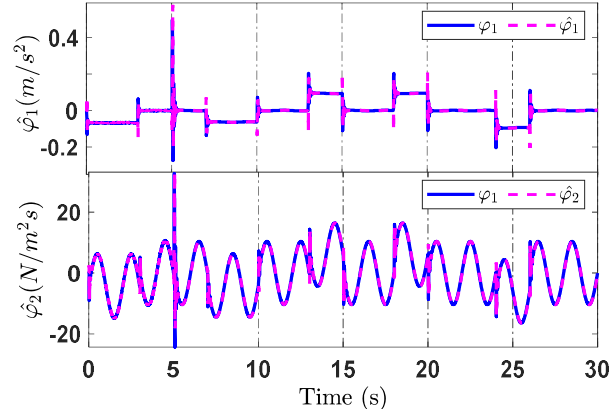


Figure 6.10 Lumped disturbance estimation of ESOs in case 2

Case 3: Multistep reference tracking with different lumped disturbance

To further validate the effectiveness of the proposed method against disturbances under sensor faults, we perform the simulation with different lumped disturbances and compare it with the DSNUIO. The matched, unmatched disturbances are adjusted which increases the challenge of the designed controller. For instance, the friction force value changes from $10x_2 + 50\text{sign}(x_2)$ to $20x_2 + 100\text{sign}(x_2)$, and the leakage disturbance $Q_f = -C_t\sqrt{|x_3|}\text{sign}(x_3)$,

$C_t = 2.5 \times 10^{-8}$ is added to matched disturbance $\varphi_2 = \frac{4\beta_e}{V_c}(Q_t + Q_f) + \Delta_2$ after 10s. The

estimation performance of the two ESOs, in this case, is displayed in Figure 6.11 while overall tracking errors are depicted in Figure 6.12. From Figure 6.12, it can be seen that the tracking error of DCNUIO becomes worse and unstable, especially after 10s, due to the lack of disturbance compensation. Meanwhile, the proposed controller brings less tracking error

thanks to ESOs as a compensation part. The result of maximum errors is 0.5324 (proposed controller) and 0.4655 (DSNUIO) in case 3, it confirms the efficacy of the proposed strategy over the DSNUIO method.

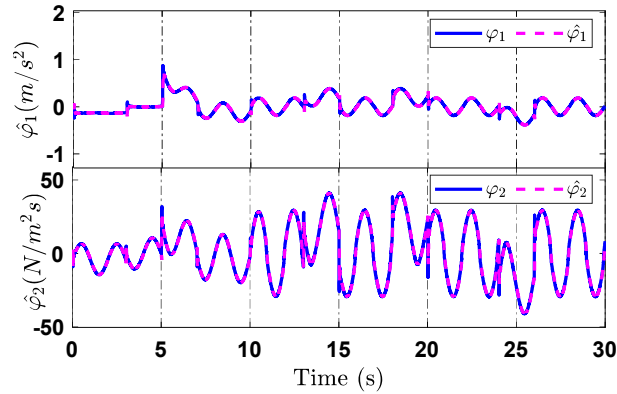


Figure 6.11 Lumped disturbance estimation of ESOs in case 3

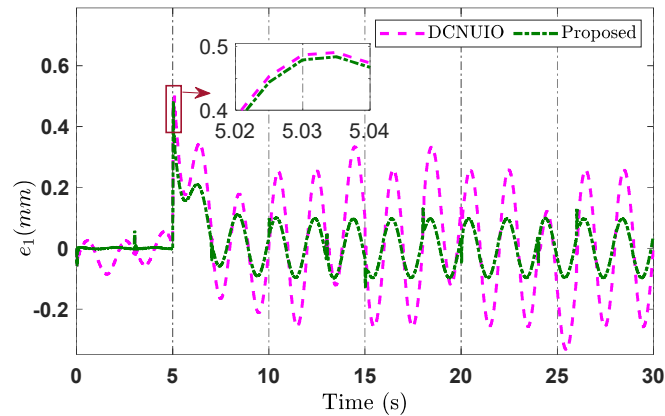


Figure 6.12 Tracking errors of two control methods in case 3

According to the achieved simulation results, we can conclude that the proposed FTC exhibits superior tracking performance and can ensure the stability condition in the presence of the matched, unmatched disturbances, multiple sensor faults.

6.6 Chapter summary

In this chapter, the proposed FTC scheme is elaborated and applied for the dynamics model of EHA to overcome the influences of the negative factors such as disturbance/uncertainties, and multiple sensor faults. This is the first time, three NUIOs are deployed to detect and estimate the simultaneously sensor faults, i.e., position, velocity, or

load pressure sensor fault. Every sensor fault is successfully identified and isolated that validates the effectiveness of the suggested NUIO. Next, the position tracking control problem is considered under the multiple sensor faults and lumped disturbance. The ESOs are employed to deal with the matched, unmatched disturbance and further enhance tracking performance of the closed-loop system. Meanwhile, the NUIO 1 is used to provide the exact estimated position value when the position sensor fault appears. The DSC handles the derivative explosion phenomena when computing the derivatives of virtual control laws. The advanced FTC scheme comprises of DSC, NUIO, ESO that provides a continuous tracking control regardless of sensor fault and disturbances. System stability and asymptotic tracking convergence were verified by the Lyapunov theory. The comparison results have been conducted to demonstrate effectiveness of the proposed algorithm.

CHAPTER 7

CONCLUSION AND FUTURE WORKS

7.1 Conclusion

This thesis presents some effective FD and fault-tolerant tracking control design for an EHA system. First of all, the overview of FD and FTC is discussed and reported. The mathematical model of EHA system is then formulated in the face of the lumped disturbance (i.e., matched and mismatched disturbance). The lumped disturbance comprises of parametric uncertainties (i.e., the unknown friction, leakage coefficients, unmodeled dynamics) and time-varying disturbance (i.e., external load). The possible system faults in the EHA system are also carried out such as actuator fault and sensor fault. For actuator faults, the internal leakage fault, the LOE fault caused by drop in supply pressure of a hydraulic power supply or fault in a servo-valve are considered. For sensor faults, the position, velocity, and pressure sensor, are given in this thesis.

To deal with disturbances/uncertainties, an effective control technique, called an observer-based nonlinear controller, was developed to cope with the disturbances and uncertainties of the EHA. The core idea of this approach is to create an observer to approximate the different disturbances in the system and then mitigate their effect through a control design procedure. Various disturbance observers were induced in this thesis, such as time delay estimation in chapter 4, nonlinear disturbance observer in chapter 5, and ESO in chapter 6. These observers are used as an efficient tool for disturbance compensation.

To cope with the internal leakage fault-tolerant tracking control problem of the real EHA system, a TDE combined FBL, adaptive ISMC (AISM) technique is presented in chapter 4. Firstly, a coordinate transformation is used to convert the original system becoming a linear system to reject the inherent nonlinear features. Besides, the new lumped uncertainty is formulated including matched, mismatched disturbance, and the fault. Next, the FDTDE technique is deployed to approximate the given lumped uncertainty. The fault is successfully detected and accommodated when the estimated new lumped uncertainty is larger than a predefined threshold. Then, the estimated value via the TDE, and an adaptive law are

integrated into the ISMC which increases the robustness property to against the lumped disturbances, and faults. The proposed FTC exhibits high precision tracking control as well as system stability under both healthy and faulty conditions.

Besides, the proposed FTC scheme in chapter 5 for an EHA system is developed by using the BLF-CFC, NDO, and an adaptive law for a reconfigurable controller that ensures the system stability and constraint condition under lumped uncertainties, and multiple actuator faults. It is noteworthy that bias fault or LOE fault is individually considered in the previous works. There are very few works that attempt to deal with both the bias fault and the LOE fault in EHA systems. This thesis investigated the FTC problem for the practical hydraulic system to simultaneously solve the position constraint, lumped disturbances, internal leakage fault, and partial LOE faults which make the designed controller more feasible for practical applications.

To solve adverse problems, including multiple sensor faults and matched and unmatched disturbances, chapter 6 provides the advanced FTC method for the EHA system. Herein, fault observers are constructed to simultaneously estimate the sensor faults (i.e., position, velocity, and load pressure sensor fault) under the influences of the lumped disturbance. The NUIO-based FDEI is accommodated to detect and isolate the sensor faults in real-time successfully even if three faults simultaneously occur.

7.2 Future works

Although this thesis considered the lumped and faults problem for EHA problem. Nonetheless, this thesis still has some limitations. Many of interesting studies relate to EHA system and its applications will be developed in future work:

- The development of the proposed FTC will be studied to deal with the simultaneous faults, i.e., sensor fault, actuator fault and achieve the prescribed tracking performance.
- The influences of the measurement noises and other type of sensor faults (i.e., bias and loss of effectiveness sensor fault) to the system control performance will be considered. In addition, the relevant experimental data with multi-sensor and actuator fault diagnosis will be investigated.

- The optimal tuning mechanism to tune control parameters of the proposed FTC will be investigated to achieve the better tracking performance.

- The observer-based finite-time trajectory tracking FTC will be investigated to improve the tracking response.

PUBLICATIONS

A. International Journals

1. V. D. Phan, C. P. Vo, H. V. Dao and K. K. Ahn, "Robust Fault-Tolerant Control of an Electro-Hydraulic Actuator with a Novel Nonlinear Unknown Input Observer," in *IEEE Access*, vol. 9, pp. 30750-30760, 2021, doi: 10.1109/ACCESS.2021.3059947.
2. V. D. Phan, C. P. Vo, H. V. Dao, and K. K. Ahn, "Actuator Fault-Tolerant Control for an Electro-Hydraulic Actuator Using Time Delay Estimation and Feedback Linearization," *IEEE Access*, vol. 9, pp. 107111-107123, 2021, doi: 10.1109/ACCESS.2021.3101038.
3. V. D. Phan and K. K. Ahn. Optimized-Based Fault-Tolerant Control of an Electro-Hydraulic System with Disturbance Rejection. *Appl. Sci.* 2022, 12.
4. V. D. Phan, H. V. A. Truong, and K. K. Ahn. Actuator failure compensation-based command filtered control of electro-hydraulic system with position constraint. *ISA Transactions*, vol. 134, pp. 561-572, 2023.
5. V. D. Phan, H.-A. Trinh, and K. K. Ahn. Design and evaluation of adaptive neural fuzzy-based pressure control for PEM fuel cell system. *Energy Rep.* 2022, 8, 12026-12037.
6. V. D. Phan, H.-A. Trinh, and K. K. Ahn. Finite-Time Command Filtered Control for Oxygen-Excess Ratio of PEM Fuel Cell Systems with Prescribed Performance. *Mathematics*, 2023, 11(4), 914.
7. V. D. Phan and K. K. Ahn, "Fault-tolerant Control for an Electro-Hydraulic Servo System with Sensor Fault Compensation and Disturbance Rejection," in *Nonlinear Dynamics*, vol. 111, pp. 10131-10146, 2023.
8. H.-A. Trinh, V. D. Phan, H. V. A. Truong, and K. K. Ahn. Energy Management Strategy for PEM Fuel Cell Hybrid Power System Considering DC Bus Voltage Regulation. *Electronics* 2022, 11, 2722.
9. H.-A. Trinh, D. G. Nguyen, V. D. Phan, T-Q. Duong, H. V. A. Truong, S-J. Choi, and K. K. Ahn, Robust adaptive control strategy for a bidirectional DC-DC converter based on extremum seeking and sliding mode control. *Sensors* 2023, 23(1), 457, doi: 10.3390/s23010457.

10. C. P. Vo, V. D. Phan, T. H. Nguyen, and K. K. Ahn, "A compact adjustable stiffness rotary actuator based on linear springs: Working principle, design, and experimental verification," in *Actuators*, vol. 9, no. 4, p. 141, Dec. 2020, doi: 10.3390/act9040141.
11. H.-A. Trinh, H. V. A. Truong, T. C. Do, M. H. Nguyen, V. D. Phan, and K. K. Ahn. Optimization-based energy management strategies for hybrid construction machinery: A review. *Energy Rep.* 2022, 8, 6035-6057.
12. V. D. Phan, C. P. Vo, and K. K. Ahn, "Adaptive neural tracking control for flexible joint robot including actuator dynamics with disturbance observer," in *International Journal of Robust and Nonlinear Control*, (Under review).
13. H.V.A. Truong, V. D. Phan, D.T. Tran, and K. K. Ahn, " A Novel Observer-based Neural-Network Finite-time Output Control for High-order Nonlinear Systems with New System Transformation," in *IEEE Transactions on Systems, Man and Cybernetics: Systems*, (Under review).
14. H. V. A. Truong, H.-A. Trinh; T. C. Do; M. H. Nguyen; V. D. Phan; S. H. Cho; K. K. Ahn. "A Modified Extremum Seeking-based Energy Management Strategy with Equivalent State for Hybrid Electric Tramway-Powered by Fuel Cell–Battery–Supercapacitors", in *eTransportation*, (Under review).

B. International Conferences

1. V. D. Phan and K. K. Ahn, " Observer-based Fault-Tolerant Control of an Electro-Hydraulic Actuator with mismatched disturbance," in *24th International Conference on Mechatronics Technology (ICMT)*, vol. 9, pp. 30750-30760, 2021, doi: 10.1109/ICMT53429.2021.9687272.
2. V. D. Phan; K. K. Ahn. Disturbance Observer-based Adaptive Fault-Tolerant Control of an Electro-Hydraulic Actuator with Output Constraint. In *Proceedings of The 13th Asian Control Conference*, Jeju Island, Korea, May 4-7, 2022.

REFERENCES

- [1] J. Yao, "Model-based nonlinear control of hydraulic servo systems: Challenges, developments and perspectives," *Frontiers of Mechanical Engineering*, vol. 13, no. 2, pp. 179-210, 2017.
- [2] J. Yao, Z. Jiao, D. Ma, and L. Yan, "High-Accuracy Tracking Control of Hydraulic Rotary Actuators With Modeling Uncertainties," *IEEE/ASME Transactions on Mechatronics*, vol. 19, no. 2, pp. 633-641, 2014.
- [3] Q.-N. Xu, K.-M. Lee, H. Zhou, and H.-Y. Yang, "Model-Based Fault Detection and Isolation Scheme for a Rudder Servo System," *IEEE Transactions on Industrial Electronics*, vol. 62, no. 4, pp. 2384-2396, 2015.
- [4] J. Yao, G. Yang, and Z. Jiao, "High dynamic feedback linearization control of hydraulic actuators with backstepping," *Proc. Inst. Mech. Eng. Part I-J Syst Control Eng.*, vol. 229, no. 8, pp. 728-737, 2015.
- [5] J. Yao, Z. Jiao, and D. Ma, "Extended-State-Observer-Based Output Feedback Nonlinear Robust Control of Hydraulic Systems With Backstepping," *IEEE Transactions on Industrial Electronics*, vol. 61, no. 11, pp. 6285-6293, 2014.
- [6] D.-T. Tran, T.-C. Do, and K.-K. Ahn, "Extended High Gain Observer-Based Sliding Mode Control for an Electro-hydraulic System with a Variant Payload," *International Journal of Precision Engineering and Manufacturing*, vol. 20, no. 12, pp. 2089-2100, 2019.
- [7] Z. Yao, J. Yao, and W. Sun, "Adaptive RISE Control of Hydraulic Systems With Multilayer Neural-Networks," *IEEE Transactions on Industrial Electronics*, vol. 66, no. 11, pp. 8638-8647, 2019.
- [8] O. Doukhi and D. J. Lee, "Neural Network-based Robust Adaptive Certainty Equivalent Controller for Quadrotor UAV with Unknown Disturbances," *International Journal of Control, Automation and Systems*, vol. 17, no. 9, pp. 2365-2374, 2019.
- [9] V. T. Yen, W. Y. Nan, and P. Van Cuong, "Robust Adaptive Sliding Mode Neural Networks Control for Industrial Robot Manipulators," *International Journal of Control, Automation and Systems*, vol. 17, no. 3, pp. 783-792, 2019.
- [10] G. Tan, Z. Wang, and C. Li, " H_∞ performance state estimation of delayed static neural networks based on an improved proportional-integral estimator," *Applied Mathematics and Computation*, vol. 370, 2020.
- [11] L. Liu, Y. J. Liu, D. Li, S. Tong, and Z. Wang, "Barrier Lyapunov Function-Based Adaptive Fuzzy FTC for Switched Systems and Its Applications to Resistance-Inductance-Capacitance Circuit System," *IEEE Trans Cybern*, vol. 50, no. 8, pp. 3491-3502, Aug 2020.
- [12] C. P. Vo, X. D. To, and K. K. Ahn, "A Novel Adaptive Gain Integral Terminal Sliding Mode Control Scheme of a Pneumatic Artificial Muscle System With Time-Delay Estimation," *IEEE Access*, vol. 7, pp. 141133-141143, 2019.
- [13] Y. Wang, X. Zhang, L. Yang, and H. Huang, "Adaptive Synchronization of Time Delay Chaotic Systems with Uncertain and Unknown Parameters via Aperiodically Intermittent Control," *International Journal of Control, Automation and Systems*, vol. 18, no. 3, pp. 696-707, 2019.
- [14] X. Yu and J. Jiang, "A survey of fault-tolerant controllers based on safety-related issues," *Annual Reviews in Control*, vol. 39, pp. 46-57, 2015.
- [15] I. Hwang, S. Kim, Y. Kim, and C. E. Seah, "A Survey of Fault Detection, Isolation, and Reconfiguration Methods," *IEEE Transactions on Control Systems Technology*, vol. 18, no. 3, pp. 636-653, 2010.

- [16] S. A. Nahian, D. Q. Truong, P. Chowdhury, D. Das, and K. K. Ahn, "Modeling and fault tolerant control of an electro-hydraulic actuator," *International Journal of Precision Engineering and Manufacturing*, vol. 17, no. 10, pp. 1285-1297, 2016.
- [17] M. S. Shaker and R. J. Patton, "Active sensor fault tolerant output feedback tracking control for wind turbine systems via T-S model," *Engineering Applications of Artificial Intelligence*, vol. 34, pp. 1-12, 2014.
- [18] J. Z. J. Poshtan, "Design of Nonlinear Unknown Input Observer for Process Fault Detection," *Ind. Eng. Chem. Res.*, vol. 49, pp. 11443–11452, 2010.
- [19] H. Chen, B. Jiang, and N. Lu, "A Multi-mode Incipient Sensor Fault Detection and Diagnosis Method for Electrical Traction Systems," *International Journal of Control, Automation and Systems*, vol. 16, no. 4, pp. 1783-1793, 2018.
- [20] S. K. Kommuri, S. B. Lee, and K. C. Veluvolu, "Robust Sensors-Fault-Tolerance With Sliding Mode Estimation and Control for PMSM Drives," *IEEE/ASME Transactions on Mechatronics*, vol. 23, no. 1, pp. 17-28, 2018.
- [21] Z. Wang, L. Liu, and H. Zhang, "Neural Network-Based Model-Free Adaptive Fault-Tolerant Control for Discrete-Time Nonlinear Systems With Sensor Fault," *IEEE Transactions on Systems, Man, and Cybernetics: Systems*, vol. 47, no. 8, pp. 2351-2362, 2017.
- [22] C. C. a. S. X. D. Zhiwei Gao, "A Survey of Fault Diagnosis and Fault-Tolerant Techniques—Part II: Fault Diagnosis With Knowledge-Based and Hybrid/Active Approaches," *IEEE TRANSACTIONS ON INDUSTRIAL ELECTRONICS*, vol. 62, no. 6, 2015.
- [23] Z. Gao, C. Cecati, and S. X. Ding, "A Survey of Fault Diagnosis and Fault-Tolerant Techniques—Part I: Fault Diagnosis With Model-Based and Signal-Based Approaches," *IEEE Transactions on Industrial Electronics*, vol. 62, no. 6, pp. 3757-3767, 2015.
- [24] P. Halder, "A Novel Approach for Detection and Diagnosis of Process and Sensor Faults in Electro-Hydraulic Actuator," *International Journal of Engineering Research and Development*, 2013.
- [25] H. Z. J. H. S. Daley, "On the use of adaptive updating rules for actuator and sensor fault diagnosis," *Automatica*, vol. 33, no. 2, pp. 217-225, 1997.
- [26] H.-J. Ma and G.-H. Yang, "Simultaneous fault diagnosis for robot manipulators with actuator and sensor faults," *Information Sciences*, vol. 366, pp. 12-30, 2016.
- [27] S. G. a. B. Yao, "Fault Detection, Identification and Accommodation for an Electro-hydraulic System: An Adaptive Robust Approach," *Proc. 17th IFAC World Congress*, 2008.
- [28] C. P. Vo, X. D. To, and K. K. Ahn, "A Novel Force Sensorless Reflecting Control for Bilateral Haptic Teleoperation System," *IEEE Access*, pp. 1-1, 2020.
- [29] S. Gautam, P. K. Tamboli, K. Roy, V. H. Patankar, and S. P. Duttagupta, "Sensors incipient fault detection and isolation of nuclear power plant using extended Kalman filter and Kullback-Leibler divergence," *ISA Trans*, vol. 92, pp. 180-190, Sep 2019.
- [30] H. Liu, D. Liu, C. Lu, and X. Wang, "Fault Diagnosis of Hydraulic Servo System Using the Unscented Kalman Filter," *Asian Journal of Control*, vol. 16, no. 6, pp. 1713-1725, 2014.
- [31] D. S. Pires and G. L. d. O. Serra, "Methodology for Evolving Fuzzy Kalman Filter Identification," *International Journal of Control, Automation and Systems*, vol. 17, no. 3, pp. 793-800, 2019.
- [32] S. Mondal, G. Chakraborty, and K. Bhattacharyy, "LMI approach to robust unknown input observer design for continuous systems with noise and uncertainties," *International Journal of Control, Automation and Systems*, vol. 8, no. 2, pp. 210-219, 2010.
- [33] T. Van Nguyen and C. Ha, "Experimental Study of Sensor Fault-Tolerant Control for an Electro-Hydraulic Actuator Based on a Robust Nonlinear Observer," *Energies*, vol. 12, no. 22, 2019.

- [34] Z. Gao, X. Liu, and M. Chen, "Unknown Input Observer Based Robust Fault Estimation for Systems Corrupted by Partially-Decoupled Disturbances," *IEEE Transactions on Industrial Electronics*, pp. 1-1, 2015.
- [35] S. A. Nahian, T. Q. Dinh, H. V. Dao, and K. K. Ahn, "An Unknown Input Observer-EFIR Combined Estimator for Electro-Hydraulic Actuator in Sensor Fault Tolerant Control Application," *IEEE/ASME Transactions on Mechatronics*, pp. 1-1, 2020.
- [36] S. K. Kommuri, M. Defoort, H. R. Karimi, and K. C. Veluvolu, "A Robust Observer-Based Sensor Fault-Tolerant Control for PMSM in Electric Vehicles," *IEEE Transactions on Industrial Electronics*, vol. 63, no. 12, pp. 7671-7681, 2016.
- [37] T. Li, T. Yang, Y. Cao, R. Xie, and X. Wang, "Disturbance-Estimation Based Adaptive Backstepping Fault-Tolerant Synchronization Control for a Dual Redundant Hydraulic Actuation System With Internal Leakage Faults," *IEEE Access*, vol. 7, pp. 73106-73119, 2019.
- [38] D. Wu, W. Liu, J. Song, and Y. Shen, "Fault Estimation and Fault-Tolerant Control of Wind Turbines Using the SDW-LSI Algorithm," *IEEE Access*, vol. 4, pp. 7223-7231, 2016.
- [39] G. Ren, M. Esfandiari, J. Song, and N. Sepehri, "Position Control of an Electrohydrostatic Actuator With Tolerance to Internal Leakage," *IEEE Transactions on Control Systems Technology*, vol. 24, no. 6, pp. 2224-2232, 2016.
- [40] J. Yao, G. Yang, and D. Ma, "Internal Leakage Fault Detection and Tolerant Control of Single-Rod Hydraulic Actuators," *Mathematical Problems in Engineering*, vol. 2014, pp. 1-14, 2014.
- [41] X. Wu, Y. Li, F. Li, Z. Yang, and W. Teng, "Adaptive Estimation-Based Leakage Detection for a Wind Turbine Hydraulic Pitching System," *IEEE/ASME Transactions on Mechatronics*, vol. 17, no. 5, pp. 907-914, 2012.
- [42] A. El-Betar, M. Abdelhamed, A. El-Assal, and R. Abdelsatar, "Fault Diagnosis of a Hydraulic Power System Using an Artificial Neural Network," *Journal of King Abdulaziz University-Engineering Sciences*, vol. 17, no. 1, pp. 115-136, 2006.
- [43] A. Maddahi, W. Kinsner, and N. Sepehri, "Internal Leakage Detection in Electrohydrostatic Actuators Using Multiscale Analysis of Experimental Data," *IEEE Transactions on Instrumentation and Measurement*, vol. 65, no. 12, pp. 2734-2747, 2016.
- [44] A. Y. Goharrizi and N. Sepehri, "A Wavelet-Based Approach for External Leakage Detection and Isolation From Internal Leakage in Valve-Controlled Hydraulic Actuators," *IEEE Transactions on Industrial Electronics*, vol. 58, no. 9, pp. 4374-4384, 2011.
- [45] A. Y. Goharrizi and N. Sepehri, "Internal Leakage Detection in Hydraulic Actuators Using Empirical Mode Decomposition and Hilbert Spectrum," *IEEE Transactions on Instrumentation and Measurement*, vol. 61, no. 2, pp. 368-378, 2012.
- [46] M. Van, M. Mavrovouniotis, and S. S. Ge, "An Adaptive Backstepping Nonsingular Fast Terminal Sliding Mode Control for Robust Fault Tolerant Control of Robot Manipulators," *IEEE Transactions on Systems, Man, and Cybernetics: Systems*, vol. 49, no. 7, pp. 1448-1458, 2019.
- [47] R. I. a. P. Ballé, "Trends in the Application of Model-Based Fault Detection and Diagnosis of Technical Processes," *Control Engineering Practice*, vol. 5, no. 5, pp. 709-719, 1997.
- [48] G. Yang, J. Yao, G. Le, and D. Ma, "Adaptive integral robust control of hydraulic systems with asymptotic tracking," *Mechatronics*, vol. 40, pp. 78-86, 2016.
- [49] T. D. Thien, D. X. Ba, and K. K. Ahn, "Adaptive Backstepping Sliding Mode Control for Equilibrium Position Tracking of an Electrohydraulic Elastic Manipulator," *IEEE Transactions on Industrial Electronics*, pp. 1-1, 2019.
- [50] G. Yang, H. Wang, and J. Chen, "Disturbance compensation based asymptotic tracking control for nonlinear systems with mismatched modeling uncertainties," *International Journal of Robust and Nonlinear Control*, 2021.

- [51] G. Yang and J. Yao, "Output feedback control of electro-hydraulic servo actuators with matched and mismatched disturbances rejection," *Journal of the Franklin Institute*, vol. 356, no. 16, pp. 9152-9179, 2019.
- [52] Q. Guo and Z. Chen, "Neural adaptive control of single-rod electrohydraulic system with lumped uncertainty," *Mechanical Systems and Signal Processing*, vol. 146, 2021.
- [53] H.-Z. T. a. N. Sepehri, "Parametric Fault Diagnosis for Electrohydraulic Cylinder Drive Units," *IEEE TRANSACTIONS ON INDUSTRIAL ELECTRONICS*, vol. 49, no. 1, 2002.
- [54] C. Kaddissi, J. P. Kenne, and M. Saad, "Identification and Real-Time Control of an Electrohydraulic Servo System Based on Nonlinear Backstepping," *IEEE/ASME Transactions on Mechatronics*, vol. 12, no. 1, pp. 12-22, 2007.
- [55] G. A. S. a. J. E. Bobrow, "Experiments and Simulations on the Nonlinear Control of a Hydraulic Servosystem," *IEEE TRANSACTIONS ON CONTROL SYSTEMS TECHNOLOGY*, vol. 7, no. 2, 1999.
- [56] M. B. A. Souza, L. de Mello Honório, and E. J. de Oliveira, "Innovative Analysis for Parameter Estimation Quality," *International Journal of Control, Automation and Systems*, vol. 19, no. 1, pp. 363-371, 2020.
- [57] H. Angue Mintsá, R. Venugopal, J.-P. Kenne, and C. Belleau, "Feedback Linearization-Based Position Control of an Electrohydraulic Servo System With Supply Pressure Uncertainty," *IEEE Transactions on Control Systems Technology*, vol. 20, no. 4, pp. 1092-1099, 2012.
- [58] V. D. Phan, C. P. Vo, H. V. Dao, and K. K. Ahn, "Actuator Fault-Tolerant Control for an Electro-Hydraulic Actuator Using Time Delay Estimation and Feedback Linearization," *IEEE Access*, vol. 9, pp. 107111-107123, 2021.
- [59] Z. Ding, "Nonlinear and Adaptive Control Systems," *The Institution of Engineering and Technology, London, United Kingdom*, 2013.
- [60] A. Levant, "Robust exact differentiation via sliding mode technique," *Automatica*, vol. 34, no. 3, pp. 379-384, 1998.
- [61] V. Mien, G. Shuzhi Sam, and R. Hongliang, "Finite Time Fault Tolerant Control for Robot Manipulators Using Time Delay Estimation and Continuous Nonsingular Fast Terminal Sliding Mode Control," *IEEE Trans Cybern*, vol. 47, no. 7, pp. 1681-1693, Jul 2017.
- [62] J. Lee, P. H. Chang, B. Yu, K.-H. Seo, and M. Jin, "An Effective Adaptive Gain Dynamics for Time-Delay Control of Robot Manipulators," *IEEE Access*, vol. 8, pp. 192229-192238, 2020.
- [63] H. K. Khalil, "Nonlinear Systems " *Prentice Hall: Upper Saddle River NJ, USA*, 2002.
- [64] X. Yang, J. Yao, and W. Deng, "Output feedback adaptive super-twisting sliding mode control of hydraulic systems with disturbance compensation," *ISA Trans*, vol. 109, pp. 175-185, Mar 2021.
- [65] W. Shen, X. Liu, and X. Su, "High-Precision Position Tracking Control of Electro-hydraulic Servo Systems Based on an Improved Structure and Desired Compensation," *International Journal of Control, Automation and Systems*, vol. 19, no. 11, pp. 3622-3630, 2021.
- [66] G. Q. Zhangbao Xu, Qingyun Liu, Jianyong Yao, "Output Feedback Disturbance Rejection Control for Full-State Constrained Hydraulic Systems with Guaranteed Tracking Performance," *Applied Mathematical Modelling*, p. doi:10.1016/j.apm.2022.06.043, 2022.
- [67] V. D. Phan and K. K. Ahn, "Observer-based Fault-Tolerant Control of an Electro-Hydraulic Actuator with mismatched disturbance," *24th International Conference on Mechatronics Technology (ICMT)*, pp. 1-6, 2021.
- [68] S.-C. Nie, L.-F. Qian, L.-M. Chen, L.-F. Tian, and Q. Zou, "Barrier Lyapunov functions-based dynamic surface control with tracking error constraints for ammunition manipulator electro-hydraulic system," *Defence Technology*, vol. 17, no. 3, pp. 836-845, 2021.

- [69] Z. Xu, C. Sun, X. Hu, Q. Liu, and J. Yao, "Barrier Lyapunov Function-Based Adaptive Output Feedback Prescribed Performance Controller for Hydraulic Systems with Uncertainties Compensation," *IEEE Transactions on Industrial Electronics*, pp. 1-10, 2023.
- [70] V. D. Phan, H. V. A. Truong, and K. K. Ahn, "Actuator failure compensation-based command filtered control of electro-hydraulic system with position constraint," *ISA Trans*, vol. 134, pp. 561-572, 2023.
- [71] W. Wu, Y. Li, and S. Tong, "Neural Network Output-Feedback Consensus Fault-Tolerant Control for Nonlinear Multiagent Systems With Intermittent Actuator Faults," *IEEE Trans Neural Netw Learn Syst*, vol. PP, Oct 13 2021.
- [72] V. D. Phan, C. P. Vo, H. V. Dao, and K. K. Ahn, "Robust Fault-Tolerant Control of an Electro-Hydraulic Actuator With a Novel Nonlinear Unknown Input Observer," *IEEE Access*, vol. 9, pp. 30750-30760, 2021.
- [73] V. D. Phan and K. K. Ahn, "Fault-tolerant control for an electro-hydraulic servo system with sensor fault compensation and disturbance rejection," *Nonlinear Dynamics*, vol. 111, pp. 10131-10146, 2023.